

WestminsterResearch

<http://www.westminster.ac.uk/research/westminsterresearch>

Compensation of nonlinear distortion in RF amplifiers for mobile communications

Mina Vaskovic

Faculty of Science and Technology

This is an electronic version of a PhD thesis awarded by the University of Westminster. © The Author, 2014.

This is an exact reproduction of the paper copy held by the University of Westminster library.

The WestminsterResearch online digital archive at the University of Westminster aims to make the research output of the University available to a wider audience. Copyright and Moral Rights remain with the authors and/or copyright owners.

Users are permitted to download and/or print one copy for non-commercial private study or research. Further distribution and any use of material from within this archive for profit-making enterprises or for commercial gain is strictly forbidden.

Whilst further distribution of specific materials from within this archive is forbidden, you may freely distribute the URL of WestminsterResearch: (<http://westminsterresearch.wmin.ac.uk/>).

In case of abuse or copyright appearing without permission e-mail repository@westminster.ac.uk

Compensation of Nonlinear Distortion in RF Amplifiers for Mobile Communications

Mina Vaskovic

A thesis submitted in partial fulfillment of the
requirements of the University of Westminster
for the degree of Doctor of Philosophy

January 2014

ACKNOWLEDGEMENT

First and foremost, I would like to acknowledge my director of studies, Dr. D. Budimir whose guidance and patience guided me through my research work. I am also grateful to my supervisors Dr. A. Tarczynski and Dr. Z. Djurovic for useful suggestions and assistance.

I would also like to express my gratitude, love and respect for those to whom I dedicate this work, my family. They were, are and always will be my inspiration and my strength for any accomplishment.

The financial supports provided by the University of Westminster and Serbian Ministry of Youth and Sport, Fund for Young Talents, are gratefully acknowledged.

To my family.

ABSTRACT

Compensation of nonlinear distortion of power amplifiers in mobile communications is an important requirement for improving power consumption performance while maintaining efficiency, since mobile phone became an essential accessory for everyone nowadays. This problem demands a good power amplifier model, in order to develop an effective predistortion system.

Current researches are focused on modelling and predistortion of power amplifiers with memory, as well as memoryless ones. Different methods for modelling are used, as the Volterra series, polynomial models, look-up tables, the Hammerstein models, the Wiener models, and artificial intelligence systems. For predistortion feedback, feedforward and digital predistortion techniques are used. Among digital predistortion methods there are artificial intelligence systems, used in this thesis for linearization of power amplifier.

This thesis presents developed robust method for modelling power amplifiers without memory effects and gives a comparison of proposed method with least squares method. Also, this research presents two novel techniques based on artificial intelligence systems for modelling and predistortion of highly nonlinear power amplifier with memory. The first approach is based on artificial neural networks, while the second one uses adaptive fuzzy logic systems. Forward and inverse models of power amplifier are created with both proposed methods. Superiority of artificial intelligence systems over partial least squares method is presented. Developed models are employed in a cascade to make a linearized system. Verification of proposed methods is carried out through the signal performance parameters and spectra of measured signal and signal from predistortion system. The feasibility and performances of the proposed digital predistortions are examined by simulations and experiments. The comparison of proposed methods is given to present advantages/disadvantages of both methods. The achieved distortion suppression from 72.2% to 93.6% and spectral regrowth improvement from 11.4 dB to 16.2 dB prove that the proposed methods have great ability to compensate the nonlinear distortion in power amplifier.

CONTENTS

ACKNOWLEDGEMENT	ii
ABSTRACT	iii
LIST OF TABLES	viii
LIST OF FIGURES	xi
1. INTRODUCTION.....	1
1.1. Background	2
1.2. Objectives of Research and Outline of Thesis	3
1.2.1 Objectives of Research.....	3
1.2.2 Outline of the Thesis	5
1.3. References	7
2. NONLINEAR ANALYSIS OF POWER AMPLIFIERS	11
2.1. Introduction	11
2.2. Power Amplifier Fundamentals	12
2.2.1 Gain	12
2.2.2 1dB Compression Point	13
2.2.3 Second- and Third-Order Intercept Points	14
2.2.4 Efficiency	16
2.3. Nonlinear Analysis.....	17
2.3.1 Two-Tone Test.....	17
2.3.2 AM/AM and AM/PM Distortions.....	21

2.3.3	Error Vector Magnitude	22
2.3.4	Adjacent Channel Power Ratio	23
2.3.5	Peak to Average Power Ratio	24
2.4.	Overview of modelling and linearization techniques.....	25
2.4.1	Behavioural Modelling Techniques	25
2.4.1	Overview of Linearization Techniques.....	31
2.5.	Conclusion	36
2.6.	References.....	37
3.	ARTIFICIAL INTELLIGENCE SYSTEMS	42
3.1.	Introduction.....	42
3.2.	Artificial Neural Networks.....	42
3.2.1	Artificial Neuron	43
3.2.2	Network Architecture.....	45
3.2.3	Learning Algorithms	48
3.3.	Fuzzy Logic.....	51
3.3.1	Fuzzy Sets and Membership Functions.....	51
3.3.2	Fuzzy Rules.....	52
3.3.3	Defuzzification.....	54
3.4.	Neuro-Fuzzy Systems	55
3.4.1	Adaptive neuro-fuzzy inference system.....	56
3.4.2	Adaptive Fuzzy Logic Systems.....	57
3.5.	Conclusion	60
3.6.	References.....	60

4. ROBUST ESTIMATION OF NONLINEAR COEFFICIENTS FOR MEMORYLESS POLYNOMIAL MODEL OF POWER AMPLIFIERS	63
4.1. Introduction	63
4.2. Memoryless polynomial model of power amplifier	64
4.3. Theoretical analysis of the baseband linearization method	66
4.4. Proposed robust method for estimation of nonlinear coefficients	69
4.5. Experimental validation of the proposed estimation method	72
4.6. Conclusion	76
4.7. References	76
5. MODELING AND PREDISTORTION OF POWER AMPLIFIERS USING NEURAL NETWORKS	79
5.1. Introduction	79
5.2. Neural Network Models – Literature Overview	79
5.3. Proposed Neural Network Structure	82
5.4. Neural Network Forward Model of Power Amplifier	85
5.4.1 Experimental Data Collection	85
5.4.2 Training the Neural Network with collected data	86
5.5. Neural Network Inverse Model of Power Amplifier	91
5.6. Power Amplifier Predistortion using Inverse Model	95
5.7. Comparison with partial least squares method	99
5.8. Conclusion	100
5.9. References	101

6. MODELING AND PREDISTORTION OF POWER AMPLIFIERS USING NEURO-FUZZY SYSTEMS.....	103
6.1. Introduction.....	103
6.2. Proposed Adaptive Fuzzy Logic System	104
6.2.1 Training of Adaptive Fuzzy Logic System	107
6.3. Experimental Results for Modelling and Predistortion of DUT	110
6.3.1 Modelling of Power Amplifier.....	110
6.3.2 Predistortion of Power Amplifier using AFLS	115
6.4. Comparison of used predistortion techniques.....	120
6.5. Conclusion	123
6.6. References.....	123
7. CONCLUSION.....	126
7.1. Thesis Summary.....	126
7.2. Contributions to Knowledge	128
7.3. Future Work	129
LIST OF PUBLICATIONS.....	130
APPENDIX-A.....	131
Data Sheets for the Power Amplifiers.....	131

LIST OF TABLES

TABLE 4.1: Power levels from the experiment

TABLE 5.1: Forward model performances compared with performances of real input and output for the LTE 1.4 MHz 64 QAM signal at 880 MHz centre frequency

TABLE 5.2: Forward model statistical performances for the LTE 1.4 MHz 64 QAM signal at 880 MHz centre frequency

TABLE 5.3: Forward model performances compared with performances of real input and output for the LTE 3 MHz 64 QAM signal at 880 MHz centre frequency

TABLE 5.4: Forward model statistical performances for the LTE 3 MHz 64 QAM signal at 880 MHz centre frequency

TABLE 5.5: Inverse model performances compared with performances of real input and output for the LTE 1.4 MHz 64 QAM signal at 880 MHz centre frequency

TABLE 5.6: Inverse model statistical performances for the LTE 1.4 MHz 64 QAM signal at 880 MHz centre frequency

TABLE 5.7: Inverse model performances compared with performances of real input and output for the LTE 3 MHz 64 QAM signal at 880 MHz centre frequency

TABLE 5.8: Inverse model statistical performances for the LTE 3 MHz 64 QAM signal at 880 MHz centre frequency

TABLE 5.9: Performances of output signal from a system with DPD compared with performances of real input and output signals from a system without DPD for the LTE 1.4 MHz 64 QAM signal at 880 MHz centre frequency

TABLE 5.10: Performances of output signal from a system with DPD compared with performances of real input and output signals from a system without DPD for the LTE 3 MHz 64 QAM signal at 880 MHz centre frequency

TABLE 5.11: ACPR of output signal from a real system with DPD compared with ACPR of real input and output signals from a system without DPD for the LTE 1.4 MHz 64 QAM signal at 880 MHz centre frequency

TABLE 5.12: Forward model statistical performances for RVTDNN and PLS for the LTE 1.4 MHz 64 QAM signal at 880 MHz centre frequency

TABLE 5.13: Inverse model statistical performances for RVTDNN and PLS for the LTE 1.4 MHz 64 QAM signal at 880 MHz centre frequency

TABLE 6.1: Forward model performances compared with performances of real input and output for the LTE 1.4 MHz 64 QAM signal at 880 MHz centre frequency

TABLE 6.2: Forward model statistical performances for the LTE 1.4 MHz 64 QAM signal at 880 MHz centre frequency

TABLE 6.3: Inverse model performances compared with performances of real input and output for the LTE 1.4 MHz 64 QAM signal at 880 MHz centre frequency

TABLE 6.4: Inverse model statistical performances for the LTE 1.4 MHz 64 QAM signal at 880 MHz centre frequency

TABLE 6.5: Performances of output signal from DPD+PA system compared with performances of real input and output signals from a system without DPD for the LTE 1.4 MHz 64 QAM signal at 880 MHz centre frequency

TABLE 6.6: Performances of output signal from PA+DPD system compared with performances of real input and output signals from a system without DPD for the LTE 1.4 MHz 64 QAM signal at 880 MHz centre frequency

TABLE 6.7: Comparative overview of used DPD techniques for the LTE 1.4 MHz 64 QAM signal at 88MHz centre frequency

TABLE 6.8: Distortion suppression for presented methods for the LTE 1.4 MHz 64 QAM signal at 88MHz centre frequency

LIST OF FIGURES

Figure 2-1: Examples of transfer characteristics of a PA: (a) ideal; (b) real

Figure 2-2: The measured gain characteristic of the PA Mini-Circuits ZFL-500

Figure 2-3: The measured output power characteristic of the PA Mini-Circuits ZFL-500, with 1dB compression point at 9dBm output power level

Figure 2-4: The second- and third-order intercept points

Figure 2-5: The measured output power and power-added efficiency curves for the Mini-Circuits ZFL-500

Figure 2-6: Output spectrum of a power amplifier under two-tone excitation

Figure 2-7: ADS simulation of the Two-tone test for the PA Mini-Circuits ZHL-1042J

Figure 2-8: ADS simulation results of the Two-tone test for the PA ZHL-1042J at 0dBm input power level: a) Spectra of the input and output signals; b) Time domain waveforms of input and output signals

Figure 2-9: An example of characteristics for a PA: a) AM/AM; b) AM/PM

Figure 2-10: Error vector

Figure 2-11: A graphical representation of ACPR

Figure 2-12: The Volterra series representation of a system

Figure 2-13: The Wiener model

Figure 2-14: The Hammerstein model

Figure 2-15: The Wiener-Hammerstein model

Figure 2-16: General feedback linearization system

Figure 2-17: ADS model for an analogue two-tone signal with feedback

Figure 2-18: ADS simulation results of feedback RF linearization for the Two-tone signal for the PA ZHL-1042J at 0dBm input power level: a) Spectra of the input and output signals; b) Time domain waveforms of input and output signals

Figure 2-19: General layout of a feedforward system

Figure 2-20: General layout of a digital predistortion system

Figure 2-21: Layout of an adaptive digital predistortion system

Figure 3-1: A single neuron model

Figure 3-2: A neuron activation functions: a) linear, b) hyperbolic tangent, c) log-sigmoid

Figure 3-3: A single-layer neural network

Figure 3-4: A multi-layer neural network fully connected

Figure 3-5: NN architectures: a) a multi-layer network not-fully connected, b) a feedforward network, c) a recurrent network

Figure 3-6: Back-propagation algorithm

Figure 3-7: Classes of parameterized membership functions: a) $triangle(x, 10, 30, 40)$, b) $trapezoid(x, 5, 10, 20, 35)$, c) $gaussian(x, 25, 10)$, d) $bell(x, 10, 2, 25)$

Figure 3-8: Fuzzy reasoning for multiple rules with multiple premises

Figure 3-9: The Mamdani defuzzification methods

Figure 3-10: The Sugeno fuzzy model

Figure 3-11: A two-input ANFIS architecture

Figure 3-12: A multi-input multi-output AFLS architecture

Figure 4-1: The experimental setup for data collection

Figure 4-2: An example of single-tone frequency response of a power amplifier in saturation

Figure 4-3: The experimental setup for PA characterisation

Figure 4-4: AM/AM characteristics of the measured and modelled PA ZHL-1042J at a 751 MHz carrier (11 data samples)

Figure 4-5: AM/AM characteristics of the measured and modelled PA ZHL-1042J at a 751 MHz carrier (19 data samples)

Figure 5-1: Power amplifier model structure with two separate networks

Figure 5-2: Power amplifier model structure with one complex-valued network

Figure 5-3: Feedforward real-valued neural network with multiple inputs and two outputs

Figure 5-4: Proposed neural network structure for modelling

Figure 5-5: The experimental setup for data collection

Figure 5-6: The hardware test-bench

Figure 5-7: Forward model results at 880 MHz: a) PA gain for the LTE 1.4 MHz 64 QAM signal; b) Power spectrum density of the RVTDNN model output vs. the real PA output for the LTE 1.4 MHz 64 QAM signal

Figure 5-8: Forward model results at 880 MHz: a) PA gain for the LTE 3 MHz 64 QAM signal; b) Power spectrum density of the RVTDNN model output vs. the real PA output for the LTE 3 MHz 64 QAM signal

Figure 5-9: Inverse model results at 880 MHz: a) Inverse PA gain for the LTE 1.4 MHz 64 QAM signal; b) Power spectrum density of the RVTDNN model output vs. the real PA input for the LTE 1.4 MHz 64 QAM signal

Figure 5-10: Inverse model results at 880 MHz: a) Inverse PA gain for the LTE 3 MHz 64 QAM signal; b) Power spectrum density of the RVTDNN model output vs. the real PA input for the LTE 3 MHz 64 QAM signal

Figure 5-11: A layout of predistortion system

Figure 5-12: Power spectrum densities at 880 MHz for an input signal before predistortion, output signal with predistortion, and output signal without predistortion for the LTE 1.4 MHz 64 QAM signal

Figure 5-13: Power spectrum densities at 880 MHz for an input signal before predistortion, output signal with predistortion, and output signal without predistortion for the LTE 3 MHz 64 QAM signal

Figure 5-14: Power spectrum densities at 880 MHz for an input signal before predistortion, output signal with predistortion, and output signal without predistortion for the LTE 1.4 MHz 64 QAM signal (using the hardware test-bench)

Figure 6-1: A multi-input multi-output AFLS architecture

Figure 6-2: A triangular shape membership function

Figure 6-3: A consequent part shape

Figure 6-4: Consequent fuzzy sets of the j -th output placed on a massless beam

Figure 6-5: Forward model results at 880 MHz: a) PA gain for the LTE 1.4 MHz 64 QAM signal; b) Power spectrum density of the AFLS model output vs. the real PA output for the LTE 1.4 MHz 64 QAM signal

Figure 6-6: Inverse model results at 880 MHz: a) PA gain for the LTE 1.4 MHz 64 QAM signal; b) Power spectrum density of the AFLS model output vs. the real PA output for the LTE 1.4 MHz 64 QAM signal

Figure 6-7: Predistortion results at 880 MHz: a) Power spectrum density of the DPD+PA model output vs. the real PA output for the LTE 1.4 MHz 64 QAM signal; b) PA gain; c) AM/AM characteristic; d) AM/PM characteristic

Figure 6-8: A layout of PA-DPD system

Figure 6-9: Comparison of simulation and experimental predistortion results at 880 MHz: a) Power spectrum density of a PA+DPD model output vs. output of the real PA for the LTE 1.4 MHz 64 QAM signal; b) PA gain; c) AM/AM characteristic; d) AM/PM characteristic

1. INTRODUCTION

Modern emerging mobile systems such as High Speed Packet Access (HSPA), Long-Term Evolution (LTE), and Mobile Interoperability for Microwave Access (Mobile WiMAX) require radio transceivers able to support high data rates and throughput. One of the main trends in the design of wireless transmitters is to provide enhanced transmitter functionalities using digital signal processing (DSP). However, the common assumption of linearity for wireless communication systems limits the efficiency of such designs, as this assumption is not realistic, for instance, due to the nonlinear properties of the front-end components and semiconductor devices in the power amplifier [1.1]-[1.2].

With the increasing demands for the performance of the system and supported data rates on one side, and the terminal flexibility and implementation costs on the other, the requirements for nonlinear distortion suppression in wideband multichannel wireless transceivers become extremely challenging to meet. In order to satisfy the abovementioned requirements, wireless systems need Multiple Input Multiple Output (MIMO) radio transceivers that cover different frequency bands, low cost and maintain low current consumption with OFDM modulation supporting multiple quadrature amplitude modulations (QAMs) with orders as high as 256 QAM on subcarriers. Such high order modulation levels demand a very high performance from the radio and dictate a highly linear architecture. High linearity and efficiency are required in the entire signal path of both transmitter and receiver, imposing the need for advanced design techniques and high power consumption. The need for reducing power/energy consumption and preventing climate change are widely acknowledged today. With the low power and low cost front-end architecture direct conversion OFDM is considered as the most promising transmission technique to support the high-speed wireless communications systems. So, here too, the requirement to design highly linear amplifiers becomes important. High power amplifiers having compact size, high efficiency and a high nonlinear distortion performance are important for the next-generation mobile, satellite and wireless systems.

1.1. Background

Power amplifier (PA) modelling and linearization techniques development increased during last decade with expansion of mobile systems and user requirements. Modelling methods used for wireless power amplifiers are theoretical and empirical [1.3]-[1.4]. Theoretical modelling utilizes describing the process partly, using knowledge about sub-models, to compose a structured process model, which also provides information about the internal state of the process [1.5]. This approach demands precise knowledge of the PA internal structure and its specific parameters and makes modelling process complicated. Empirical modelling is based on determination of system model using set of input-output observations [1.3]. Naturally, it must be regarded that the identified process model is only valid within the analysed range and does not necessarily comprise physically relevant parameters. This type of modelling is called the black-box modelling. Both approaches are used for modelling memoryless power amplifiers, as well as power amplifiers with memory effects.

A highly linear and efficient transmitter can be achieved by linearization of power amplifiers, which is an important task aimed to satisfy the exacting requirements put on modern wireless transmitters. For linearization of PAs authors use different methods. Feedback linearization techniques, which imply feedback loops in a system, can be found in [1.6]-[1.13]. On the other hand, in order to avoid feedback and possibility of instability, other authors use feedforward techniques for linearization [1.14]-[1.17]. These methods add components for linearization in a forward chain. Digital predistortion (DPD) is mostly used during the last decades. It is based on introducing nonlinear distortion which is complementary to PA distortion in baseband part of system, to make a cascade that will be linear in overall input-output characteristic. Digital predistortion methods can be divided to conventional and advanced techniques [1.18]. Look-up tables (LUT) and polynomial techniques presented in [1.19]-[1.28] are conventional techniques. Performance of polynomial methods is limited by the order of the function, while LUTs suffer from nonlinearity if the entries in the table are not interpolated [1.18]. Artificial intelligence systems, such as neural networks, fuzzy systems and neuro-fuzzy systems published in [1.18], [1.29]-[1.37] are categorized as advanced systems. These have ability to track highly nonlinear dynamics of power amplifier and have been successfully used in modelling of memory effects of PAs.

Artificial intelligence systems are frequently used DPD methods during the last twenty years as they are capable to adapt to changes in power amplifier behaviour. Predistortion is based on creation of a predistortion signal in baseband, as an output of inverse model of power amplifier. In this way, a signal at the very end of the system, containing predistorter and amplifier, has suppressed distortion effects.

1.2. Objectives of Research and Outline of Thesis

This thesis is focused on modelling of highly nonlinear power amplifiers, and nonlinear distortion suppression, future power/energy consumption reduction and improving the efficiency of wireless communication systems. The overall aim is to create the advanced digital signal processing techniques for adaptive compensation of nonlinear distortions in radio transmitters within innovative telecommunication applications. The main goal of this research is to develop an adaptive algorithm for suppression of nonlinear distortions that unlike existing solutions, e.g. those based on large look-up tables, will not require extensive calibrations before development.

1.2.1 Objectives of Research

1. Studying non-linear analysis of power amplifiers and identification methods
2. Investigation of polynomial modelling of RF power amplifiers for the development of digital predistortion systems
3. Literature review on the newest achievements in the area of adaptive digital predistortion of power amplifiers in the wireless communication industry
4. Creating ADS simulation circuits with ZHL-1042J block and two tone analogue signal and realization of feedback compensation of intermodulation components
5. Developing a robust method for extracting PA polynomial coefficients from instantaneous nonlinear behaviour based on a frequency response analysis

6. Setting up an experimental test-bed for developing and testing new estimation method. Setup contains two real power amplifiers, Mini Circuits ZHL-1042J and Mini Circuits ZFL500, Agilent ESG-D Series Signal Generator E4433B, and Agilent VSA Series Transmitter Tester E4406A and MATLAB as software tool
7. Creating LAN and GPIB connections between PC and instruments: signal generators Agilent E4433B and MXG N5182A and spectrum analyser Agilent E4406A for faster offline and online data processing and further developing of an adaptive system which requires all components to be connected
8. Setting up an experimental test-bed for developing and testing new methods. Setup contains real power amplifiers MIMIX CFH2162-P3, Agilent ESG-D Series Signal Generator E4433B, Agilent MXG Vector Signal Generator N5182A and Agilent VSA Series Transmitter Tester E4406A and MATLAB, Agilent Signal Studio Toolkit and Agilent Distortion Suite 89604A, as software tools
9. Developing modelling technique based on artificial intelligence systems
10. Modelling power amplifier MIMIX CFH2162-P3 using neural network approach
11. Developing a digital processing technique for digital predistortion using neural networks with the aim to improve linearity of real-life device under test
12. Implementing the neural network predistorter for linearising a nonlinear power amplifier exhibiting memory effects
13. Experimentally verifying the complete DPD system with the MIMIX CFH2162-P3 power amplifier for the LTE 1.4 MHz 64 QAM signal at 880MHz as centre frequency
14. Modelling of device under test using neuro-fuzzy systems

15. Developing a digital predistortion technique using adaptive fuzzy logic system with the aim to improve linearity of MIMIX CFH2162-P3
16. Implementing the neuro-fuzzy predistorter for linearising a nonlinear power amplifier exhibiting memory effects
17. Verifying the complete system with the adaptive fuzzy logic system predistorter and power amplifier for the LTE 1.4 MHz 64 QAM signal at 880MHz as centre frequency

1.2.2 Outline of the Thesis

This thesis investigates and implements novel techniques in modelling power amplifiers without memory effects and digital predistortion linearization. Presented research work concentrates on the linearization of wireless transmitters by digital methods, which are cost effective, small size, easily integrated, tuneable and maintain high overall efficiency of a system.

Chapter 2 covers nonlinear theory of power amplifiers. Nonlinear parameters of power amplifiers are defined and its characteristics are given in related figures. Performance parameters used for examination of nonlinear effects of power amplifiers are introduced. Furthermore, an overview of modelling and linearization techniques is carried out. Models exhibiting memory effects and models for memoryless power amplifiers used in existing literature are reviewed. Simulation analysis of the nonlinear Mini-Circuits ZHL-1042J power amplifier using Advanced Design System software is presented. The analysis is carried out using the two-tone test. A RF feedback compensation of distortion components in a two-tone signal is validated through ADS simulations.

Chapter 3 is dedicated to artificial intelligence systems. Neural networks are defined. Neuron, as the basic element of neural network, is defined. Mostly used activation functions, network structures and learning algorithms are presented. After that, a brief introduction to fuzzy systems is given, for better understanding the

combinational part called neuro-fuzzy. Final subsection in this Chapter explains the adaptive neuro-fuzzy inference system and adaptive fuzzy logic systems, as two main types of neuro-fuzzy structures.

Chapter 4 concentrates on memoryless polynomial model of power amplifiers. Analytical description of an output signal distortion caused by a memoryless nonlinearity of a PA is presented. General formulas are derived, which relate an analytical expression for the fundamental frequency signal and in-band distortion components to the order of a PA polynomial model. Theoretical analysis of the baseband linearization method is depicted. Furthermore, a robust method for estimation of coefficients of a nonlinear model is proposed. This method is applied and tested for the Mini-Circuits ZHL-1042J power amplifier and the results are provided at the end of this Chapter.

Chapter 5 is dedicated to the issues of nonlinear modelling and predistortion of highly nonlinear power amplifiers with memory using neural networks. A novel neural network structure is proposed. The proposed structure, in contrast to literature results published by now, has the activation function in the output layer different from the linear. The experimental setup and measured results for verifying the feasibility and linearizing performances of the proposed DPD are presented. Signals used for characterisation and linearization of the power amplifier MIMIX CFH2162-P3 are the LTE 1.4 MHz 64 QAM signal and the LTE 3 MHz 64 QAM signal at 880MHz as centre frequency. Verification of forward and inverse models of DUT is obtained through spectra of input and output signals and signal performance parameters. Chapter presents the implementation and verification of a complete predistortion system based on the proposed structure. First, the predistortion is tested using a cascade of inverse and forward model derived using neural networks, and finally, the predistorter is validated for the LTE 1.4 MHz 64 QAM signal at 880 MHz through the hardware test-bench. At the end of this chapter comparison of the neural network forward and inverse models of power amplifier and models based on partial least squares regression is given.

Chapter 6 is dedicated to an adaptive fuzzy logic systems technique used for the first time for modelling and predistortion of power amplifiers. This chapter also presents a detailed structure with area of balance defuzzification method as alternative to the

centroid defuzzification. Learning procedure and update functions for all parameters of a neuro-fuzzy structure are defined. As for the previously proposed neural network based method, the same verification is performed through MATLAB simulations using a developed forward model of power amplifier. Furthermore, predistortion system based on cascade layout that is formed of power amplifier and after that inverse model of power amplifier is implemented, based on neural networks and adaptive fuzzy logic systems. Simulation and experimental results are presented. Performances of the proposed predistortion methods are discussed and comparative overview of training procedures and modelling results for the MIMIX CFH2162-P3 highly nonlinear power amplifier is conferred.

Chapter 7 gives summary of the research undertaken within this work and gives suggestions and potential future research directions.

1.3. References

- [1.1] F. H. Raab, P. Asbeck, S. Cripps, P. B. Kenington, Z. B. Popovic, N. Pothecary, J. F. Sevic, and N. O. Sokal, "Power Amplifiers and Transmitters for RF and Microwave", *IEEE Transactions on Microwave Theory and Techniques*, vol. 50, no. 3, pp. 814-826, March 2002.
- [1.2] P. B. Kenington, *High Linearity RF Amplifier Design*, Artech House, 2000.
- [1.3] J. C. Pedro, and S. A. Maas, "A comparative overview of microwave and wireless power-amplifier behavioral modeling approaches," *IEEE Transactions on Microwave Theory and Techniques*, vol. 53, no. 4, pp. 1150-1163, April 2005.
- [1.4] J. C. Pedro, and N. B. Carvalho, *Intermodulation Distortion in Microwave and Wireless Circuits*, Artech House, Norwood, 2003.
- [1.5] Cellier, F. E, *Continuous system modeling*, Springer-Verlag, 1991.
- [1.6] Y. Yang, and B. Kim, "A new linear amplifier using low-frequency second-order intermodulation component feedforwarding", *IEEE Microwave and Guided Wave Letters*, vol. 9, no. 10, pp. 419-421, October 1999.
- [1.7] M. Faulkner, "Amplifier linearization using RF feedback and feedforward techniques", *IEEE Transactions on Vehicular Technology*, vol. 47, pp. 209-215, February 1998.

-
- [1.8] G. Gajda, and R. Douville, "A linearization system using RF feedback", in *Proc. IEEE International Electrical and Electronics Conference*, Toronto, Canada, pp. 30-33, 1983.
- [1.9] T. Sowlati, D. Rozenblit, E. MacCarthy, M. Damgaard, R. Pullela, D. Koh, D. Ripley, "Quad-band GSM/GPRS/EDGE polar loop transmitter", *IEEE Journal of Solid-State Circuits*, vol. 39, no 12, pp. 2179- 2189, December 2004.
- [1.10] J. L. Dawson, and T. H. Lee, "Automatic phase alignment for a fully integrated cartesian feedback power amplifier system", *IEEE Journal of Solid-State Circuits*, vol. 38, no. 12, pp. 2269-2279, December 2003.
- [1.11] M. Johansson, and L. Sundstrom, "Linearisation of RF multicarrier amplifiers using Cartesian feedback", *IEE Electronics Letters*, vol. 30, no. 14, pp. 1110-1111, July 1994.
- [1.12] S. Chung, J. W. Holloway, and J. L. Dawson, "Energy-efficient digital predistortion with lookup table training using analog cartesian feedback", *IEEE Transactions on Microwave Theory Tech.* vol. 56, no. 10, pp. 385-392, October 2008.
- [1.13] S. Chung, J. W. Holloway, and J. L. Dawson, "Open-loop digital predistortion using Cartesian feedback for adaptive RF power amplifier linearization", in *Proc. IEEE MTT-S Int. Microw. Symp. Dig.*, pp. 1449–1452, June 2007.
- [1.14] M. T. Hickson, D. K. Paul, P. Gardner, and K. Konstantinou, "High efficiency feedforward linearizers," In *Proc. 24th European Microwave Conference*, vol. 1, pp. 819-824, 1994.
- [1.15] Y. K. G. Hau, V. Postoyalko, and J. R. Richardson, "Design and characterization of a microwave feed-forward amplifier with improved wide-band distortion cancellation", *IEEE Transactions on Microwave Theory Tech.* vol. 49, no. 1, pp. 200-203, January 2001.
- [1.16] H. Seidel, "A feedforward experiment applied to an L-4 carrier system amplifier", *IEEE Transactions on Communication Technology*, vol. COM-19, no. 3, pp.320-325, June 1971.
- [1.17] S. P. Stapleton, "Adaptive feedforward linearization for RF power amplifiers", *55th ARFTG Conference Digest-Spring*, vol. 37, pp. 1-7, June 2000.
- [1.18] K. C. Lee, and P. Gardner, "Adaptive neuro-fuzzy inference system (ANFIS) digital predistorter for RF power amplifier linearization", *IEEE Trans. Veh. Technol.*, vol. 55, no. 1, pp. 43–51, January 2006.

-
- [1.19] D. Bondar, and D. Budimir, "A digital predistorter for wireless transmitters", *International Journal of RF and Microwave Computer-Aided Engineering*, 2009.
- [1.20] T. J. Liu, S. Boumaiza, F. M. Ghannouchi, "Augmented Hammerstein predistorter for linearization of broad-band wireless transmitters", *IEEE Transactions on Microwave Theory and Techniques*, vol. 54, no. 4, pp. 1340–1349, April 2006.
- [1.21] S. Boumaiza, et al., "Adaptive digital/RF predistortion using a nonuniform LUT indexing function with built-in dependence on the amplifier nonlinearity", *IEEE Transactions on Microwave Theory and Techniques*, vol.52, no.12, pp. 2670-2677, December 2004.
- [1.22] P. L. Gilabert, et al., "Multi-lookup table FPGA implementation of an adaptive digital predistorter for linearizing RF power amplifiers with memory effects", *IEEE Transactions on Microwave Theory and Techniques*, vol.56, no.2, pp.372-384, February 2008.
- [1.23] K.J. Muhonen, M. Kavehrad, R. Krishnamoorthy, "Look-up table techniques for adaptive digital predistortion: a development and comparison", *IEEE Transactions on Vehicular Technology*, vol.49, no.5, pp.1995-2002, September 2000.
- [1.24] J. K. Cavers, "The effect of quadrature modulator and demodulator errors on adaptive digital predistorters for amplifier linearization", *IEEE Trans. Veh. Technol.*, vol. 46, pp. 456-466, May 1997.
- [1.25] M. Ghaderi, S. Kumar, D.E. Dodds, "Adaptive predistortion lineariser using polynomial functions", *IEE Proceedings on Communications*, vol.141, no.2, pp.49-55, April 1994.
- [1.26] L. Ding, et al., "A robust digital baseband predistorter constructed using memory polynomials", *IEEE Transactions on Communications*, vol.52, no.1, pp. 159-165, January 2004.
- [1.27] S. Hong, et al., "Weighted polynomial digital predistortion for low memory effect doherty power amplifier", *IEEE Transactions on Microwave Theory and Techniques*, vol.55, no.5, pp.925-931, May 2007.
- [1.28] N. Mizusawa, and S. Kusunoki, "Third and fifth order base-band component injection for linearization of the power amplifier in a cellular phone", In *2005 IEEE MTT-S International Microwave Symposium Digest*, pp. 1565-1568, June 2005.

-
- [1.29] D. Culibrk, O. Marques, D. Socek, H. Kalva, and B. Furht, “Neural network approach to background modeling for video object segmentation”, *IEEE Trans. Neural Netw.*, vol. 2, no. 5/6, pp. 673–689, June 2005.
- [1.30] T. Takagi and M. Sugeno, “Fuzzy identification of systems and its Applications to modeling and control”, *IEEE Trans. Syst., Man, Cybern.*, vol. 15, no. 1, pp. 116–132, 1985.
- [1.31] N. Bawane, A. G. Kothari, and D. P. Kothari, “ANFIS based HVDC control and fault identification of HVDC converter”, *HAIT J. Sci. Eng. B*, vol. 18, no. 6, pp. 1614–1627, November 2007.
- [1.32] J. S. R. Jang, “ANFIS: Adaptive-network-based fuzzy inference system”, *IEEE Trans. Syst., Man, Cybern.*, vol. 23, no. 3, pp. 665–685, June 1993.
- [1.33] V. P. G. Jimenez, Y. Jabrane, A. G. Armada, B. A. Es Said, and A. A. Ouahman, “High Power Amplifier Pre-Distorter Based on Neural-Fuzzy Systems for OFDM Signals”, *IEEE Transactions on Broadcasting*, vol. 57, no. 1, March 2011.
- [1.34] H. M. Deng, S. B. He, and J. B. Yu, ”An adaptive predistorter using modified neural networks combined with a fuzzy controller for nonlinear power amplifiers“, *International Journal of RF and Microwave Computer-Aided Engineering*, vol. 14, no. 1, pp. 15-20, January 2004.
- [1.35] K. C. Lee and P. Gardner, ”Neuro-fuzzy approach to adaptive digital predistortion“, *Electronics Letters*, vol. 40, no. 3, February 2004.
- [1.36] Y. Li, and P. Yang, “Data predistortion with adaptive fuzzy systems”, *In Proc. IEE Int. Conf. Syst., Man, Cybern.*, vol. 6, pp. 168–172, 1999.
- [1.37] K. C. Lee, and P. Gardner, “A novel digital predistorter technique using an adaptive neuro-fuzzy”, *IEEE Commun. Lett.*, vol. 7, no. 2, pp. 55–57, February 2003.

2. NONLINEAR ANALYSIS OF POWER AMPLIFIERS

2.1. Introduction

Nowadays mobile communications have become one of the most consumed connection category. The main block of transceiver in emerging wireless radio systems is power amplifier (PA), which provides high gain to the input signal, and supports it to be transmitted over a radio channel. A power amplifier which has large linear region makes a whole transmitter very power inefficient, and that comes as a big problem if the transmitter is engaged in a mobile device, because a battery is intended to be used for as much time as possible. To overcome this problem, nonlinear PAs working in range close to saturation point are used. In that range, a power amplifier produces in-band and out-of-band distortions which makes signal impossible to detect correctly at a receiver. Thus a linearization of the power amplifier is required, which means expansion of the linear region of the PA up to a higher input power level. In this way we can maintain the power efficiency of the whole transmitter without generation of distortion components.

Ideally, a PA would have linear gain over the whole working range. The output signal in that case would be as described in (2.1):

$$V_{out}(t) = G \cdot V_{in}(t), \quad (2.1)$$

where G denotes voltage gain of the power amplifier, and $V_{in}(t)$ and $V_{out}(t)$ are the voltages at the input and output of the PA, respectively. On the other hand, a real PA has nonlinear region, e.g. a saturation operating range, where the output signal does not follow the input one with ideal gain. Examples of ideal and real transfer characteristics of a power amplifier are shown in the Figure 2-1.

In this Chapter, fundamentals of power amplifiers will be presented, as well as nonlinear analysis of PAs and overview of approaches in modelling and linearization techniques.

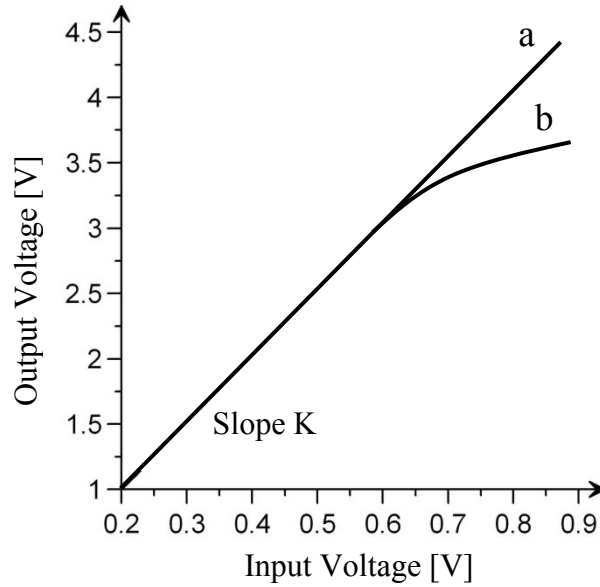


Figure 2-1: Examples of transfer characteristics of a PA: (a) ideal; (b) real

2.2. Power Amplifier Fundamentals

2.2.1 Gain

One of the most important characteristics of a power amplifier is gain. There are three main types of gain: transducer gain, power gain and available gain [2.1]. The delivered power at the end of the overall amplification system differs from the available power because of the imperfections of the matching circuits. Commonly, the transducer gain is used for the characterisation of an amplifier, as it is easy to measure. It is denoted just as “gain”, and represents the ratio of the output power to the input power, expressed in dB:

$$G[dB] = 10 \log_{10} \left(\frac{P_{out}[W]}{P_{in}[W]} \right) = P_{out}[dBm] - P_{in}[dBm] \quad (2.2)$$

An input power and output power are usually expressed in dBm, and gain is expressed in dB, as a power difference. The Figure 2-2 shows the gain characteristic for the power amplifier Mini-Circuits ZFL-500.

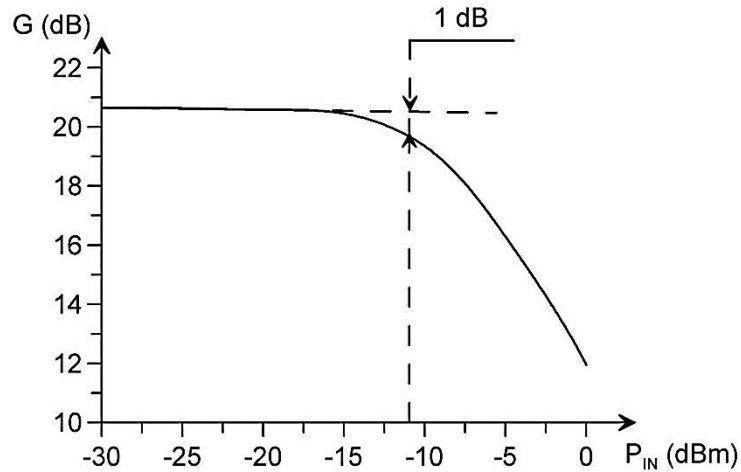


Figure 2-2: The measured gain characteristic of the PA Mini-Circuits ZFL-500

2.2.2 1dB Compression Point

The output power level at which gain of a real amplifier decreases for 1dB with respect to gain in linear region is called 1dB compression point:

$$G_{1dB} = G_{lin} - 1dB \quad (2.2)$$

In (2.2) G_{1dB} denotes the power amplifier gain at a 1dB compression point, and G_{lin} is the PA gain in the linear region, e.g. in the ideal case. The Figure 2-2 indicates the gain at 1dB compression point for the commercially available power amplifier Mini-Circuits ZFL-500. Representation for the output power at 1dB compression point is P_{1dB} . For the PA mentioned above the output power characteristic is presented in the Figure 2-3, with 1dB compression point at 9dBm output power level.

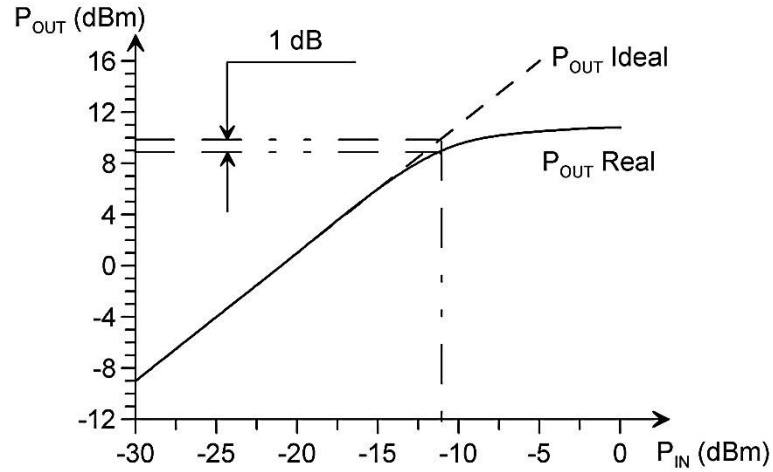


Figure 2-3: The measured output power characteristic of the PA Mini-Circuits ZFL-500, with 1dB compression point at 9dBm output power level

2.2.3 Second- and Third-Order Intercept Points

Nonlinear characteristic of the real power amplifier shown in the Figure 2-1 can be represented by third-order polynomial function [2.2]:

$$V_{out}(t) = K_1 V_{in}(t) + K_2 V_{in}^2(t) + K_3 V_{in}^3(t), \quad (2.2)$$

where $K_1, K_2, K_3 \in \mathbb{R}$ represent the coefficients of nonlinear function.

Assume the input as a single frequency stimulus:

$$V_{in}(t) = V_m \cos(\omega t), \quad (2.3)$$

with amplitude V_m and frequency ω . After substituting (2.3) into (2.2) and completing trigonometric transformations:

$$\begin{aligned} \cos^2(x) &= \frac{1}{2} - \frac{1}{2} \cos(2x), \\ \cos^3(x) &= \frac{1}{4} \cos(3x) + \frac{3}{4} \cos(x), \end{aligned}$$

the following expression is obtained:

$$V_{out}(t) = \frac{K_2}{2}A^2 + \left(K_1A + \frac{3}{4}K_3A^3\right)\cos(\omega t) + \frac{K_2}{2}A^2\cos(2\omega t) + \frac{K_3}{4}A^3\cos(3\omega t) \quad (2.4)$$

Although the excitation signal is at a single frequency, ω , two new frequencies, 2ω and 3ω , are generated, as the result of a nonlinear characteristic of an amplifier. These frequencies are called the harmonic frequencies. Usually the stimulus frequency is called the fundamental frequency. First term in (2.4), $\frac{K_2}{2}V_m^2$ is the DC component and the second-order component $\frac{K_2}{2}V_m^2\cos(2\omega t)$ in (2.4) appear as a product of the second-order term. The third-order products are $\frac{3}{4}K_3V_m^3\cos(\omega t)$ and $\frac{K_3}{4}V_m^3\cos(3\omega t)$. The components at the second harmonic and third harmonic are called second- and third-harmonic distortions, respectively. These increase faster than the component at the fundamental frequency. In other words, when the fundamental frequency product increase for 1dB, the second-order product will have 2dB growth and the third-order product will rise for 3dB. Power levels at which the harmonic distortion magnitudes and the linear characteristic magnitude become equal are called the second-order intercept point (SOI) and third-order intercept point (TOI), usually expressed in logarithmic values of dBm for the input or output power (Figure 2-4).

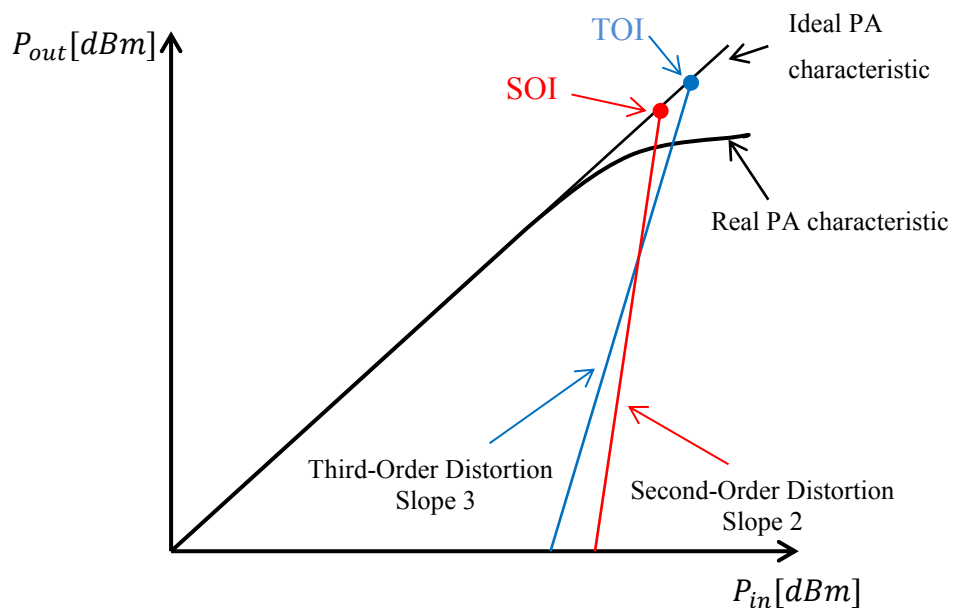


Figure 2-4: The second- and third-order intercept points

As the third harmonic component brings an in-band distortion, e.g. component at the fundamental frequency, the linear part of the fundamental characteristic must be extrapolated in order to find the TOI. Further, the in-band distortion is a result of odd-order terms of nonlinear function, and cannot be filtered out.

The SOI and TOI are a convenient way of describing the PA nonlinearity, as they have fixed values for each PA, and therefore can be used to predict the distortion behaviour in a particular operation mode.

2.2.4 Efficiency

Efficiency characterises how much of the DC power supply energy is converted into the RF signal. This characteristic should be as high as possible in order to make the PA consume less power. Efficiency is particularly important for battery-operated handset applications.

There are three main definitions of efficiency: DC-to-RF efficiency (or drain efficiency), power-added efficiency (PAE) and overall efficiency [2.3].

The power-added efficiency is the ratio of the difference between the RF output power and the RF input power to the DC input power:

$$PAE = \frac{P_{RF}^{out} - P_{RF}^{in}}{P_{DC}^{in}} \quad (2.5)$$

Efficiency of the power amplifier increases with the rise of the RF power level. The Figure 2-5 illustrates that, where one can see the dependences of the output power and the PAE on the input power presented for the PA Mini-Circuits ZFL-500. This amplifier has 20dB gain in the linear region.

The PAE is maximised when the PA operates near to the compression region. Consequently, non-linear distortions may appear at the output. Therefore, linearisation techniques are becoming very important with the aim to keep the output signal linearly amplified.

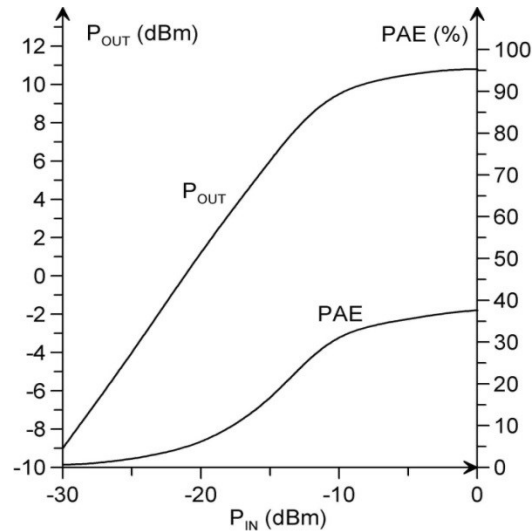


Figure 2-5: The measured output power and power-added efficiency curves for the Mini-Circuits ZFL-500

2.3. Nonlinear Analysis

A PA is required to amplify the signal which is excited to its input, and it is desirable to have constant gain over the whole dynamic range, or frequency spectrum. This is not possible for the input signals reaching the saturation range of the PA, where the gain compression exists. Besides the gain reduction, the input signal experiences phase variations near the compression region.

2.3.1 Two-Tone Test

Widely used method for the evaluation of the PA behaviour is the Two-tone test [2.4]. Using this technique the number of intermodulation products can be clearly seen, as described in text below. The output signal can be divided into DC zone, fundamental zone, second- and third-harmonic zones. The intermodulation distortion products will be defined further.

If the excitation signal to the PA has two frequencies, and the same amplitude:

$$V_{in}(t) = V_m(\cos(\omega_1 t) + \cos(\omega_2 t)), \quad (2.6)$$

after driving it to the power amplifier described with third-order polynomial function (2.2), and carrying out trigonometric transformations, the resulting output is derived:

$$\begin{aligned}
 V_{out}(t) = & K_2 V_m^2 + \left(K_1 A + \frac{9}{4} K_3 V_m^3 \right) (\cos(\omega_1 t) + \cos(\omega_2 t)) + \\
 & + \frac{1}{2} K_2 V_m^2 (\cos(2\omega_1 t) + \cos(2\omega_2 t)) + \\
 & + K_2 V_m^2 (\cos((\omega_1 - \omega_2)t) + \cos((\omega_1 + \omega_2)t)) + \\
 & + \frac{1}{4} K_3 V_m^3 (\cos(3\omega_1 t) + \cos(3\omega_2 t)) + \\
 & + \frac{3}{4} K_3 V_m^3 (\cos((2\omega_1 - \omega_2)t) + \cos((2\omega_1 + \omega_2)t)) + \\
 & + \frac{3}{4} K_3 V_m^3 (\cos((2\omega_2 - \omega_1)t) + \cos((2\omega_2 + \omega_1)t))
 \end{aligned} \tag{2.7}$$

In this case, there are more frequency components than just harmonic ones. These components are defined as the intermodulation products (IM). The Figure 2-6 illustrates the spectrum which assumes that the DC and harmonic components are not filtered out.

Observed products at frequencies $2\omega_1 - \omega_2$ and $2\omega_2 - \omega_1$ are of the most interest, because they are close to the fundamental frequencies and cannot be filtered out without problems. As the power level of these intermodulation products is proportional to the power of three of the input signal amplitude V_m , in comparison with the fundamental tone which is approximately linear to V_m , they make a challenge to a linear power amplifier design.

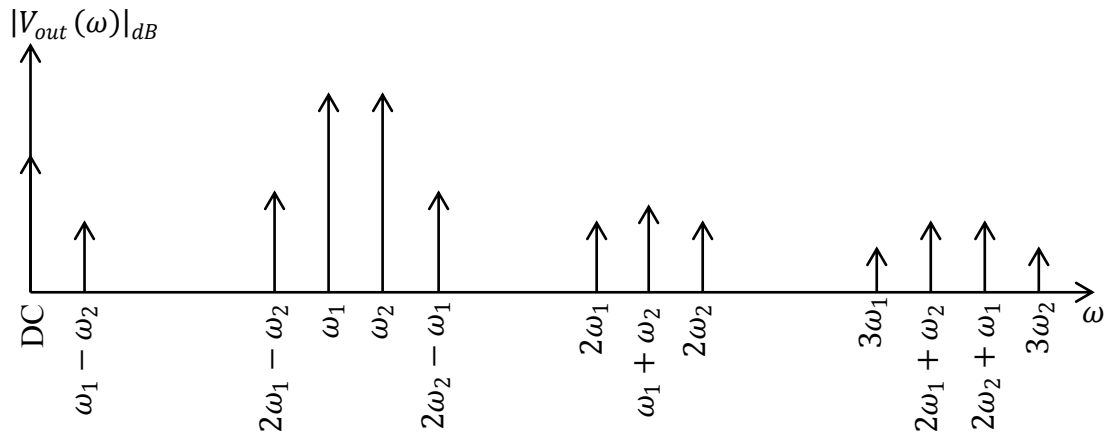


Figure 2-6: Output spectrum of a power amplifier under two-tone excitation

The distortion components produced by the nonlinear power amplifier can be divided into two groups: the in-band and out-of-band distortions. The out-of-band distortions are DC and harmonic products, and they can be easily filtered out. The in-band distortion components are the main problem, but can be filtered out using a RF feedback linearization, which will be presented later on in this Chapter. When the complex digitally modulated signals are used, sinusoidal analysis is not valid any more, and different measurement characteristics are used for measuring the PA distortion.

2.3.1.1 ADS Simulation of Two-Tone Test

An analogue simulation model for the commercially available Mini-Circuits ZHL-1042J power amplifier, with 1dB compression point at the output power level of 26dBm, created in Advanced Design System (ADS) is presented on the Figure 2-7. The analogue two-tone signal at frequencies $f_1 = 2.14$ GHz and $f_2 = 2.15$ GHz and amplitude 1 ($P_{in} = 0$ dBm) is driven as the input to the PA. Figure 2-8 (a) shows the fundamental zone of the output spectrum, with markers showing the distortion in power level. Intermodulation distortion components at frequencies $2f_1 - f_2$ and $2f_2 - f_1$ can be observed. It can be seen that these products have big influence on the signal at the output, and make the recovery of the output signal impossible (Figure 2-8 (b)). The output signal is plotted in dots, in order to make the input signal visible.

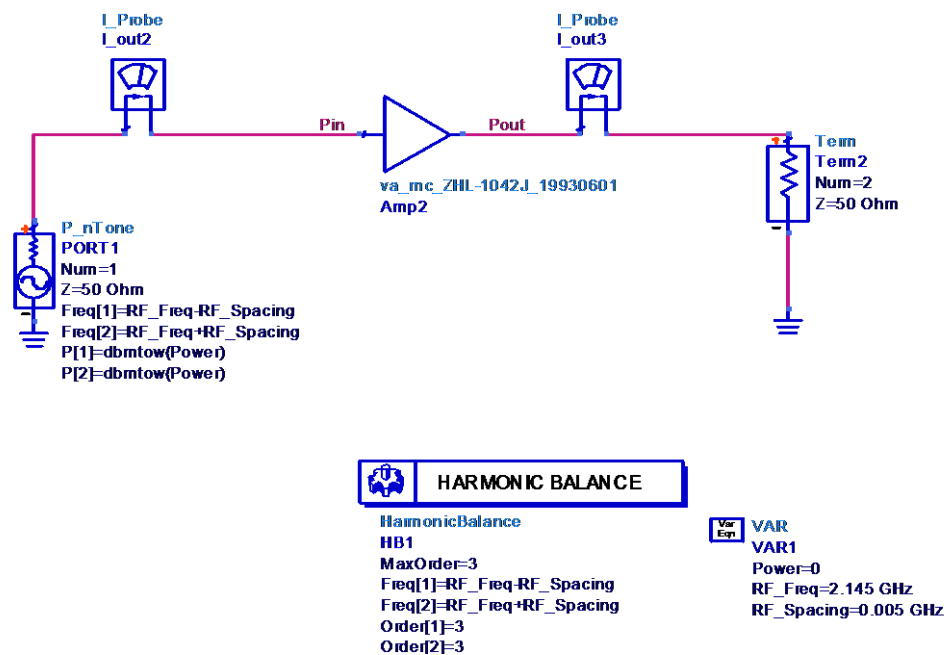


Figure 2-7: ADS simulation of the Two-tone test for the PA Mini-Circuits ZHL-1042J

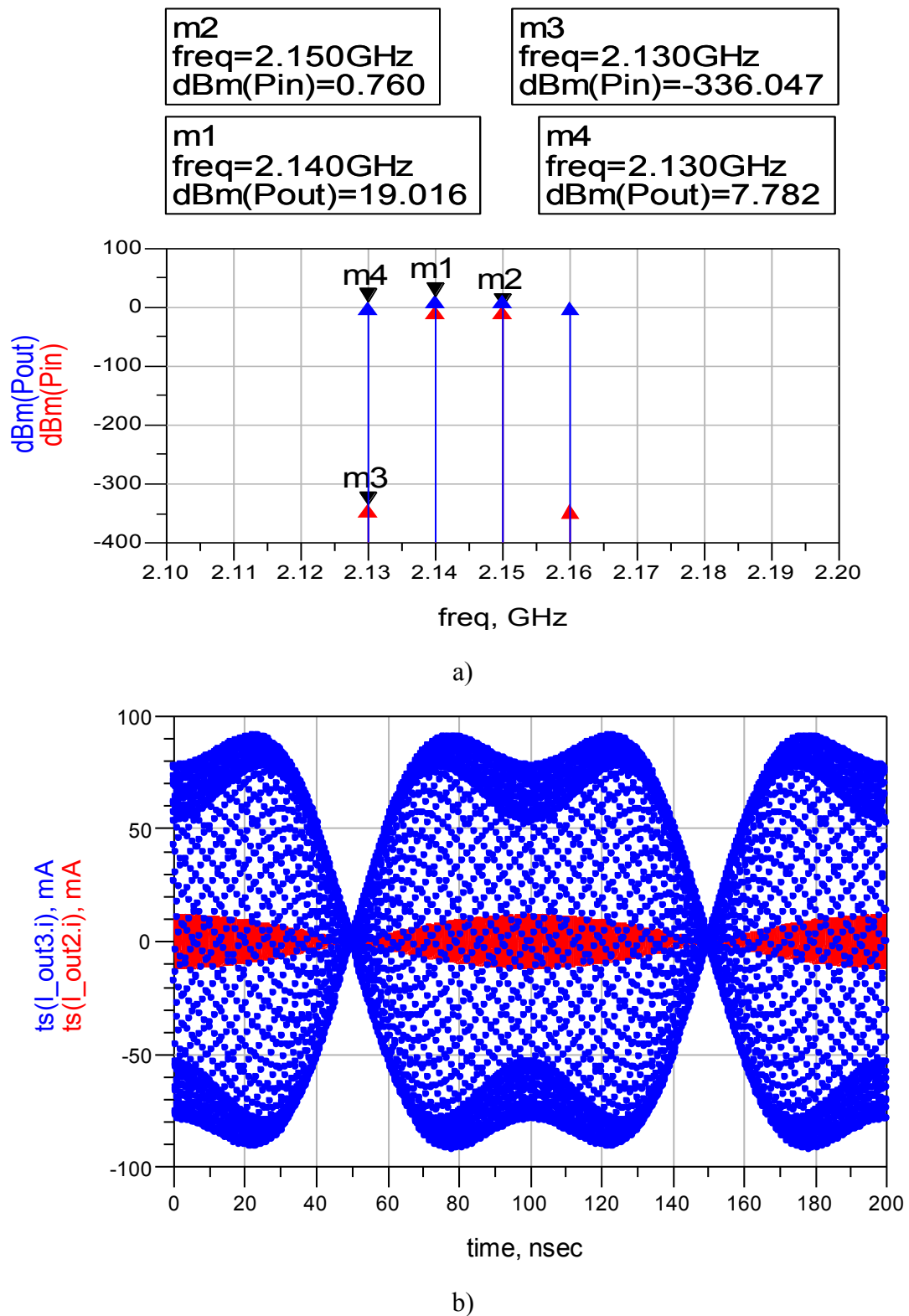
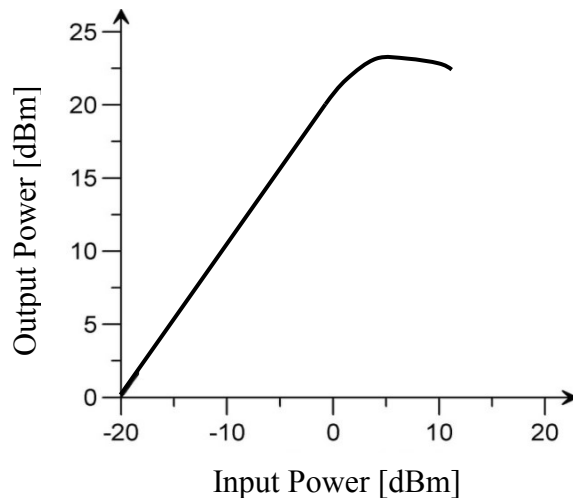


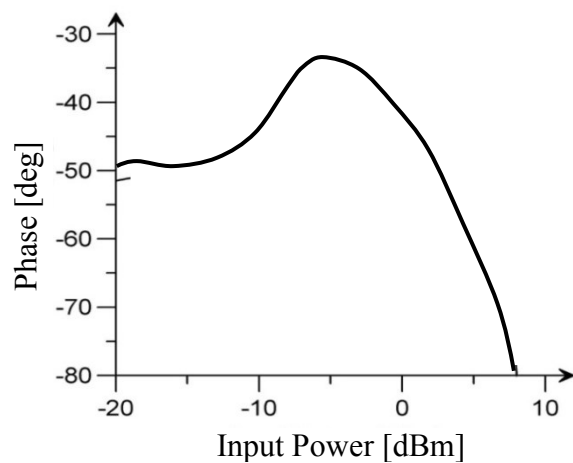
Figure 2-8: ADS simulation results of the Two-tone test for the PA ZHL-1042J at 0dBm input power level: a) Spectra of the input and output signals; b) Time domain waveforms of input and output signals

2.3.2 AM/AM and AM/PM Distortions

Amplitude-Amplitude (AM/AM) and Amplitude-Phase (AM/PM) distortions represent the dependence of the fundamental output signal phase and amplitude on the input signal amplitude [2.2]. Amplitude-amplitude distortion characteristic is also called the gain compression characteristic. The main cause of AM/AM distortion is nonlinearity of the transfer characteristic, while AM/PM distortion comes as a consequence of the memory effects [2.4]-[2.5]. The memory effects are produced by reactive elements in the PA, and result in the signal delays. This thesis deals with nonlinear PAs with the memory effects, so the phase shift will be also a problem to be solved. Illustration of AM/AM and AM/PM distortion for a MOSFET PA is given in the Figure 2-9.



a)



b)

Figure 2-9: An example of characteristics for a PA: a) AM/AM; b) AM/PM

2.3.3 Error Vector Magnitude

As mentioned before, when the signal is digitally modulated, there are different performance parameters that show the amplifier nonlinearity. One of them is error vector magnitude (EVM). It is defined as the difference between magnitudes of the ideal reference signal and the measured output (transmitted) signal (Figure 2-10), after the compensation in time, amplitude, frequency, phase and DC offset [2.4]. It is represented in percents (2.8), but it can be also represented in dB (2.9).

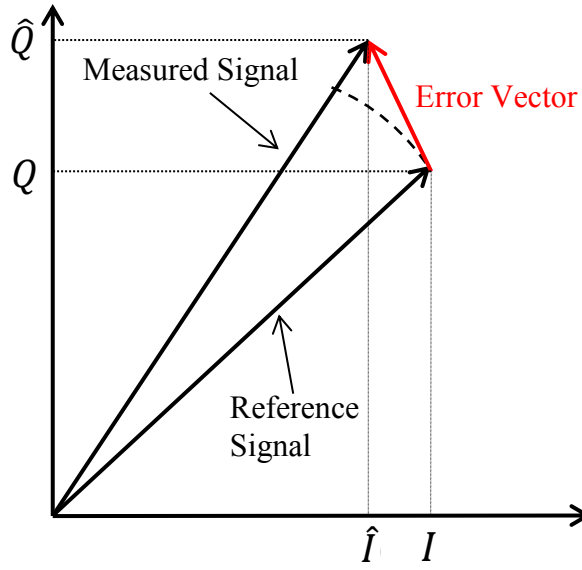


Figure 2-10: Error vector

$$EVM [\%] = \frac{\sum_{i=1}^n \sqrt{[I(i) - \hat{I}(i)]^2 + [Q(i) - \hat{Q}(i)]^2}}{\sum_{i=1}^n \sqrt{I(i)^2 + Q(i)^2}} \cdot 100\% \quad (2.8)$$

$$EVM [dB] = 10 \log_{10} \left(\frac{\sum_{i=1}^n \sqrt{[I(i) - \hat{I}(i)]^2 + [Q(i) - \hat{Q}(i)]^2}}{\sum_{i=1}^n \sqrt{I(i)^2 + Q(i)^2}} \right) \quad (2.9)$$

In (2.8)-(2.9) $I(i)$ and $\hat{I}(i)$ are reference and measured I components of the i -th symbol, respectively. Likewise, $Q(i)$ and $\hat{Q}(i)$ are reference and measured Q components of the i -th symbol. Because it changes continuously during the every

symbol transition, EVM is defined as the root-mean-square value of the error vector over time.

2.3.4 Adjacent Channel Power Ratio

Another distortion effect is the power leakage in adjacent channels. The power ratio between the adjacent channels and the main channel is called the adjacent channel power ratio (ACPR), and it is defined in (2.10):

$$ACPR = \frac{\int_{\omega_L}^{\omega_1} S(\omega)d\omega + \int_{\omega_2}^{\omega_U} S(\omega)d\omega}{\int_{\omega_1}^{\omega_2} S(\omega)d\omega} \quad (2.10)$$

In (2.10) $S(\omega)$ is the power density function of the output signal, ω_1 and ω_2 are the frequency bounds of occupied bandwidth of the fundamental signal and ω_L and ω_U are the lower and upper frequency limits for the lower and upper adjacent channels, in that order. In a logarithmic representation ACPR can be presented as:

$$ACPR [dB] = P_{adj}[dBm] - P_{fund}[dBm], \quad (2.11)$$

where P_{fund} denotes overall power integrated in the main channel, expressed in dBm, while P_{adj} is:

$$P_{adj}[dBm] = 10 \log_{10}(P_{adjL} + P_{adjU}), \quad (2.12)$$

where P_{adjL} and P_{adjU} are powers integrated in adjacent channels. There are two different approaches to measuring ACPR. Using the first approach, ACPR is calculated as the ratio between the power in adjacent channels and overall output power. The second one considers ACPR as the ratio between sum of powers integrated in adjacent channels and the power in the main channel (Figure 2-11). As can be seen from the figure, adjacent channels are of the same bandwidth as the main channel. The second method for estimation of the ACPR parameter is used most frequently, because it's easier practical implementation.

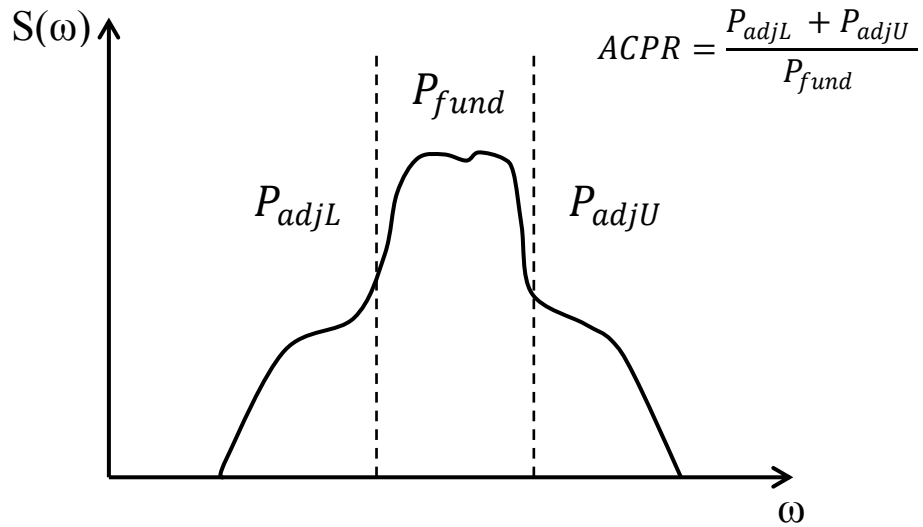


Figure 2-11: A graphical representation of ACPR

2.3.5 Peak to Average Power Ratio

Peak to average power ratio (PAPR) is defined as the ratio between the maximum instantaneous power in time and the average power of the output signal:

$$PAPR [dB] = 10 \log_{10} \frac{\max_{0 \leq n < N-1} |x(n)|^2}{P_{avg}} \quad (2.13)$$

Single-carrier systems are not exposed to the impairments in the frontend, as the OFDM transceivers. The high PAPR problem associated with multicarrier signals is one of the principal impairments in the implementation of OFDM systems. The linear operation of the PA over a large dynamic range increases the implementation cost and reduces the power efficiency.

2.4. Overview of modelling and linearization techniques

2.4.1 Behavioural Modelling Techniques

Modelling power amplifiers can be accomplished in two ways: using the physical knowledge of the PA internal composition or by blackbox modelling from the empirical input-output observations [2.6]-[2.7]. The first approach relates to the physical models, whereas the second one implies the behavioural models. Theoretical modelling utilizes abstraction, decomposition and aggregation of the sub-models describing the process partly to compose a structured process model, which also provides information about the internal state of the process [2.8]. These models are more accurate, but they require precise knowledge of the PA internal structure and its specific parameters. This complicates the modelling process and in some cases makes it almost impossible to complete. For these reasons, when a complete system-level evaluation is required, the behavioural models are usually preferred. They are concerned with the generation of mathematical system models from the data. Naturally, the system must already exist and it must be regarded that the identified process model is only valid within the analysed range and does not necessarily comprise physically relevant parameters. Therefore, this approach treats a PA as a black-box and determines its model from appropriately selected set of the input-output observations [2.6].

Used experiment must be planned carefully to acquire suitable data, an appropriate model structure must be found and a suitable parameter estimation method must be applied. Besides, the identified process model must be validated against the real process behaviour. The parameter estimation is often achieved by finding the estimates that minimize a specific loss function. Different loss functions lead to different methods of identification.

Appropriate model structure must be designed with awareness of possible over- or under- parameterization. An over-parameterised structure can lead to unnecessary complicated computations for finding the parameter estimates and for using the estimated model. An under-parameterised model may be very inaccurate. As the number of model parameters directly determines the complexity of the calculation, simple models that compromise between model accuracy and simplicity are often

preferred. As described in the previous subsection, analysis of the power amplifiers is adjustable for simple cases. When frequency of the signals grows, e.g. when the envelope variations become more rapid and random, the distortion increases, and the analysis is not easy to be carried out with the paper and pencil. In that case, simulations are likely to be used in order to determine all distortion parameters of a PA. Even in simulations, a compromise is preferable, because of the long simulations runtime. For a power amplifier, the number of parameters, e.g. model order, can be estimated by the number of harmonics appearing at the PA maximum operational power level output. [2.9]

Amplifiers can be divided in two groups: the ones with memory and PAs without memory, e.g. memoryless power amplifiers.

2.4.1.1 Memoryless Modelling Techniques

Memoryless power amplifier nonlinearity can be presented as a function of instantaneous input signal sample (2.14). This type of nonlinear behavioural model can be used for PAs with small memory effects, or even for PAs with memory, where the dominant distortion arises from the memoryless part of the amplifier. Memoryless modelling is widely used because of the low cost computations and acceptable efficiency in system simulations [2.10]-[2.11].

$$V_{out}(t) = G(V_{in}(t)), \quad (2.14)$$

where $G(\cdot)$ is memoryless nonlinear function, which means that the output is derived just from the current input signal sample.

Saleh model

The Saleh model represents (2.14) over two functions, from which one function represents the static AM/AM characteristic and the other function is the AM/PM characteristic [2.12]-[2.13]:

$$V_{out}(t) = G_{AM/AM}(V_m(t))e^{j(\arg\{V_{in}(t)\}+G_{AM/PM}(V_m(t)))}, \quad (2.15)$$

where $G_{AM/AM}(\cdot)$ and $G_{AM/PM}(\cdot)$ are AM/AM and AM/PM functions, respectively, depending on the input signal amplitude $V_m(t)$. If the excitation signal is single stimulus at the frequency ω_0 , with the amplitude $V_m(t)$ and the phase $\varphi(t)$:

$$V_{in}(t) = V_m(t) \cos(\omega_0 t + \varphi(t)), \quad (2.16)$$

(2.15) becomes:

$$V_{in}(t) = G_{AM/AM}(V_m(t)) \cos[\omega_0 t + \varphi(t) + G_{AM/PM}(V_m(t))], \quad (2.17)$$

where $G_{AM/AM}(V_m(t))$ and $G_{AM/PM}(V_m(t))$ are parametric frequency-independent function described by (2.18)-(2.19). Only four parameters of these two functions, which make the model simple, are the reasons why the Saleh model is poor in terms of modelling dynamics of the nonlinear power amplifiers.

$$G_{AM/AM}(V_m) = \frac{\alpha_{AM} V_m}{1 + \beta_{AM} V_m^2} \quad (2.18)$$

$$G_{AM/PM}(V_m) = \frac{\alpha_{PM} V_m}{1 + \beta_{PM} V_m^2} \quad (2.19)$$

Simplicity of this model make it widely used for modelling and linearization techniques [2.14].

Memoryless polynomial model

Memoryless polynomial model is a nonlinear behaviour representation by the power series [2.1], [2.15]-[2.16]. Nonlinear transfer characteristic can be approximated by a polynomial expression [2.16]:

$$V_{out}(t) = \sum_{n=1}^{\infty} g_n V_{in}^n(t) \quad (2.20)$$

Coefficients g_n correspond to the power terms $V_{in}^n(t)$. Detailed explanation of this behavioural modelling method will be given in Chapter 4.

2.4.1.2 Memory Modelling Techniques

General discrete-time form of an arbitrary power amplifier with memory is given in (2.21). $V_{in}(n)$ and $V_{out}(n)$ are the input and output uniform time samples with sampling time T_s . Unlike systems without memory effects, here the output of the system depends on the current and previous time samples of the input signal [2.6].

$$V_{out}(n) = G(V_{in}(n), V_{in}(n-1), V_{in}(n-2), \dots, V_{in}(n-Q)) \quad (2.21)$$

In above equation $G(\cdot)$ is the function depending on the input signal at the sample time n , and Q previous input signal samples, and its result is the output at the time sample n .

Modelling of this type of nonlinearity is most comprehensively carried out using the Volterra series [2.17].

Volterra series

The Volterra series are generic models that are used for modelling of a PA with memory. It is a sum of responses of a number of *Volterra kernels* [2.17]-[2.18].

$$V_{out}(t) = \sum_{n=1}^{\infty} H_n(V_{in}(t)), \quad (2.22)$$

where $H_n(V_{in}(t))$ is the n -th Volterra operator depending on the input function $V_{in}(t)$, stated as:

$$H_n(V_{in}(t)) = \int_{-\infty}^{\infty} \dots \int_{-\infty}^{\infty} h_n(\tau_1, \tau_2, \dots, \tau_n) V_{in}(t - \tau_1) V_{in}(t - \tau_2) \dots V_{in}(t - \tau_n) d\tau_1 d\tau_2 \dots d\tau_n \quad (2.23)$$

The Figure 2-12 shows generalized block diagram of the Volterra series, corresponding to (2.22).

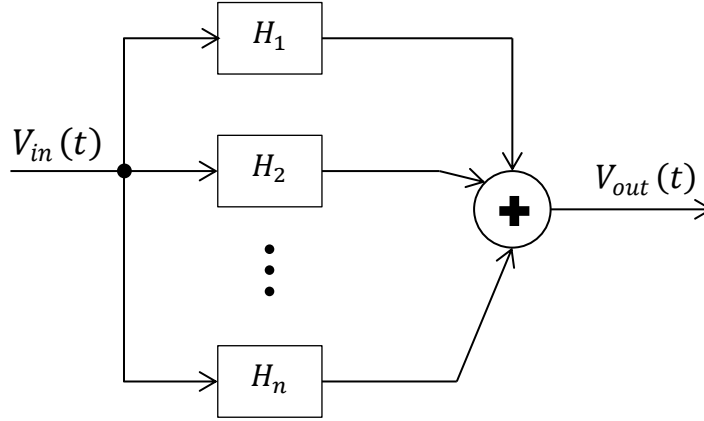


Figure 2-12: The Volterra series representation of a system

Wiener model

The Wiener model is a special case of the Volterra series model, where the nonlinearity and memory of the system are presented by two independent blocks [2.19]-[2.20]. This model is a linear time-invariant (LTE) system, representing memory effects, followed by a memoryless nonlinearity (Figure 2-13). Subsystems in discrete-time form are expressed as:

$$H(n) = \sum_{m=0}^{L-1} h_m V_{in}(n - m), \quad (2.24)$$

$$V_{out}(n) = \sum_{k=1}^K a_k H^k(n), \quad (2.25)$$

where L is the memory depth, and K is the order of memoryless nonlinearity.

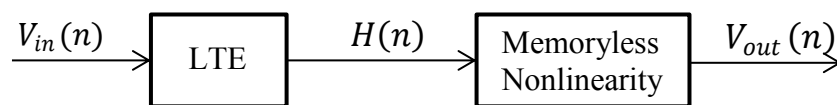


Figure 2-13: The Wiener model

Hammerstein model

The Hammerstein model is memoryless nonlinearity followed by the LTE system presented in the Figure 2-14 [2.21]-[2.22]. Systems are described by:

$$H(n) = \sum_{k=1}^K a_k V_{in}^k(n) \quad (2.26)$$

$$V_{out}(n) = \sum_{m=0}^{L-1} h_m H(n-m) \quad (2.27)$$

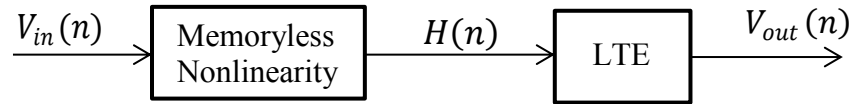


Figure 2-14: The Hammerstein model

Wiener-Hammerstein model

The Wiener-Hammerstein model is three-box model that has two memory LTE blocks, and one memoryless nonlinear block illustrated in the figure below [2.23]-[2.24].

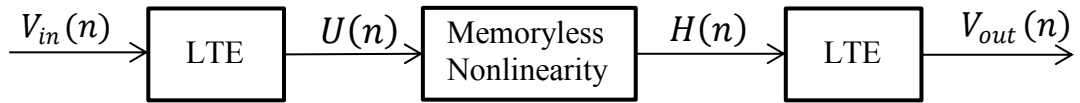


Figure 2-15: The Wiener-Hammerstein model

Subsystems in this model are described by:

$$U(n) = \sum_{m=0}^{L_1-1} h_m V_{in}(n-m) \quad (2.28)$$

$$H(n) = \sum_{k=1}^K a_k V_{in}^k(n) \quad (2.29)$$

$$V_{out}(n) = \sum_{m=0}^{L_2-1} h_m H(n-m) \quad (2.30)$$

The Wiener-Hammerstein is generally used when a power amplifier is driven near saturation to exploit the maximum power efficiency for the downlink [2.25].

The models described above are polynomial based models, which are easy to derive, but the performance of these models could be limited by the order of polynomial function to some extent. Another disadvantage of polynomial models is the use of the demanding fast Fourier transforms when involving polynomial models in the predistortion of power amplifiers [2.53]. A few alternatives to polynomial based models are developed in recent years, based on artificial neural networks and fuzzy logic systems. Artificial intelligence systems have capability to approximate any dynamic nonlinear function, and have been successfully exploited in modelling of power amplifiers behaviour and for the construction of the corresponding predistortion [2.26]-[2.27]. Next chapter will explain the structures of artificial intelligence systems.

2.4.1 Overview of Linearization Techniques

A highly linear and efficient transmitter can be achieved by increasing the power amplifier efficiency at the cost of linearity and providing the external linearization afterwards in order to fulfil the linearity requirements [2.4]. Consequently, the linearization of power amplifiers is an important task aimed to satisfy the exact requirements put on modern wireless transmitters.

Many linearization techniques have been developed recently and they can be classified into three major categories: feedback, feedforward and predistortion techniques.

2.4.1.1 Feedback Linearization

Feedback linearization is based on adjustment of the future input samples using the current output driven through the feedback loop. General block diagram of a feedback is given in the Figure 2-16. By comparing the output signal to the desired output, an error signal is substituted from the next input sample. Several linearization techniques can be found in the literature dealing with a feedback [2.28]-[2.40]. They can be classified as active RF feedback, passive RF feedback, modulation or envelope feedback, including polar and Cartesian loops. The RF feedback involves comparison between RF components of a signal, whereas the modulation feedback implies comparison of the baseband modulation components of the signal. Feedback branch is mandatory in a linearization process if the power amplifier engaged in the system changes its behaviour through time. This can be caused by changes in the temperature, supply voltage variations, or just due to the aging of the PA [2.54]. Adaptation to system changes is not possible without feedback information. Stability of an overall system in this case can be a problem and can limit the performance of the linearization process.

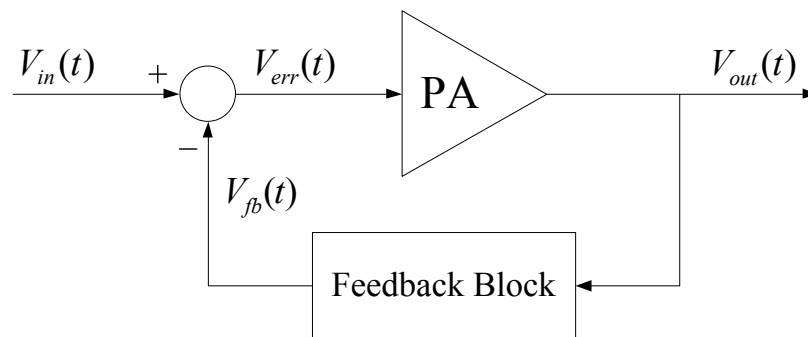


Figure 2-16: General feedback linearization system

Compensation of intermodulation components of two tone signal using RF feedback loop

Feedback circuit for analogue two-tone signal at frequencies $f_1 = 2.14$ GHz and $f_2 = 2.15$ GHz is simulated using ADS simulation block shown on Figure 2-17. Power amplifier used for simulations is Mini-Circuits ZHL-1042J. If we have signal $V_{IN}(t) = \sin(\omega_1 t) + \sin(\omega_2 t)$, e.g. two-tone signal, the intermodulation distortion components

formed passing this signal through the PA are at two frequencies $2f_1 - f_2$ and $2f_2 - f_1$, and they can be filtered with bandpass raised cosine filters through feedback branch and multiplied by a for amplitude tuning and rotated θ for phase tuning. Adding these two components to the original signal, unwanted tones will be suppressed (Figure 2-18). Simulation results show that is possible to annulate nonlinear effects of this PA using RF feedback linearization method. This method is useful if we have two-tone excitation, but when the digitally modulated signals are observed, it is hard to implement RF linearization.

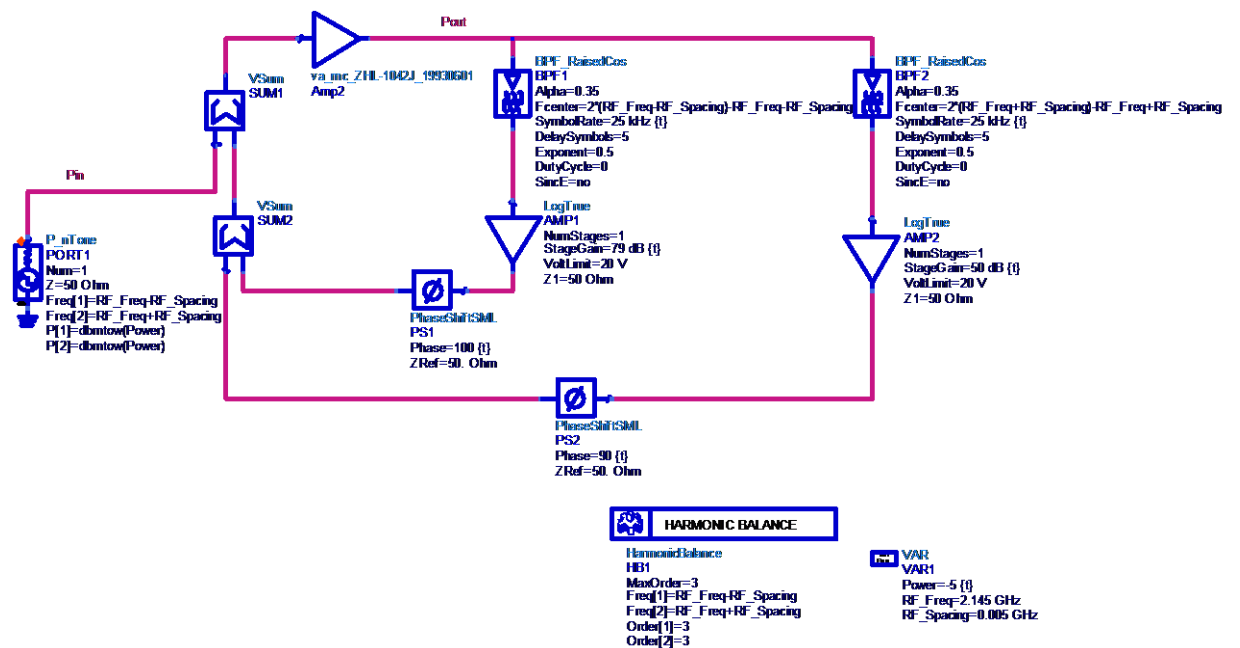
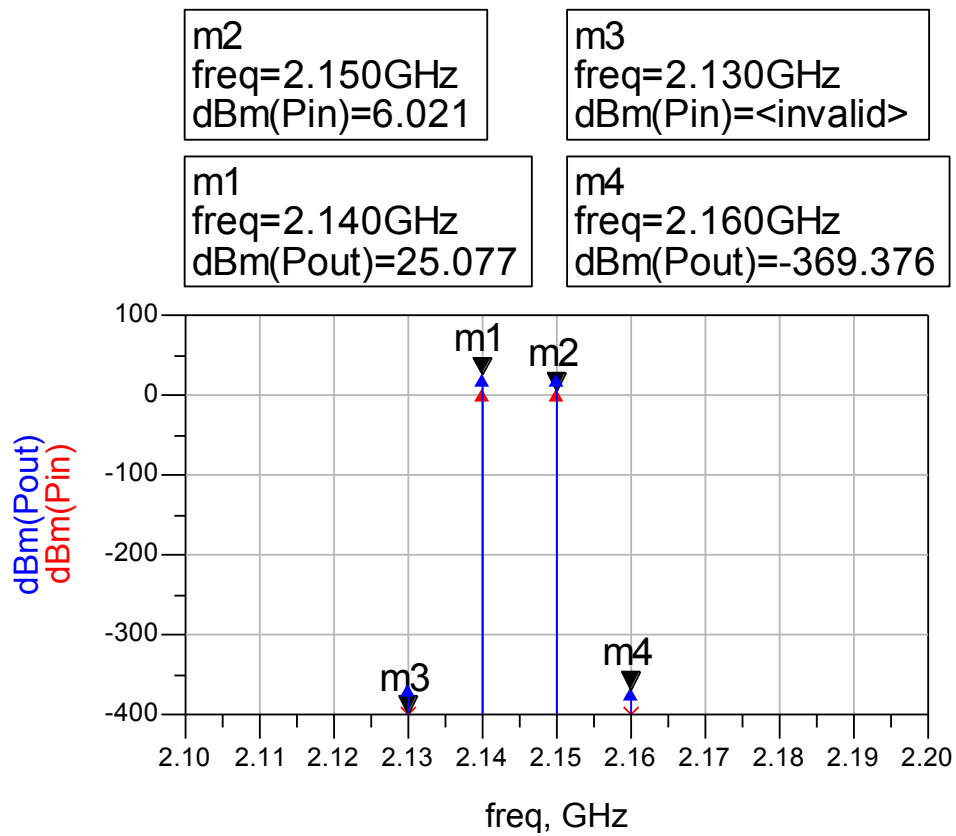
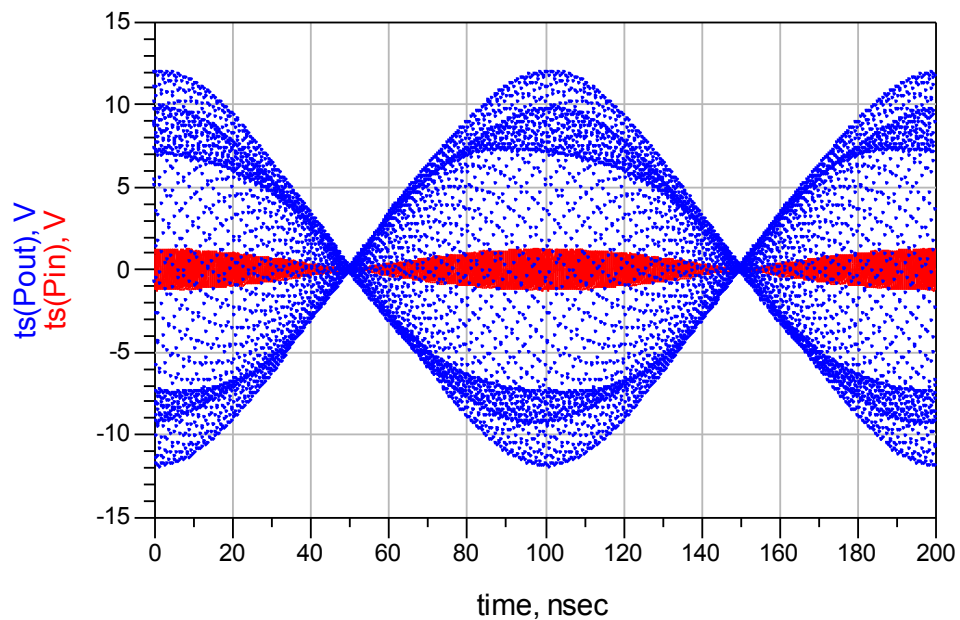


Figure 2-17: ADS model for an analogue two-tone signal with feedback

Simulations are carried out for input two-tone signal at 0dBm input power level and passed through simulation models with feedback (Figure 2-17) and without feedback (Figure 2-7). Tuning of a and θ coefficients is done to make as better suppression of unwanted signals as possible. Improvement of linear performance of power amplifier ZHL-1042J is more than 300dB for analog signal. Parameters a and θ are manually adjusted for individually input, according to input signal power. The difference between these parameters argument the linearization method described above.



a)



b)

Figure 2-18: ADS simulation results of feedback RF linearization for the Two-tone signal for the PA ZHL-1042J at 0dBm input power level: a) Spectra of the input and output signals; b) Time domain waveforms of input and output signals

2.4.1.2 Feedforward Linearization

The principle block diagram of feedforward linearizer is presented in Figure 2-19.

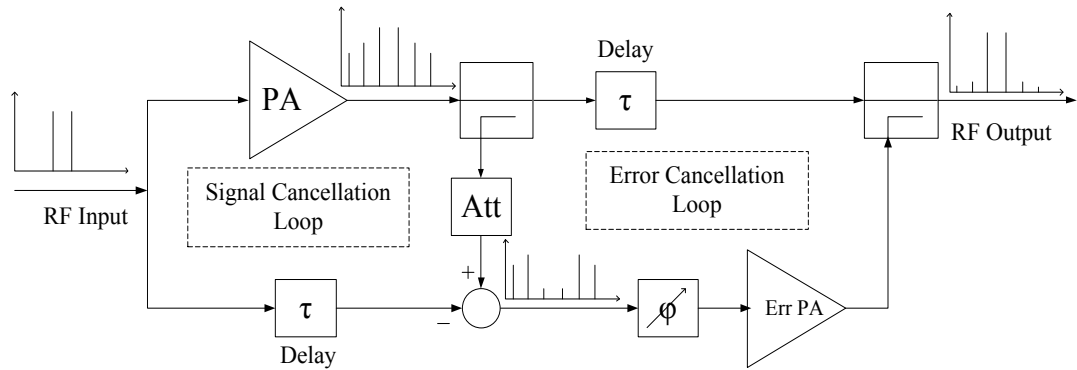


Figure 2-19: General layout of a feedforward system

Feedforward technique is used to linearize PAs for many years [2.29], [2.33], [2.41]-[2.44]. The distortion components are obtained and delivered to the output through the feedforward chain. PA distortion at the output is compensated by subtracting the distortion components from the overall output signal. The first loop is used to remove the fundamental signal from the PA output and obtain the IMD products. The second loop is necessary to subtract the adjusted distortion products from the overall output in order to obtain the linear amplified signal.

2.4.1.3 Digital Predistortion Techniques

Digital predistortion (DPD) techniques are based on introducing nonlinear distortion which is complementary to PA distortion in baseband part of system, to make cascade that will be linear in overall input-output characteristic (Figure 2-20) [2.16],[2.22], [2.45]-[2.52]. Some of the advantages of baseband processing are reliability, immunity to aging and temperature drift, compact implementation, ability to handle complex algorithms, and reconfigurability. Among digital predistortion techniques are adaptive techniques also, where the parameters of DPD are adjusted during the training procedure (Figure 2-21).

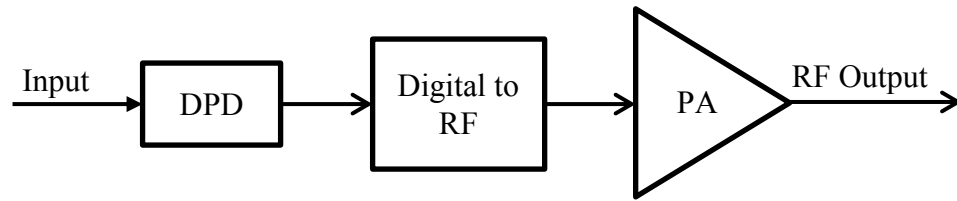


Figure 2-20: General layout of a digital predistortion system

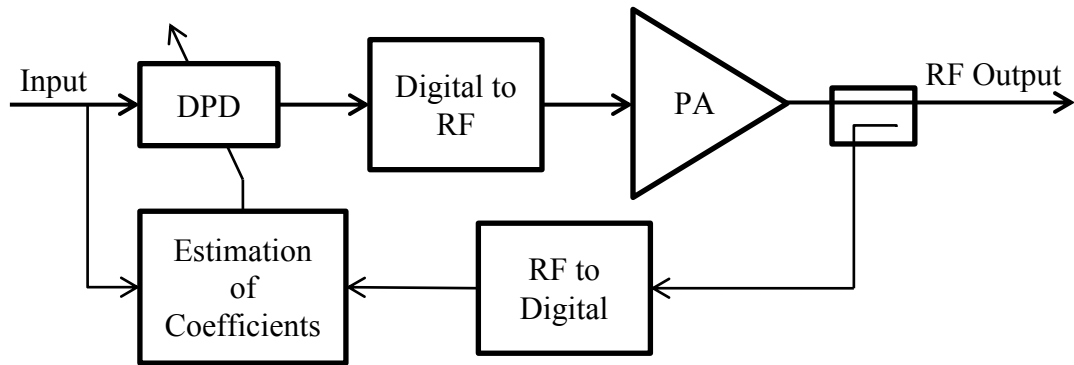


Figure 2-21: Layout of an adaptive digital predistortion system

Adaptive digital predistortions will be presented in Chapters 5 and 6, based on artificial intelligence models.

2.5. Conclusion

This chapter presents the nonlinear analysis of power amplifiers and briefly explains possible predistortion structures. Nonlinear parameters of power amplifiers have been defined. Performance parameters used for examination of nonlinear effects of power amplifiers were introduced. An overview of modelling and linearization techniques was presented. Simulation analysis of nonlinear Mini-Circuits ZHL-1042J power amplifier using Advanced Design System software was presented. The analysis was carried out using two-tone test. A RF feedback compensation of distortion components in two-tone signal is validated through ADS simulations.

2.6. References

- [2.1] S. Maas, *Nonlinear Microwave and RF Circuits*, Artech House Publishers, 2003.
- [2.2] P. B. Kenington, *High Linearity RF Amplifier Design*, Artech House Inc., 2000.
- [2.3] F. H. Raab, et al., "Power amplifiers and transmitters for RF and microwave", *IEEE Transactions on Microwave Theory and Techniques*, vol. 50, no. 3, pp. 814–826, March 2002.
- [2.4] J. Vuolevi, T. Rahkonen, *Distortion in RF Power Amplifiers*, Artech House Inc., 2003.
- [2.5] G. Collins, and D. W. Runton, "Nonlinear analysis of power amplifiers", *Microwave Journal*, vol. 50, no. 9, p. 164, September 2007.
- [2.6] J. C. Pedro, and S. A. Maas, "A comparative overview of microwave and wireless power-amplifier behavioral modeling approaches", *IEEE Transactions on Microwave Theory and Techniques*, vol. 53, no. 4, pp. 1150-1163, April 2005.
- [2.7] J. C. Pedro, and N. B. Carvalho, *Intermodulation Distortion in Microwave and Wireless Circuits*, Artech House, Norwood, 2003.
- [2.8] Cellier, F. E, *Continuous system modeling*, Springer-Verlag, 1991.
- [2.9] D. Bondar, D. Budimir, and B. Shelkovnikov, "A new approach for nonlinear analysis of power amplifiers", in *Proc. 18th Int. Crimean Conf. Microw. and Telecommun. Technology*, Sebastopol, Ukraine, vol. 1, pp. 125-128, September 2008.
- [2.10] D. D. Silveira, M. E. Gardringer, P. L. Gilabert, G. Montoro, Y. Lei, E. R. Srinidhi, E.G. Lima, V. Camarchia, G. Magerl, E. Bertran, A. Goacher, M. O'Droma, G. Kompa, and M. Pirola, "A Performance Comparison of Six RF Power Amplifier Behavioural Models", *Target Meets Industry Int. Colloquium*, Frascati, Rome, November 2006.
- [2.11] M. O'Droma, Y. Lei, A. Meza, S. Camarchia, and M. Pirola, *RF Power Amplifier Behavioural Modelling*, Chapter 3, Cambridge University Press, Cambridge, United Kingdom, June 2009.
- [2.12] A. M. Saleh, "Frequency-Independent and Frequency-Dependent Nonlinear Models of TWT Amplifiers", *IEEE Transactions on Communication*, vol. 29, pp. 1715-1720, November 1981.

- [2.13] Y. Yan, T. Liu, and F. M. Ghannouchi, “Linear and Nonlinear Memory Effects of RF Power Amplifiers”, *2008 Asia-pacific Microwave Conference*, pp. 1-4, December 2008.
- [2.14] T. Nguyen, J. Yoh, C. Lee, H. Tran, and D. Johnson, “Modeling of HPA and HPA linearization through a predistorter: Global broadcasting service applications”, *IEEE Transactions in Broadcasting*, vol. 49, no. 2, pp. 132 – 141, June 2003.
- [2.15] J. C. Pedro, and N. B. De Carvalho, “On the use of multitone techniques for assessing RF components' intermodulation distortion”, *IEEE Transactions on Microwave Theory and Techniques*, vol. 47, no. 12, pp. 2393-2402, December 1999.
- [2.16] D. Bondar, and D. Budimir, “A digital predistorter for wireless transmitters”, *International Journal of RF and Microwave Computer-Aided Engineering*, 2009.
- [2.17] M. Schetzen, *The Volterra and Wiener Theories of Nonlinear Systems*, New York: Wiley, 1980.
- [2.18] J. Mathews and G. Sicuranza, *Polynomial Signal Processing*, New York: Wiley, 2000.
- [2.19] H. W. Kang, Y. S. Cho, and D. H. Youn, “Adaptive precompensation of Wiener systems”, *IEEE Transactions on Signal Processing*, vol. 46, no. 10, pp. 2825–2829, October 1998.
- [2.20] P. Celka, N. J. Bershad, and J.-M. Vesin, “Stochastic gradient identification of polynomial Wiener systems: analysis and application”, *IEEE Transactions on Signal Processing*, vol. 49, no. 2, pp. 301–313, February 2001.
- [2.21] A. E. Nordsjo and L. H. Zetterberg, “Identification of certain time-varying nonlinear Wiener and Hammerstein systems”, *IEEE Transactions on Signal Processing*, vol. 49, no. 3, pp. 577–592, March 2001.
- [2.22] T. J. Liu, S. Boumaiza, F. M. Ghannouchi, “Augmented Hammerstein predistorter for linearization of broad-band wireless transmitters”, *IEEE Transactions on Microwave Theory and Techniques*, vol. 54, no. 4, pp. 1340–1349, April 2006.
- [2.23] D. R. Morgan, Z. Ma, J. Kim, M. G. Zierdt, and J. Pastalan, “A generalized memory polynomial model for digital predistortion of RF power amplifiers”, *IEEE Transactions on Signal Processing*, vol. 54, no. 10, pp. 3852–3860, October 2006.

- [2.24] N. J. Bershad, P. Celka, and S. McLaughlin, “Analysis of stochastic gradient identification of Wiener–Hammerstein systems for nonlinearities with Hermite polynomial expansions”, *IEEE Transactions on Signal Processing*, vol. 49, no. 5, pp. 1060–1072, May 2001.
- [2.25] S. Benedetto, and E. Biglieri, “Nonlinear equalization of digital satellite channels”, *IEEE J. Select. Areas Commun.*, vol. SAC-1, pp. 57–62, January 1983.
- [2.26] A. Ahmed, E. R. Srinidhi, and G. Kompa, “Efficient PA modelling using neural network and measurement setup for memory effect characterization in the power device”, *IEEE MTT-S International Microwave Symposium Digest*, June 2005.
- [2.27] S. Boumaiza, and F. Mkadem, “Wideband RF Power Amplifier Predistortion using Real-Valued Time-Delay Neural Networks”, *European Microwave Conference, EuMC2009*, pp. 1449-1452, October 2009.
- [2.28] Y. Hu, J. C. Mollier, and J. Obregon, “A new method of third-order intermodulation reduction in nonlinear microwave systems”, *IEEE Transactions on Microwave Theory and Techniques*, vol. MTT-34, no. 2, pp 245 – 250, February 1986.
- [2.29] Y. Yang, and B. Kim, “A new linear amplifier using low-frequency second-order intermodulation component feedforwarding”, *IEEE Microwave and Guided Wave Letters*, vol. 9, no. 10, pp. 419–421, October 1999.
- [2.30] A. F. Mitchell, “A 135 MHz feedback amplifier”, *IEE Colloq. Broadband High Frequency Amplifiers: Practice and Theory*, pp. 2/1-2/6, London, November 1979.
- [2.31] F. Perez, E. Ballesteros, J. Perez, “Linearisation of microwave power amplifiers using active feedback networks”, *IEE Electronics Letters*, vol. 21, no. 1, pp. 9-10, January 1985.
- [2.32] E. Ballesteros, F. Perez, J. Perez, “Analysis and design of microwave linearized amplifiers using active feedback”, *IEEE Transactions on Microwave Theory and Techniques*, vol. 36, no. 3, pp. 499–504, March 1988.
- [2.33] M. Faulkner, “Amplifier linearization using RF feedback and feedforward techniques”, *IEEE Transactions on Vehicular Technology*, vol. 47, pp. 209-215, February 1998.
- [2.34] G. Gajda, and R. Douville, “A linearization system using RF feedback”, in *Proc. IEEE International Electrical and Electronics Conference*, Toronto, Canada, pp. 30-33, 1983.

- [2.35] T. Arthanayake, and H. B. Wood, "Linear amplification using envelope feedback", *IEE Electronics Letters*, vol. 7, no. 7, pp. 145-146, April 1971.
- [2.36] T. Sowlati, D. Rozenblit, E. MacCarthy, M. Damgaard, R. Pallela, D. Koh, D. Ripley, "Quad-band GSM/GPRS/EDGE polar loop transmitter", *IEEE Journal of Solid-State Circuits*, vol. 39, no 12, pp. 2179- 2189, December 2004.
- [2.37] J. L. Dawson, and T. H. Lee, "Automatic phase alignment for a fully integrated cartesian feedback power amplifier system", *IEEE Journal of Solid-State Circuits*, vol. 38, no. 12, pp. 2269-2279, December 2003.
- [2.38] M. Johansson, and L. Sundstrom, "Linearisation of RF multicarrier amplifiers using Cartesian feedback", *IEE Electronics Letters*, vol. 30, no. 14, pp. 1110-1111, July 1994.
- [2.39] S. Chung, J. W. Holloway, and J. L. Dawson, "Energy-efficient digital predistortion with lookup table training using analog cartesian feedback", *IEEE Transactions on Microwave Theory Tech.* vol. 56, no. 10, pp. 385-392, October 2008.
- [2.40] S. Chung, J. W. Holloway, and J. L. Dawson, "Open-loop digital predistortion using Cartesian feedback for adaptive RF power amplifier linearization", in *Proc. IEEE MTT-S Int. Microw. Symp. Dig.*, pp. 1449–1452, June 2007.
- [2.41] M. T. Hickson, D. K. Paul, P. Gardner, and K. Konstantinou, "High efficiency feedforward linearizers", In *Proc. 24th European Microwave Conference*, vol. 1, pp. 819-824, 1994.
- [2.42] Y. K. G. Hau, V. Postoyalko, and J. R. Richardson, "Design and characterization of a microwave feed-forward amplifier with improved wide-band distortion cancellation", *IEEE Transactions on Microwave Theory Tech.* vol. 49, no. 1, pp. 200-203, January 2001.
- [2.43] H. Seidel, "A feedforward experiment applied to an L-4 carrier system amplifier", *IEEE Transactions on Communication Technology*, vol. COM-19, no. 3, pp.320-325, June1971.
- [2.44] S. P. Stapleton, "Adaptive feedforward linearization for RF power amplifiers", *55th ARFTG Conference Digest-Spring*, vol. 37, pp. 1-7, June 2000.
- [2.45] S. Boumaiza, et al., "Adaptive digital/RF predistortion using a nonuniform LUT indexing function with built-in dependence on the amplifier nonlinearity", *IEEE Transactions on Microwave Theory and Techniques*, vol.52, no.12, pp. 2670-2677, December 2004.

-
- [2.46] P. L. Gilabert, et al., “Multi-lookup table FPGA implementation of an adaptive digital predistorter for linearizing RF power amplifiers with memory effects”, *IEEE Transactions on Microwave Theory and Techniques*, vol.56, no.2, pp.372-384, February 2008.
- [2.47] K.J. Muhonen, M. Kavehrad, R. Krishnamoorthy, “Look-up table techniques for adaptive digital predistortion: a development and comparison”, *IEEE Transactions on Vehicular Technology*, vol.49, no.5, pp.1995-2002, September 2000.
- [2.48] J. K. Cavers, “The effect of quadrature modulator and demodulator errors on adaptive digital predistorters for amplifier linearization”, *IEEE Trans. Veh. Technol.*, vol. 46, pp. 456-466, May 1997.
- [2.49] M. Ghaderi, S. Kumar, D.E. Dodds, “Adaptive predistortion lineariser using polynomial functions”, *IEE Proceedings on Communications*, vol.141, no.2, pp.49-55, April 1994.
- [2.50] L. Ding, et al., “A robust digital baseband predistorter constructed using memory polynomials”, *IEEE Transactions on Communications*, vol.52, no.1, pp. 159-165, January 2004.
- [2.51] S. Hong, et al., “Weighted polynomial digital predistortion for low memory effect doherty power amplifier”, *IEEE Transactions on Microwave Theory and Techniques*, vol.55, no.5, pp.925-931, May 2007.
- [2.52] N. Mizusawa, and S. Kusunoki, “Third and fifth order base-band component injection for linearization of the power amplifier in a cellular phone”, In *2005 IEEE MTT-S International Microwave Symposium Digest*, pp. 1565-1568, June 2005.
- [2.53] K. C. Lee, and P. Gardner, “Adaptive neuro-fuzzy inference system (ANFIS) digital predistorter for RF power amplifier linearization”, *IEEE Trans. Veh. Technol.*, vol. 55, no. 1, pp. 43–51, January 2006.
- [2.54] S.P. Stapleton, and J.K. Cavers, “A new technique for adaptation of linearizing predistorters”, *41st IEEE Vehicular Technology Conference*, pp.753-758, May 1991.

3. ARTIFICIAL INTELLIGENCE SYSTEMS

3.1. Introduction

The most important developments in the area of artificial intelligence are neural networks and fuzzy logic systems. They have been successfully applied to a wide range from pattern recognition to industry. Neural networks are based on emulation of biological neurons, while the fuzzy systems use expert skills and thinking process in the artificial intelligence mechanism. The ability and limitations of these systems to learn to imitate the desired device or human thinking is an attractive problem for researchers in recent years. Sometimes neural networks (NNs) require millions of iterative calculations, and their training is time-consuming. On the other hand, fuzzy logic systems require knowledge from an expert who encodes his knowledge into IF-THEN rules. The problem arises when the system for imitation becomes complicated in terms of the number of inputs and outputs. Many researchers try to combine these two techniques to overcome the problems related to individual systems.

This chapter will describe the neural network architecture, fuzzy logic principle and neuro-fuzzy artificial intelligence systems. As these research areas are complex and widely developed, focus will be on the structures that are used later on in this thesis.

3.2. Artificial Neural Networks

A lot of different types of neural networks are developed. This subsection will give brief description of the neurons, as the basic of every network, network architectures and learning algorithms. In the area of modelling and predistortion of power amplifiers mostly used structures are multilayer perceptron with gradient descent learning algorithm [3.1]-[3.12].

3.2.1 Artificial Neuron

The Figure 3-1 shows the typical artificial neuron. It consists of the input weights, summing junction and activation function. The weights are connection strengths between the outputs of previous neurons and integration (summation) node in the neuron, called synapses. The output of summation junction will be the input for activation function which will give the overall neuron output.

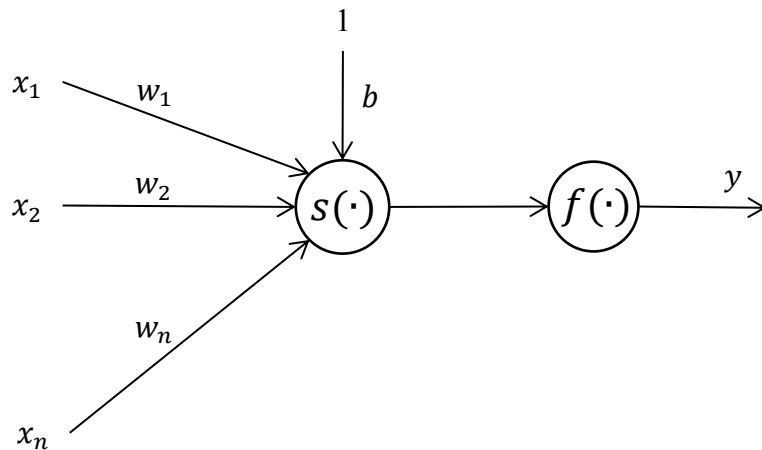


Figure 3-1: A single neuron model

3.2.1.1 Input Weights and Bias

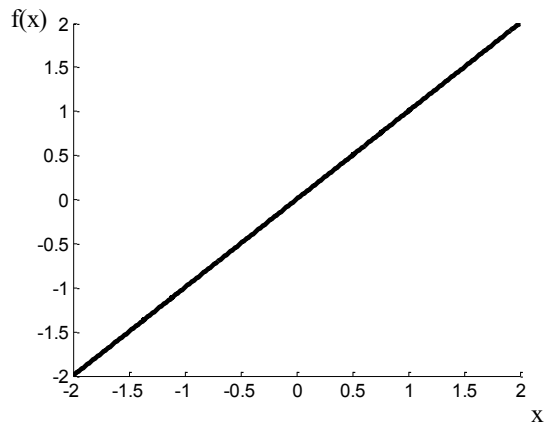
The input weights w_i and bias b are free parameters in the neuron model which are used for the network training. Bias is a special neuron input with constant value 1, and weight b . Number of the free parameters is $n + 1$, where n is the number of inputs coming from other neurons in the system. Summing function is defined as:

$$s(\mathbf{x}, \mathbf{w}, b) = b + \sum_{i=1}^n x_i w_i \quad (3.1)$$

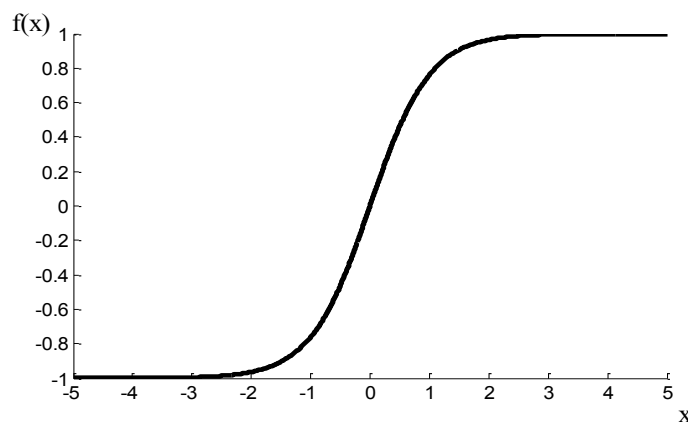
Bolded letters \mathbf{x} and \mathbf{w} are notations for the vectors of inputs and weights, respectively. During the training process bias and weights are adjusted to make the network error acceptable for the wanted application.

3.2.1.2 Activation Function

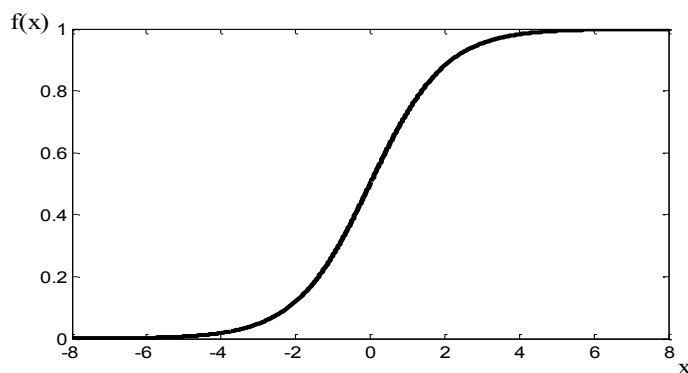
Most commonly used activation functions $f(\cdot)$ in NNs are linear (*Purelin*) (3.2) (Figure 3-2 (a)), hyperbolic tangent transfer function (*Tansig*) (3.3) (Figure 3-2 (b)) or log-sigmoid, function (*Logsig*) (3.4) (Figure 3-2 (c)).



a)



b)



c)

Figure 3-2: A neuron activation functions: a) linear, b) hyperbolic tangent, c) log-sigmoid

$$f(x) = \text{Purelin}(x) = x \quad (3.2)$$

$$f(x) = \text{Tansig}(x) = \frac{e^{2x} - 1}{e^{2x} + 1} \quad (3.3)$$

$$f(x) = \text{Logsig}(x) = \frac{1}{1 + e^{-x}} \quad (3.4)$$

First, *purelin*, activation function transfers summation output to the neuron's output, while the other two nonlinear functions *tansig* and *logsig*, for input range $(-\infty, \infty)$, provide output in range $(-1,1)$ and $(0,1)$, respectively. Depending on nature of phenomena which has to be imitated by network, user chooses activation function for neuron.

3.2.2 Network Architecture

Only one neuron is rarely sufficient to present the input-output transfer function. In that situation more neurons organized in one or more layers are incorporated in NN system.

3.2.2.1 Single-Layer Network

A network with one layer is presented in the Figure 3-3. The input layer is the layer which does not process any computations over the input values. The output layer is the only layer in this architecture that derives the input-output relationship.

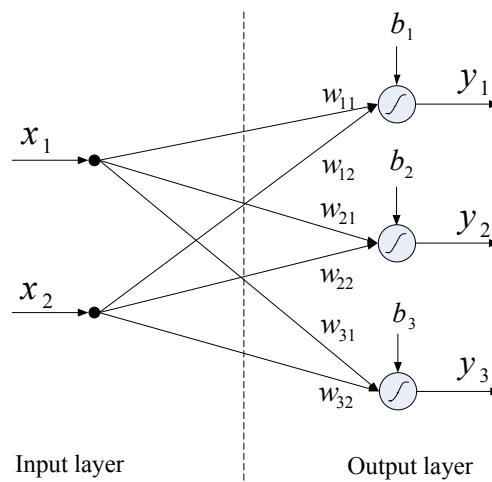


Figure 3-3: A single-layer neural network

The output vector $\mathbf{y} = [y_1 \ y_2 \ y_3]^T$ can be defined as:

$$\mathbf{y} = \mathbf{f}(\mathbf{W}\mathbf{x} + \mathbf{b}) \quad (3.5)$$

$$\mathbf{W} = \begin{bmatrix} w_{11} & w_{12} \\ w_{21} & w_{22} \\ w_{31} & w_{32} \end{bmatrix} \quad (3.6)$$

$$\mathbf{x} = \begin{bmatrix} x_1 \\ x_2 \end{bmatrix} \quad (3.7)$$

$$\mathbf{b} = \begin{bmatrix} b_1 \\ b_2 \\ b_3 \end{bmatrix} \quad (3.8)$$

$$\mathbf{f} = \begin{bmatrix} f_1(\cdot) \\ f_2(\cdot) \\ f_3(\cdot) \end{bmatrix} \quad (3.9)$$

Matrix \mathbf{W} is the matrix of weights, and vectors \mathbf{x} , \mathbf{b} and \mathbf{f} are vectors of layer inputs, biases, and activation functions, respectively.

3.2.2.2 Multi-Layer Network

Multi-layer NN has more than just an output layer. Layers between the input and output layer are called hidden layers (Figure 3-4).

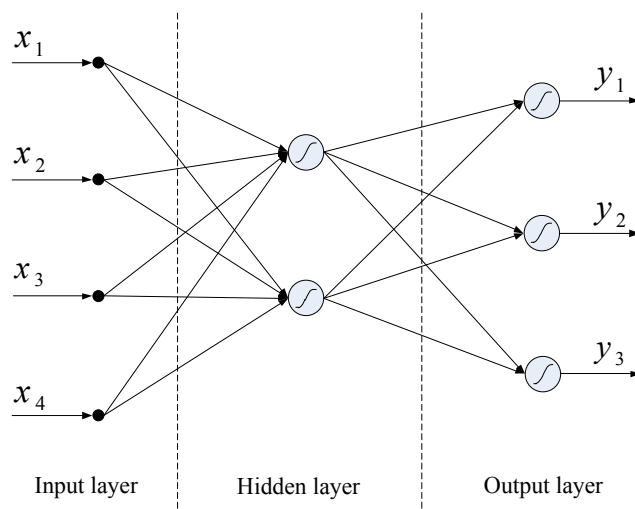


Figure 3-4: A multi-layer neural network fully connected

Output of one of the layers is described by (3.5). The overall network output is the output of the last layer (output layer).

Type of connections of neurons divides NN architectures in few groups: fully connected networks (Figure 3-4), not-fully connected networks, feedforward networks (FFNN) and recurrent networks (RNN).

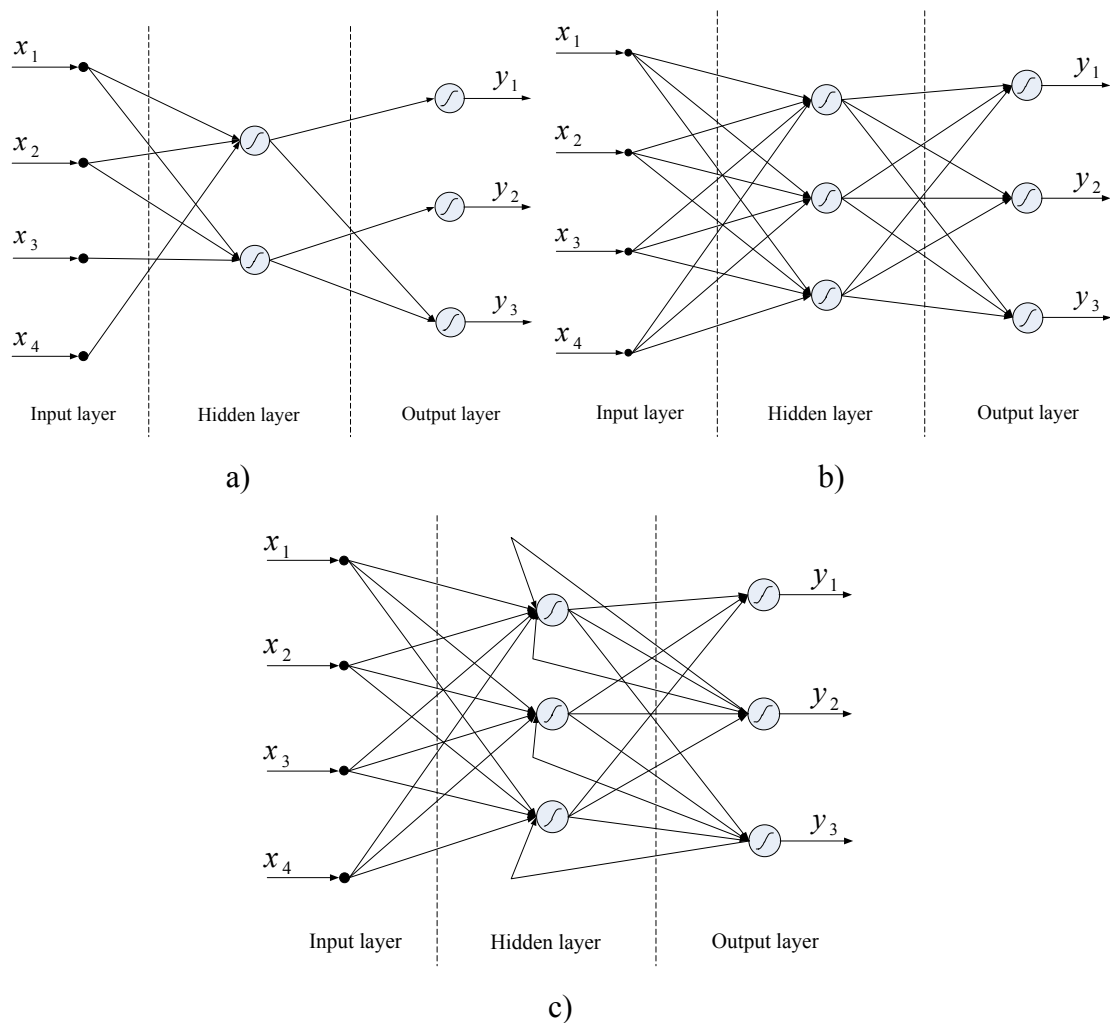


Figure 3-5: NN architectures: a) a multi-layer network not-fully connected, b) a feedforward network, c) a recurrent network

Fully connected networks have every output from the previous layer as an input to the neurons in the next layer. If user has previous knowledge about the process, neurons from one layer do not have to be connected to all of the next layer neurons. FFNNs allow signals to pass only in one direction, from input to output, while RNNs have the signals passing through feedback branches to the neurons in hidden layers, or back as the inputs to the neurons from which they come. In that way the memory of some

system can be incorporated to the model. RNNs training process is more complex and lasts longer than the training of FFNNs, and also suffers from instability in some cases. Because of that, in this thesis FFNN architecture is used and a memory is artificially simulated driving delayed signals to the network input. This will be described in the next Chapter.

3.2.3 Learning Algorithms

Learning or training process is adjusting of weights and biases of NN until a certain criterion is encountered. The criterion can be a number of training epochs, a defined number of validation tests performed or a training error falls below defined value. The training process can be supervised or unsupervised.

3.2.3.1 Supervised Learning

During the supervised learning input datasets and desired output sets are given to the network and the error between desired output and network output is minimized. This type of learning is called learn by example.

One of the most powerful algorithm for the supervised learning is back-propagation [3.13]-[3.14].

Back-propagation learning algorithm

This learning algorithm is organized in two phases. The first one is the forward pass where the error is computed. The second pass is a backward pass, from the output layer down to the input layer, where the adjustment of weights and biases is done. The algorithm is presented in the Figure 3-6.

Network parameters are adjusted using chosen method. The basic method is gradient method, which gives the most rapid decrease of the performance function (3.10). The performance function in this method is the negative of the error gradient.

$$p_{n+1} = p_n - \alpha \frac{\partial e_n}{\partial p_n} \quad (3.10)$$

α represents the learning rate, defined by the user, before the training process, n is the iteration index, p is the weight or bias and e is the error between the network outputs and desired outputs. The learning rate controls the speed of convergence. Smaller learning rate makes the network learn slowly, convergence is smoother, but large number of iterations is required, while larger value for the learning rate makes the convergence rougher, number of iterations is smaller, but the network diverge sometimes. Another learning parameter, which is a solution of oscillatory descent, is momentum η . It adds the prehistory to the current update of the parameters, e.g. determines the relative contribution of the current and past errors to the parameters update.

$$p_{n+1} = p_n - \alpha \frac{\partial e_n}{\partial p_n} + \eta \frac{\partial e_{n-1}}{\partial p_{n-1}} \quad (5.7)$$

The parameters update can be done either after each input pattern (Sequential mode), or after processing all input patterns (Batch mode).

3.2.3.1 Unsupervised Learning

Training model where the network is fed only by the input dataset is called unsupervised learning model. NN must explore shared properties of the dataset and learn how to classify the input data into appropriate categories. The unsupervised algorithm does not have information about what the output should be. It is used for clustering the input data without a priori information.

As the measurements carried out with the power amplifiers used in this research consist of the input and output data, the supervised learning scheme will be used for the modelling and predistortion of DUT.

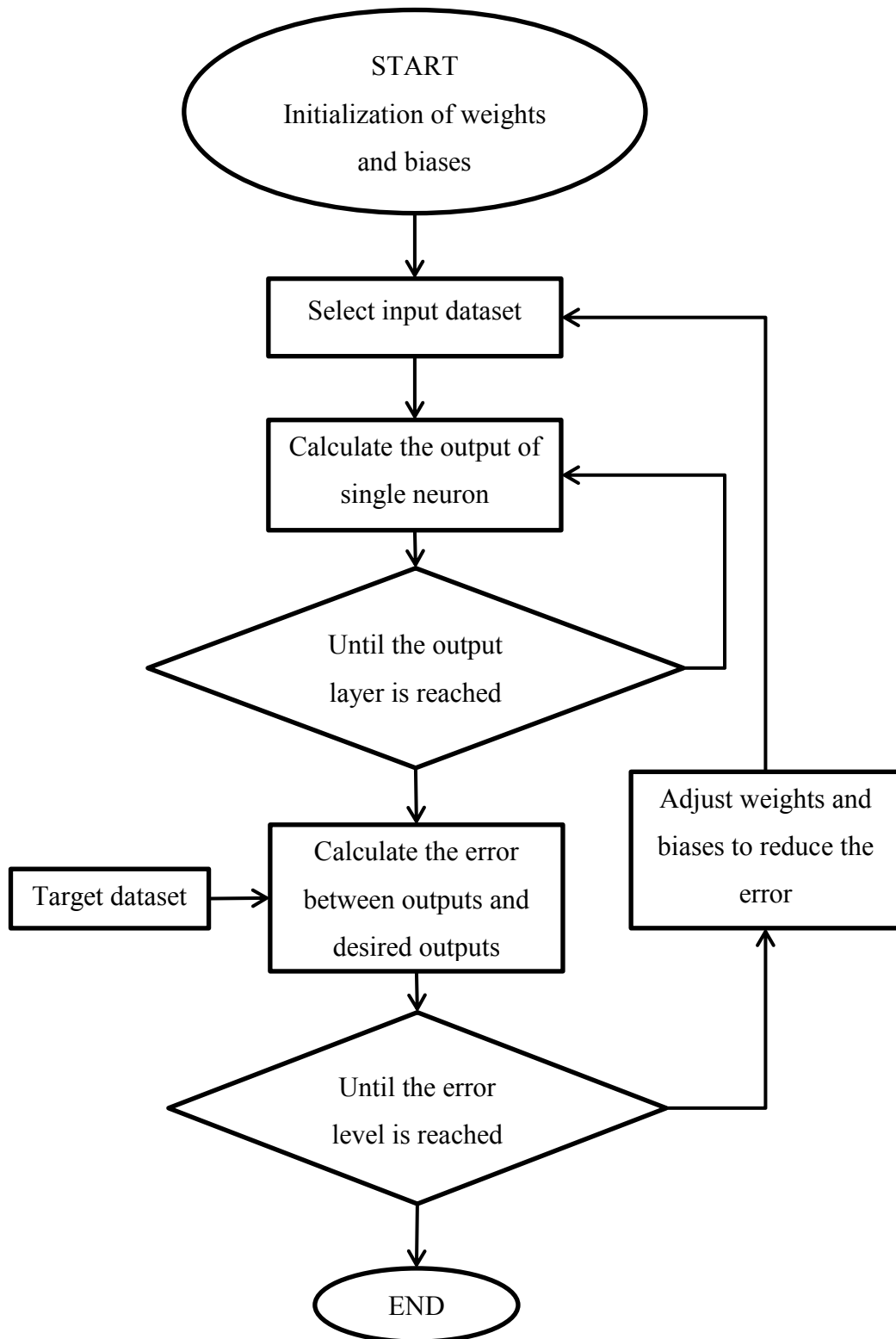


Figure 3-6: Back-propagation algorithm

3.3. Fuzzy Logic

Formalizer of fuzzy set theory is Zadeh [3.15]-[3.17]. According to him, values that are normally characterized by words, like “young”, “not young”, “very young”, etc., have compatibility values from range [0, 1]. Thus, age 21 will have compatibility with “young” 0.75, and age 37 will have compatibility with “young” 0.2. Compatibility function is defined by an expert in the area of research aiming fuzzy theory. Fuzzy logic, regardless of the mathematical bivalent logic of zero and one, allows half-truth. In field of modelling and predistortion of power amplifiers fuzzy logic is not used individually, because of the inability to create proper compatibility functions as the signals in the mobile communications are too complex. This subsection will give a brief introduction to fuzzy sets and fuzzy logic, as the next one will deal with neuro-fuzzy systems.

3.3.1 Fuzzy Sets and Membership Functions

By definition [3.18], if X is collection of objects denoted generically by x , then a **fuzzy set** A in X is a set of ordered pairs:

$$A = \{(x, \mu_A(x)) | x \in X\}, \quad (3.11)$$

where $\mu_A(x)$ is called **membership function** (or MF for short) for the fuzzy set A . The MF maps each element of X to a membership grade (or membership value) between 0 and 1.

For example, the variable x is “age 27”, fuzzy set A is “young”, and the membership value is $\mu_A(x) = 0.75$.

In fuzzy theory the determination of fuzzy sets and MF relies on the knowledge of human experts. Mostly used MFs of one dimension are given in the Figure 3-7 and defined by (3.12)-(3.15).

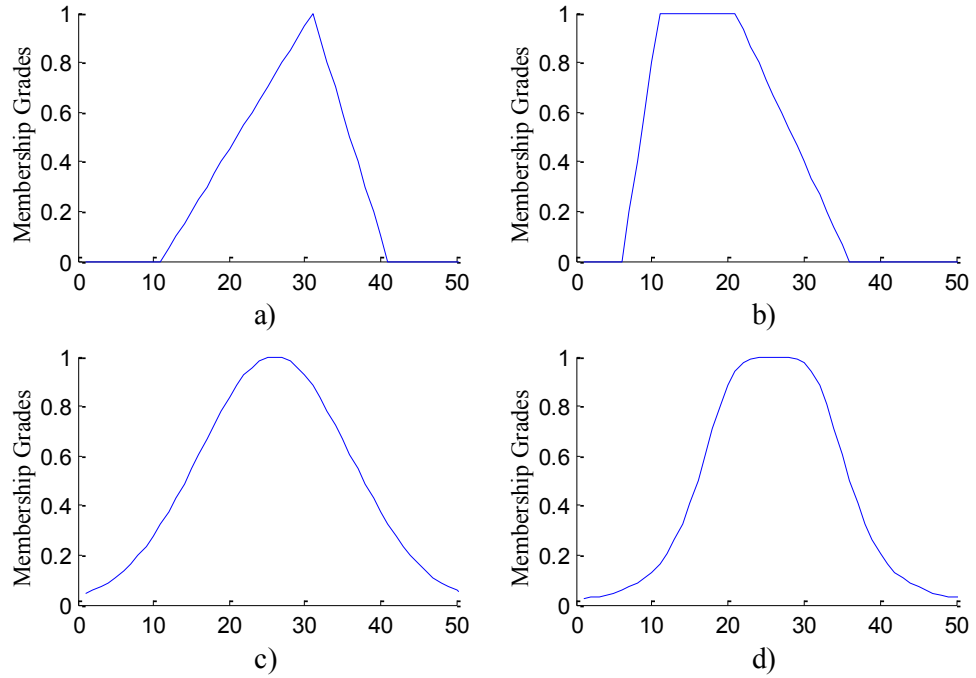


Figure 3-7: Classes of parameterized membership functions:

- a) $triangle(x, 10, 30, 40)$, b) $trapezoid(x, 5, 10, 20, 35)$, c) $gaussian(x, 25, 10)$,
d) $bell(x, 10, 2, 25)$

$$triangle(x, a, b, c) = \max\left(\min\left(\frac{x-a}{b-a}, \frac{c-x}{c-b}\right), 0\right) \quad (3.12)$$

$$trapezoid(x, a, b, c, d) = \max\left(\min\left(\frac{x-a}{b-a}, 1, \frac{d-x}{d-c}\right), 0\right) \quad (3.13)$$

$$gaussian(x, c, \sigma) = e^{-\frac{1}{2}\left(\frac{x-c}{\sigma}\right)^2} \quad (3.14)$$

$$bell(x, a, b, c) = \frac{1}{1 + \left|\frac{x-c}{a}\right|^{2b}} \quad (3.15)$$

3.3.2 Fuzzy Rules

When more fuzzy sets are incorporated in a system, they can be connected using IF-THEN statements, forming a sequence of fuzzy rules. A form of IF-THEN rule in a fuzzy system is shown below [3.18]:

$$\mathbf{IF} \ x \text{ is } A \ \mathbf{THEN} \ y \text{ is } B, \quad (3.16)$$

where A and B are fuzzy sets. The first part “ x is A ” of the rule evaluates the antecedent or premise, and involves fuzzification of the input. The second part “ y is B ” applies result of IF-part to the consequent or conclusion.

IF-part can have multiple antecedents, which are connected with fuzzy operators. Three main operators defined by Zadeh [3.15]: fuzzy intersection “ \cap ” (AND), fuzzy union “ \cup ” (OR) and fuzzy complement “ $\bar{\cdot}$ ” (NOT) are described in following equations (3.16)-(3.18). It is assumed that A and B are fuzzy sets with MFs $\mu_A(x)$ and $\mu_B(x)$.

$$\mu_{A \cap B}(x) = \min(\mu_A(x), \mu_B(x)) \quad (3.16)$$

$$\mu_{A \cup B}(x) = \max(\mu_A(x), \mu_B(x)) \quad (3.17)$$

$$\mu_{\bar{A}}(x) = 1 - \mu_A(x) \quad (3.18)$$

After deriving IF-part, the output of THEN-part will be the result of fuzzy reasoning process by applying the appropriate fuzzy operators in order to obtain the fuzzy set to be accumulated in the output member function (Figure 3-8).

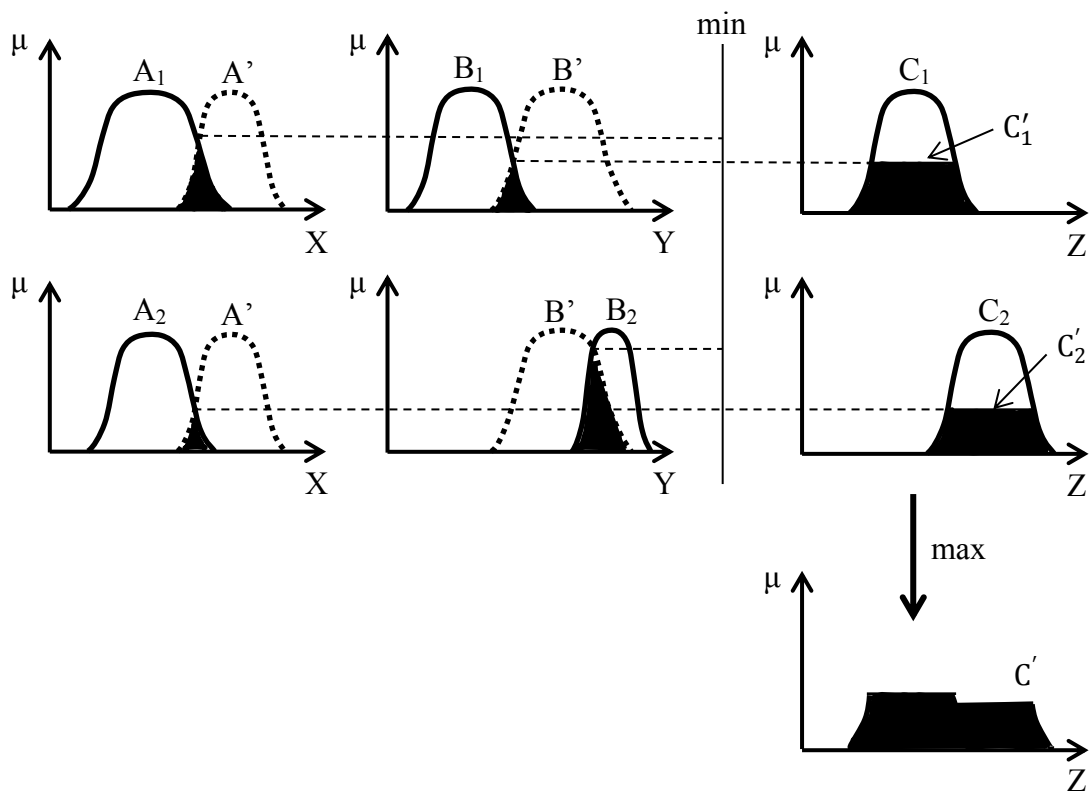


Figure 3-8: Fuzzy reasoning for multiple rules with multiple premises

3.3.3 Defuzzification

Defuzzification is transferring the fuzzy output MF (C' from Figure 3-8) into a crisp output using chosen defuzzification method. Principle shown in the Figure 3-8 is common for the Mamdani method [3.19]. In the Mamdani method consequents are fuzzy sets, and the final output is based on the defuzzification of the overall fuzzy output using various types of defuzzification methods: centroid of area, bisector of area, mean of maximum, smallest of maximum, or largest of maximum (Figure 3-9) [3.18].

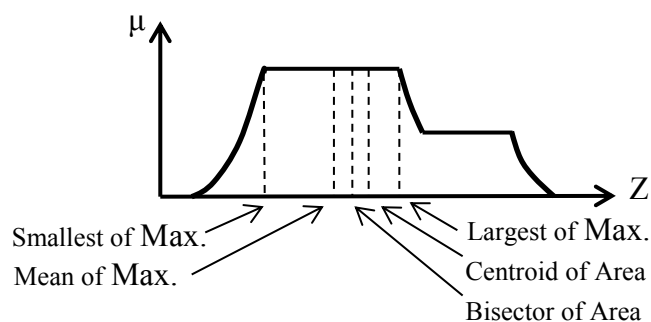


Figure 3-9: The Mamdani defuzzification methods

Second most commonly used method is proposed by Sugeno [3.20]. In this method consequents are real numbers (3.19), which can be either linear or constant. The final output, called singleton output membership function, is the weighted average of each rule's output.

$$\text{IF } x \text{ is } A \text{ AND } y \text{ is } B \text{ THEN } z = ax + by + c \quad (3.16)$$

The Figure 3-10 illustrates the Sugeno model where each rule has a crisp output, and the overall output is obtained via the weighted average, thus avoiding time-consuming defuzzification required in the Mamdani model.

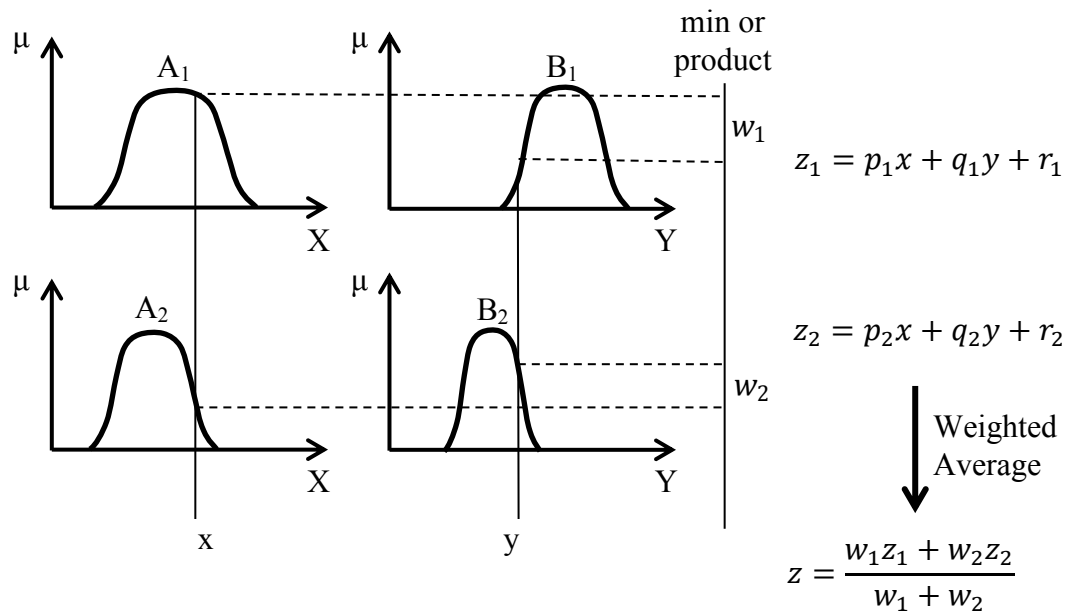


Figure 3-10: The Sugeno fuzzy model

3.4. Neuro-Fuzzy Systems

Combination of neural networks and fuzzy logic has increased researchers interest. It is still developing, but already has very good results in many fields, like medicine, system control, pattern recognition, data analysis, etc. Neuro-fuzzy systems (NFS) are an efficient tool to deal with complicated systems, in which there are linguistic information and data information, simultaneously. By Nauck [3.21] combination of these two artificial intelligence systems can be accomplished in few different ways: cooperative NFS, concurrent NFS and hybrid NFS.

In cooperative neuro-fuzzy system NN is used at the initial phase to determine the fuzzy sets and/or fuzzy rules and then the fuzzy system is fully utilised for execution.

Concurrent NFSs use NNs to provide an input for a fuzzy system, or to change an output of the fuzzy system. In this approach, the parameters of the fuzzy system are fixed, not changed by the learning process.

Hybrid NFS, mostly used in the field of interests of the author, uses neural networks to determine fuzzy system parameters through pattern processing.

In this thesis the hybrid neuro-fuzzy systems are used, thus two of the hybrid architectures will be described further.

3.4.1 Adaptive neuro-fuzzy inference system

One of the most frequently used neuro-fuzzy systems in modelling and predistortion of PAs are adaptive neuro-fuzzy inference systems (ANFIS) [3.22]-[3.25]. This structure is proposed by Jang [3.17] and it is presented in the Figure 3-11.

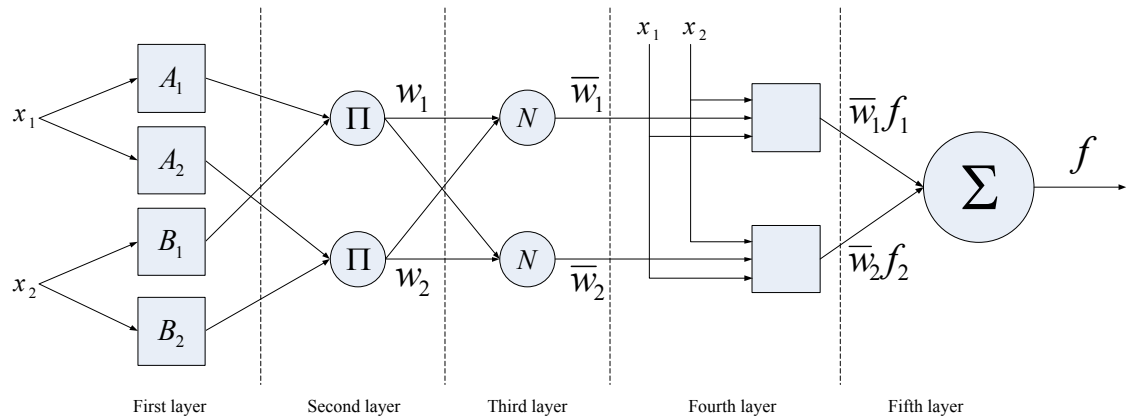


Figure 3-11: A two-input ANFIS architecture

Explanation of five layers from this structure will is given below.

First layer has nodes which represents the membership functions of A_i . The membership function can be one of the (3.12)-(3.15).

$$\begin{aligned} o_{A_i} &= \mu_{A_i}(x), \\ o_{B_i} &= \mu_{B_i}(y), \end{aligned} \quad (3.17)$$

where i goes through all nodes in the first layer.

Second layer has nodes which are the multiplication of the incoming signals, and obtain the weights:

$$w_i = \mu_{A_i} \times \mu_{B_i}, \quad (3.18)$$

where i goes through all nodes in the second layer.

Third layer calculates the ratio of the rules:

$$\bar{w}_i = \frac{w_i}{w_1 + w_2}, i = 1..n \quad (3.19)$$

Fourth layer calculates the output for each consequent:

$$\bar{w}_i f_i = \bar{w}_i (p_i x + q_i y + r_i), i = 1..n \quad (3.20)$$

n is the number of nodes in the third and fourth layer.

Fifth layer is a single node layer which summarises all incoming signals from the layer 4, and gives the overall output of ANFIS:

$$f = \sum_{i=1}^n \bar{w}_i f_i = \frac{w_1 f_1 + w_2 f_2}{w_1 + w_2} \quad (3.21)$$

Disadvantage of this system is inability to make the multiple-input multiple-output (MIMO) system. For example, if we want to make a model for a power amplifier which will give in-phase and quadrature components at the output, that could not be done using one ANFIS structure. Mizutani [3.18] proposed the generalized ANFIS structure, called coactive neuro-fuzzy interference system (CANFIS) which is suitable for the multiple-input multiple-output systems. As this structure is more complex, authors use rather two ANFIS networks for modelling the power amplifiers [3.23]-[3.25]. ANFIS structures have the number of rules equal to the number of membership functions to the power of the number of inputs. That makes the training of ANFIS networks more time consuming if the number of inputs or the number of membership functions increase.

3.4.2 Adaptive Fuzzy Logic Systems

Fuzzy logic systems (AFLSs) were first presented by Wang [3.27]. Method is developed to generate fuzzy rules from numerical data. Adaptivity of these systems is achieved by training the fuzzy parameters from the input-output data like in NN approach. This type of neuro-fuzzy systems can be a multi-input multi-output. General

ANFIS architecture for R inputs, N rules, and P outputs is given in the Figure 3-12. It consists of three layers: fuzzifier, inference engine and defuzzifier.

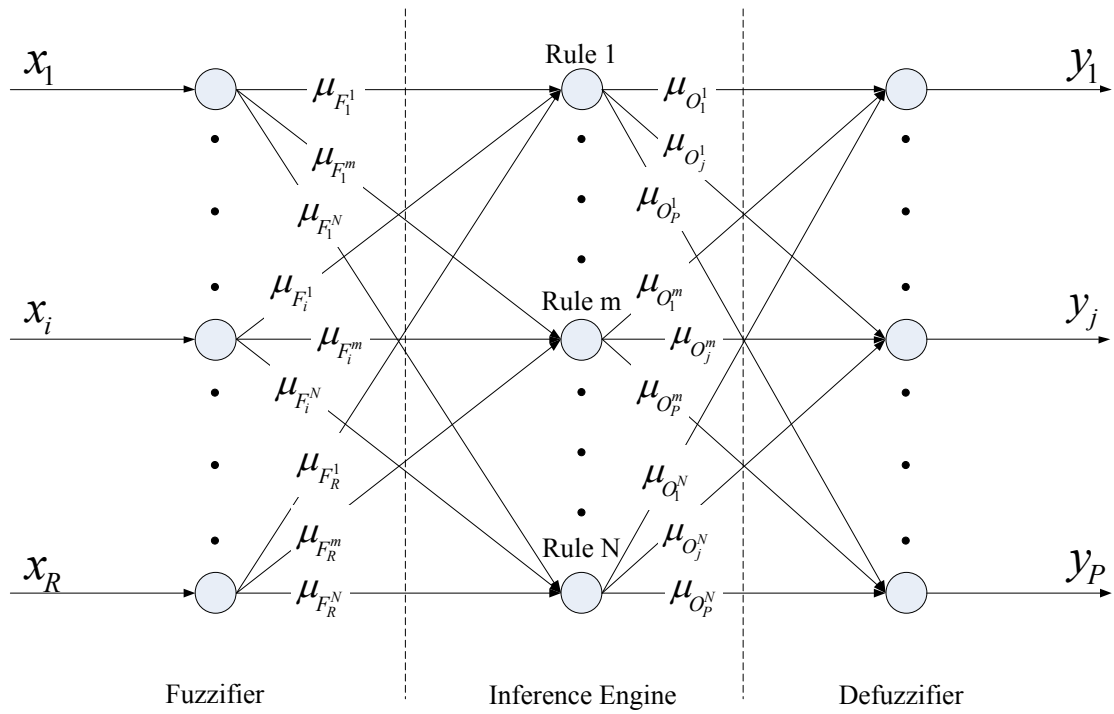


Figure 3-12: A multi-input multi-output AFLS architecture

3.4.2.1 Fuzzifier

The membership function of a fuzzifier is chosen by the user, and in case of the Gaussian shape membership function of the i -th input of the m -th rule will be in form:

$$\mu_{F_i^m}(x_i) = e^{-\frac{1}{2} \left(\frac{x_i - c_i^m}{\sigma_i^m} \right)^2}, \quad (3.22)$$

where c_i^m and σ_i^m are the centre and spread parameters of the membership function of the i -th input of the m -th rule. The membership function can be any of the four presented in (3.12)-(3.15).

3.4.2.2 Inference engine

Inference engine can have different operators engaged. In [3.26]-[3.27] AFLS uses product inference. By combining the antecedents of the m -th fuzzy rule using product operation the output membership function of the m -th rule is determined.

$$\mu_{O_j^m} = \prod_{i=1}^n \mu_{F_i^m}(x_i), \quad (3.23)$$

where $\mu_{F_i^m}(x_i)$ is the membership value of the i -th input of the m -th rule, and n is the number of rules. O_j^m is the output fuzzy region of the m -th rule for the j -th output.

3.4.2.3 Defuzzifier

The output of the inference engine O_j^m (m is the index of the rule, j is the index of the output) is area with an irregular shape depending on the membership functions used in fuzzification part, the membership value of each rule and the inference type used. Defuzzifier converts this area to a real value, using defuzzification method such as centre average (CA), centroid of area, bisector of area, mean of maximum, smallest of maximum, etc. Centroid of area defined by (3.24) would be a logical choice because it uses all information available to compute the output. The problem with this defuzzifier is an intensive computation. On the other hand, CA does not use entire shape of O_j^m , but is easy to compute and use. This method has the same result regardless of the inference operation used (min-max or max-product).

$$y_j = \frac{\sum_{i=1}^n \mu_{O_j^m}(\bar{y}_j^m) \cdot \bar{y}_j^m}{\sum_{i=1}^n \mu_{O_j^m}(\bar{y}_j^m)} \quad (3.24)$$

\bar{y}_j^m denotes centre of the fuzzy set O_j^m which is the output fuzzy region of the m -th rule for the j -th overall output and n is the number of quantization levels of the output.

Training of AFLS parameters is done by a back-propagation learning algorithm. This architecture is less time-consuming than the ANFIS models.

3.5. Conclusion

This chapter introduced the artificial intelligence systems. Brief description of neural network, fuzzy logic systems and neuro-fuzzy systems was presented. This was due to the usage of these structures later in the thesis. Neural network based approach will be described in Chapter 5. As for the authors' knowledge, there is no usage of AFLS type of artificial intelligence system in the field of power amplifiers modelling or predistortion. Thus, this AFLS with "area of balance" defuzzification will be used in Chapter 6 for modelling and predistortion of DUT.

3.6. References

- [3.1] Q. J. Zhang and K. C. Gupta, *Neural Networks for RF and Microwave Design*, Norwood, MA: Artech House, 2000.
- [3.2] H. Holma, A. Toskala, *LTE for UMTS: Evolution to LTE-Advanced, 2nd Edition*, Wiley, 2011.
- [3.3] M. Ibnkahla, N. J. Bershad, J. Sombrin, F. Castanie, "Neural network modeling and identification of nonlinear channels with memory: algorithms, applications, and analytic models", *IEEE Transactions on Signal Processing*, vol.46, no.5, pp.1208-1220, May 1998.
- [3.4] B. E. Watkins, R. North, "Predistortion of nonlinear amplifiers using neural networks", *Military Communications Conference, MILCOM '96, Conference Proceedings, IEEE*, vol.1, pp.316-320, 21-24. October 1996.
- [3.5] A. Ahmed, E. R. Srinidhi,; G. Kompa, "Efficient PA modeling using neural network and measurement setup for memory effect characterization in the power device", *Microwave Symposium Digest, 2005 IEEE MTT-S International*, 12-17. June 2005.
- [3.6] M. S. Kim, C. C. Guest, "Modification of backpropagation networks for complex-valued signal processing in frequency domain", *1990 IJCNN International Joint Conference on Neural Networks*, vol.3, pp.27-31, 17-21. June 1990.
- [3.7] H. Qian and G. T. Zhou, "A neural network predistorter for nonlinear power amplifiers with memory", *Digital Signal Processing Workshop, 2002 and the 2nd*

- Signal Processing Education Workshop. Proceedings of 2002 IEEE*, no. 10, pp. 312-316, October 2002.
- [3.8] H. Leung, S. Haykin, “The complex backpropagation algorithm”, *Signal Processing, IEEE Transactions on*, vol.39, no.9, pp.2101-2104, September 1991.
- [3.9] N. Benvenuto, F. Piazza, A. Uncini, “A neural network approach to data predistortion with memory in digital radio systems”, *Communications, 1993. ICC '93 Geneva. Technical Program, Conference Record, IEEE International Conference on*, vol.1, pp.232-236, 23-26 May 1993.
- [3.10] L. Taijun, S. Boumaiza, F.M. Ghannouchi, “Dynamic behavioral modeling of 3G power amplifiers using real-valued time-delay neural networks”, *Microwave Theory and Techniques, IEEE Transactions on*, vol.52, no.3, pp.1025-1033, March 2004.
- [3.11] H. Zihong, C. Wenhua, F. Zhenghe, F.M. Ghannouchi, “Forward behavioral modeling of concurrent dual-band power amplifiers using extended real valued time delay neural networks”, *Microwave and Millimeter Wave Technology (ICMMT), 2012 International Conference on*, vol.5, pp.1-4, 5-8. May 2012.
- [3.12] F. Mkadem, M.B. Ayed, S. Boumaiza, J. Wood, P. Aaen, “Behavioral modeling and digital predistortion of Power Amplifiers with memory using Two Hidden Layers Artificial Neural Networks”, *Microwave Symposium Digest (MTT), 2010 IEEE MTT-S International*, pp.656-659, 23-28. May 2010.
- [3.13] S. Haykin, *Neural Networks: A Comprehensive Foundation, 2nd edition*, Prentice Hall, 1999.
- [3.14] F. O. Karray, and C. De Silva, *Soft Computing and Intelligent Systems Design: Theory, Tools and Applications*, Addison Wesley, 2004.
- [3.15] L. A. Zadeh, “Fuzzy Sets”, *Information and Control*, pp. 338 – 353, June 1965.
- [3.16] L. A. Zadeh, “Outline of a New Approach to the Analysis of Complex Systems and Decision Processes”, *IEEE Transactions on Systems, Man, and Cybernetics*, pp. 28 – 44, January 1973.
- [3.17] L. A. Zadeh, “The concept of a linguistic variable and its applications to approximate reasoning”, *Information Sciences* 8, 199–249, 1975.
- [3.18] J. S. R Jang, C. T. Sun, and E. Mizutani, *Neuro-Fuzzy and Soft Computing: A Computational Approach to Learning and Machine Intelligence*, Prentice Hall, 1997.

-
- [3.19] E. H. Mamdani, and S. Assilian, “An experiment in linguistic synthesis with a fuzzy logic controller”, *International Journal of Man-Machine Studies* 7, pp. 1–13, 1975.
- [3.20] M. Sugeno, *Industrial applications of fuzzy control*, Elsevier Science Pub. Co., 1985.
- [3.21] D. Nauck, “Neuro-fuzzy systems: Review and prospects”, *In Fifth European Congress on Intelligent Techniques and Soft Computing, EUFIT97*, pp. 1044–1053, 1997.
- [3.22] K. C. Lee and P. Gardner, “Adaptive neuro-fuzzy inference system (ANFIS) digital predistorter for RF power amplifier linearization”, *IEEE Transactions on Vehicular Technology*, vol. 55, no. 1, pp. 43-51, January 2006.
- [3.23] H. M. Deng, S. B. He, and J. B. Yu, “An adaptive predistorter using modified neural networks combined with a fuzzy controller for nonlinear power amplifiers”, *International Journal of RF and Microwave Computer-Aided Engineering*, vol. 14, no. 1, pp. 15-20, January 2004.
- [3.24] V. P. G. Jimenez, Y. Jabrane, A. G. Armada, B. A. Es Said, and A. A. Ouahman, “High Power Amplifier Pre-Distorter Based on Neural-Fuzzy Systems for OFDM Signals”, *IEEE Transactions on Broadcasting*, vol. 57, no. 1, March 2011.
- [3.25] K. C. Lee and P. Gardner, “Neuro-fuzzy approach to adaptive digital predistortion”, *Electronics Letters*, vol. 40, no. 3, February 2004.
- [3.26] L. X. Wang, *Adaptive Fuzzy System and Control*, Prentice-Hall, 1994.
- [3.27] L. X. Wang, and J. M. Mendel, “Generating Fuzzy Rules by Learning from Examples”, *IEEE Transactions on Systems, Man, and Cybernetics*, vol. 22, no. 6, December 1992.

4. ROBUST ESTIMATION OF NONLINEAR COEFFICIENTS FOR MEMORYLESS POLYNOMIAL MODEL OF POWER AMPLIFIERS

4.1. Introduction

Modelling of power amplifiers can be accomplished in two ways: using the physical knowledge of the PA internal composition or by an empirical set of the input-output observations. The first approach relates to physical models, whereas the second one implies behavioural models. The physical models are more accurate, but they require precise knowledge of the PA internal structure, which increases simulation time or may be unavailable. For these reasons, when a complete system-level evaluation is required, the behavioural models are usually preferred, which treat a PA as a black-box and are determined by a properly selected set of the input-output relations.

Generally, any power amplifier can be seen as an operator function, which transforms the input signal $x(t)$ into the output signal $y(t)$ according to the following nonlinear differential equation [4.1]:

$$f \left\{ y(t), \frac{dy(t)}{dt}, \dots, \frac{d^p y(t)}{dt^p}, x(t), \frac{dx(t)}{dt}, \dots, \frac{d^r x(t)}{dt^r} \right\} = 0 \quad (4.1)$$

which means that the system output and its time derivatives are related in a nonlinear way to the input and its time derivatives. A solution to (4.1), which expresses the system output function $y(t)$ in terms of the input function $x(t)$ and their time derivatives, serves as a behavioural model for the PA.

This chapter will give analytical description of the output signal distortion caused by the memoryless nonlinearity of the PA. General formulas are derived which relate the analytical expression for the fundamental frequency signal and the in-band distortion components to the order of PA polynomial model. A robust method for estimation of coefficients of a nonlinear model will be presented and applied to a particular amplifier.

4.2. Memoryless polynomial model of power amplifier

A memoryless polynomial model for representing a nonlinear behaviour of a power amplifier with the input signal $V_{in}(t)$ and the output signal $V_{out}(t)$ is given by (2.20) [4.2]-[4.3]. In practice (2.20) can be represented with sufficient accuracy using a finite number of terms, m :

$$V_{out}(t) = \sum_{n=1}^m g_n V_{in}^n(t) \quad (4.2)$$

The input signal in modern wireless communication systems is usually a high frequency carrier modulated with the amplitude $V_m(t)$ and phase $\varphi(t)$ and can be written as:

$$V_{in}(t) = V_m(t) \cdot \cos(\omega t + \varphi(t)) \quad (4.3)$$

As the quadrature modulation is commonly used, it is convenient to re-write the input signal in the Cartesian form by introducing the in-phase $I(t)$ and quadrature $Q(t)$ components:

$$V_{in}(t) = V \cdot [I(t) \cdot \cos(\omega t) - Q(t) \cdot \sin(\omega t)], \quad (4.4)$$

where V is the root mean square value of the modulating signal amplitude $V_m(t)$ expressed as:

$$V = \sqrt{\text{average}(V_m(t)^2)} \quad (4.5)$$

and the in-phase $I(t)$ and quadrature $Q(t)$ components are calculated using the following formulas:

$$I(t) = \frac{V_m(t)}{V} \cdot \cos(\varphi(t)) \quad (4.6)$$

$$Q(t) = \frac{V_m(t)}{V} \cdot \sin(\varphi(t)) \quad (4.7)$$

From (4.5)-(4.7) it can be shown that:

$$\text{average}(I^2(t) + Q^2(t)) = 1 \quad (4.8)$$

When (4.4) is substituted in (4.2) a lot of parasitic components will be generated. Those whose frequencies are different from the frequency of the input signal could be eliminated by the suitable filtering. Thus, focus is on the components of the same frequency as the input, in-band distortions. First, (4.2) is truncated to the initial three summands, e.g. $m = 3$ and then the substitution of (4.4) in (4.2) is carried out:

$$\begin{aligned} V_{out}(t) = & \frac{V^2 g_2}{2} \cdot (I^2(t) + Q^2(t)) + \\ & + \left[g_1 + \frac{3V^2 g_3}{4} \cdot (I^2(t) + Q^2(t)) \right] \cdot V_{in}(t) + \\ & + \frac{V^2 g_2}{2} \cdot [(I^2(t) - Q^2(t)) \cdot \cos(2\omega t) - 2 \cdot I(t) \cdot Q(t) \cdot \sin(2\omega t)] + \\ & + \frac{V^3 g_3}{4} \cdot [I(t) \cdot (I^2(t) - 3Q^2(t)) \cdot \cos(3\omega t)] - \\ & - \frac{V^3 g_3}{4} \cdot [Q(t) \cdot (3I^2(t) - Q^2(t)) \cdot \sin(3\omega t)] \end{aligned} \quad (4.9)$$

Therefore, the fundamental-frequency part of the output signal is:

$$V_{out}^{fund}(t) = \left[g_1 + \frac{3V^2 g_3}{4} \cdot (I^2(t) + Q^2(t)) \right] \cdot V_{in}(t), \quad (4.10)$$

or, equivalently:

$$V_{out}^{fund}(t) = g_1 \cdot V_{in}(t) + V_{3dist}^{fund}(t), \quad (4.11)$$

where $g_1 \cdot V_{in}(t)$ is the required output of the PA and $V_{3dist}^{fund}(t)$ is the in-band distortion component. We note that the in-band distortion was created by presence of the third-order component in (4.2). The same procedure could be used for deriving other odd-order distortion components, giving:

$$V_{(2k+1)dist}^{fund}(t) = b_{2k+1} V^{2k} g_{2k+1} (I^2(t) + Q^2(t))^k V_{in}(t), \quad (4.12)$$

where the coefficient b_{2k+1} is in form:

$$b_{2k+1} = \frac{(4k+1)!}{2^{4k+2} (2k+1)! (2k)!}, \quad k = 1, 2, 3, \dots \quad (4.13)$$

These coefficients are derived in [4.4]-[4.7]. Hence the fundamental-frequency output signal for any order of nonlinearity can be rewritten using the general formula:

$$V_{out}^{fund}(t) = g_1 \cdot V_{in}(t) + \left[\sum_{k=1}^m b_{2k+1} V^{2k} g_{2k+1} (I^2(t) + Q^2(t))^k \right] \cdot V_{in}(t) \quad (4.14)$$

in the in-band distortion components can be cancelled using for example a baseband injection of nonlinear components, like in [4.5]-[4.6] if the parameters g_{2k+1} of the PA nonlinearity are identified. The next subsection will briefly explain the basics of a baseband linearization method.

4.3. Theoretical analysis of the baseband linearization method

Nonlinearity of a power amplifier is expressed in the polynomial form (4.2). In order to compensate the distortion of a modulated signal, the analysis of I and Q components of the input signal is carried out in (4.3)-(4.9). A general representation of a distorted output signal at fundamental frequency is given in (4.14). The baseband linearization presented below is from [4.2], [4.5], [4.10]-[4.13]. Equation (4.14) can be rewritten:

$$V_{out}^{fund}(t) = \left[g_1 + \sum_{k=1}^{\infty} G_{2k+1}(t) \right] \cdot V_{in}(t), \quad (4.15)$$

where G_{2k+1} stands for:

$$G_{2k+1}(t) = b_{2k+1} V^{2k} g_{2k+1} (I^2(t) + Q^2(t))^k \quad (4.16)$$

For simplicity of explanation, a third order polynomial model is considered below:

$$V_{out}(t) = g_1 \cdot V_{in}(t) + g_2 \cdot V_{in}^2(t) + g_3 \cdot V_{in}^3(t) \quad (4.17)$$

The output signal at fundamental frequency in this case is a sum of the linearly amplified input signal and the in-band distortion component which is product of the third order nonlinearity:

$$V_{out}^{fund}(t) = g_1 \cdot V_{in}(t) + G_3(t) \cdot V_{in}(t), \quad (4.18)$$

where

$$G_3(t) = b_3 V^2 g_3 (I^2(t) + Q^2(t))^k \quad (4.19)$$

As described in [4.12]-[4.14], in order to compensate for the distortion which appears in the output signal (4.18), the input signal, called the predistorted signal, is:

$$V_{in}^{DPD}(t) = V_{in}(t) + \left(-\frac{G_3(t)}{g_1} \right) \cdot V_{in}(t) \quad (4.20)$$

The idea is to bring as an input signal a primary one with distortion component, with the opposite phase and the same amplitude. Driving such predistorted signal at the input, e.g. substituting (4.20) in (4.18), the initial distortion component is compensated, as shown below, but other distortion components are made:

$$V_{out}^{fund}(t) = g_1 \cdot V_{in}(t) \cdot \left[1 - 3 \cdot \left(\frac{G_3(t)}{g_1} \right)^2 + 3 \cdot \left(\frac{G_3(t)}{g_1} \right)^3 - \left(\frac{G_3(t)}{g_1} \right)^4 \right] \quad (4.21)$$

Being smaller than the initial one, the new distortion components, however, lead to degradation of the output signal. The first term in brackets in (4.21) represents the desired undistorted output signal, whereas the last three arise from the newly injected component and become the reason for the distortion compensation limit. Therefore, the iterative distortion component injection should be used, which will also compensate the newly generated distortion components, which cannot be ignored in the system with strong nonlinearity [4.3], [4.5]. The predistortion for the first iteration is given by (4.20). For m iterations general formula for the predistorted signal is obtained [4.3], [4.5]:

$$V_{in}^{DPD(m)}(t) = V_{in}(t) - \frac{\sum_{k=1}^p G_{2k+1}^{(m-1)}(t)}{g_1} \cdot V_{in}(t), \quad (4.22)$$

for which the output signal converges to the linearly amplified input signal.

$$V_{out}^{fund(m)}(t) = g_1 \cdot V_{in}(t) + \left(\sum_{k=1}^p G_{2k+1}^{(m-1)}(t) \right) \cdot V_{in}(t) \quad (4.23)$$

Coefficients $G_{2k+1}^{(m)}(t)$ for m iterations are defined as:

$$G_{2k+1}^{(m)}(t) = G_{2k+1}^{(m-1)}(t) \cdot \left(-1 + \left(1 - \frac{\sum_{l=1}^p G_{2l+1}^{(m-1)}(t)}{g_1} \right)^{2k+1} \right) \quad (4.24)$$

For the systems with strong nonlinearities, this technique is developed in its iterative form, including a compensation of all the original and introduced in-band distortion components. The computational complexity of this method is determined by the number of iterations m and the order of the PA model $n=2p+1$ [4.5]. A storage of complex LUTs is not required, only g and b coefficients need to be tabulated, the number of which is very small and depends on the model order n . b coefficients are described in

(4.13), which results in only g coefficients being unknown in order to proceed with the linearization. A robust estimation method for deriving these coefficients is proposed in further text.

4.4. Proposed robust method for estimation of nonlinear coefficients

In order to derive the values of g_{2k+1} from the experimental data we chose the input signal to have $\varphi(t)=0$ and the constant amplitude $V_m^i(t) = V_m^i$, where i is the experiment number.

$$V_{in}^i(t) = V_m^i \cdot \cos(\omega t) \quad (4.25)$$

Data will be derived from different experiments which includes the same type of the input signal, but with various amplitudes. As the input has the form (4.25), that results in:

$$I(t) = 1 \quad (4.26)$$

$$Q(t) = 0 \quad (4.27)$$

After substituting (4.26)-(4.27) in (4.14), we get:

$$V_{out}^{fund}(t) = g_1 \cdot V_{in}(t) + \left[\sum_{k=1}^m b_{2k+1} g_{2k+1} V_m^{i 2k} \right] \cdot V_{in}(t) \quad (4.28)$$

The power amplifier is excited by a single-tone signal. The corresponding output signal at the same frequency is a sinusoid with the amplitude $V_{out_amp}^{fund(i)}$, where i is the experiment number:

$$V_{out_amp}^{fund(i)} = \sum_{k=0}^{\frac{m-1}{2}} a_{2k+1} V_m^{i 2k+1}, \quad (4.29)$$

where coefficients a_{2k+1} are:

$$a_{2k+1} = b_{2k+1}g_{2k+1} \quad (4.30)$$

The coefficients a_{2k+1} of the nonlinear model (4.29) are estimated by minimization of criterion function. Once a coefficients are derived, g coefficients come from (4.30). By choosing the correct function we are able to achieve robustness of the modeling algorithm, which is important when the noise which affects the measuring has normal distribution, but is also very efficient if the distribution is not normal and has long tails, generating outliers. The least-square method seems to be a natural choice for their estimation if the signal is disturbed by a normal distribution. But this method is not suitable for the impulsive noise. Measured signals, as they come from a power supply, can be disturbed by the impulsive changes of current or voltage, especially if the electrical network is old, or close to a substation. In that case, the robust method will give a good estimation. The robust estimation theory represents a suitable tool for coping with an impulsive noise environment or with the outliers [4.15]-[4.17].

Criterion function arguments are the coefficients of the nonlinear model (4.29) $\theta^T = [a_1 \ a_3 \ \dots \ a_m]$. Therefore, a criterion function can be written as [4.18]-[4.19]:

$$J_n(\theta) = \frac{1}{n} \sum_{i=1}^n \rho(v(i, \theta)), \quad (4.31)$$

where $v(i, \theta) = y(i) - \hat{y}(i, \theta)$ is the output prediction error, $y(i)$ is the measured output of i -th experiment, and $\hat{y}(i, \theta)$ is the estimated output. n is the number of measured data, $n > m$, where m is the order of the PA nonlinearity. $\rho(\cdot)$ is a loss function, which in case of the maximum likelihood scheme (ML), is chosen as $\rho(\cdot) = -\ln p(\cdot)$, where $p(\cdot)$ is the noise probability density function (pdf). For the Gaussian noise $\rho(\cdot)$ is a quadratic function, but in order to make a more robust algorithm Huber [4.16] proposed that we use for our robust estimator the ML estimator associated with the pdf that is like a normal in the middle, but like a double exponential in the tails. The Huber's function $\rho(\cdot)$ is the ML loss function:

$$\rho(x) = -\ln(p(x)) = \begin{cases} \frac{x^2}{2\sigma^2}, & \text{if } |x| \leq k \\ \frac{k|x|}{\sigma^2} - \frac{k^2}{2\sigma^2}, & \text{if } |x| > k \end{cases} \quad (4.32)$$

where σ^2 is the noise variance. More precisely, this pdf represents the worst-case pdf, minimizing the maximum asymptotic estimation error variance, within the class of ε -contaminated normal pdf's [4.16], [4.19]. The tuning constant k depends on the contamination index ε , i.e. $k = k(\varepsilon)$ [4.16], [4.19]. The tuning parameter k in (4.32) has to be chosen so as to provide the desired efficiency at the nominal Gaussian observation model, say more than 90%. The derivative of the $\rho(\cdot)$ function in (4.32) is [4.15]-[4.16]:

$$\Psi(x) = \rho'(x) = \min\left(\max\left(\frac{x}{\sigma^2}, -\frac{k}{\sigma^2}\right), \frac{k}{\sigma^2}\right) \quad (4.33)$$

and is bounded and continuous. A recursive minimization of the nonlinear criterion in (4.31) can be performed, for example, applying the approximate Newton-Raphson-type method [4.18]:

$$\theta(i) = \theta(i-1) - [i\nabla_{\theta}^2 J_i(\theta(i-1))]^{-1} [i\nabla_{\theta} J_i(\theta(i-1))] \quad (4.34)$$

where ∇_{θ} is the partial derivative operator. Using approximation truth of the optimality conditions [4.20] and applying the matrix inversion lemma [4.18], the Gauss-Newton stochastic gradient-type algorithm is obtained:

$$\theta(i) = \theta(i-1) + \Gamma(i)Z(i)\Psi\left(v(i, \theta(i-1))\right); \theta(0) = \theta_0 \quad (4.35)$$

$$v(i, \theta(i)) = y(i) - Z^T \theta(i) \quad (4.36)$$

$$\Gamma(i) = \Gamma(i-1) - \frac{\Gamma(i-1)Z(i)Z^T(i)\Gamma(i-1)}{w^{-1} + Z^T(i)\Gamma(i-1)Z(i)} \quad (4.37)$$

$$\Gamma(0) = \gamma^2 I; \gamma = \text{const} \quad (4.38)$$

$$w \approx w(i) = \Psi\left(v(i, \theta(i-1))\right) \quad (4.39)$$

$$Z^T(i) = [x(i) \ x(i)^3 \ \dots \ x(i)^m] \quad (4.40)$$

$x(i)$ is the input sample of i -th experiment. Since the influence function Ψ in is not differentiable, a common approximation of its derivative is $\Psi(x) \approx \frac{\Psi(x)}{x}$. By choosing adequate initial values for $\theta(0)$, which is usually a result observed with the least square (LS) procedure, and $\Gamma(0)$, it is possible to make a robust estimated nonlinear model which will provide more accurate characteristic than, for example, simple LS procedure.

4.5. Experimental validation of the proposed estimation method

In case of extracting a model from AM/AM characteristic, the power amplifier is excited by a single-tone signal with the discretely varying magnitude V_m^i and the corresponding maximum output signal magnitude at the same frequency $V_{out_amp}^{fund(i)}$ is measured, where i is the number of the experiment. The Figure 4-1 presents the experimental setup used for measurements.

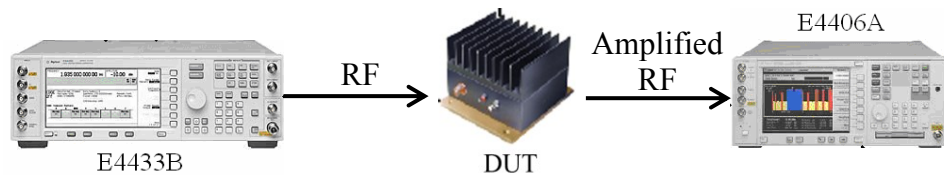


Figure 4-1: The experimental setup for data collection

Using the setup shown in the Figure 4-1, the output power is measured. The setup consist of the Agilent E4433B signal generator used to provide the single-tone signal at 751MHz frequency; the Agilent E4406A vector signal analyser for measuring the power of the output signal; the 27dB gain Mini-Circuits ZHL-1042J power amplifier with 1dB compression point at the 26dBm output power level. The input RF tone at the frequency of 751 MHz has been generated and passed thought the PA at different power levels and further transferred to the vector signal analyser for measurements. The input voltage

data are derived from input power levels, and equivalently, the output voltage data are derived from corresponding measured output power levels.

First task was to estimate the order of the polynomial model. This can be estimated by the number of harmonics appearing at the maximum operational power level. An example of frequency response of a power amplifier is shown in the Figure 4-2. In this experiment, the PA is intended to be used at the power level of its 1dB compression point, and at this level, the PA generates five harmonics. Thus we take the fifth order model.

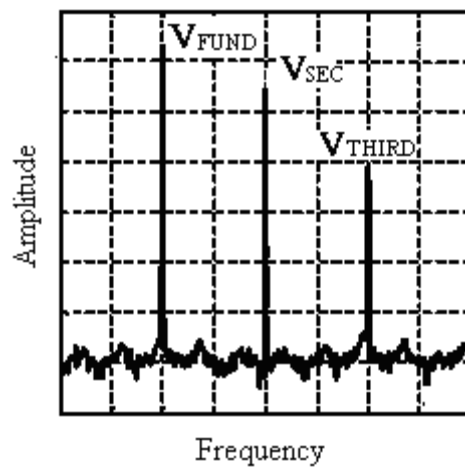


Figure 4-2: An example of single-tone frequency response of a power amplifier in saturation

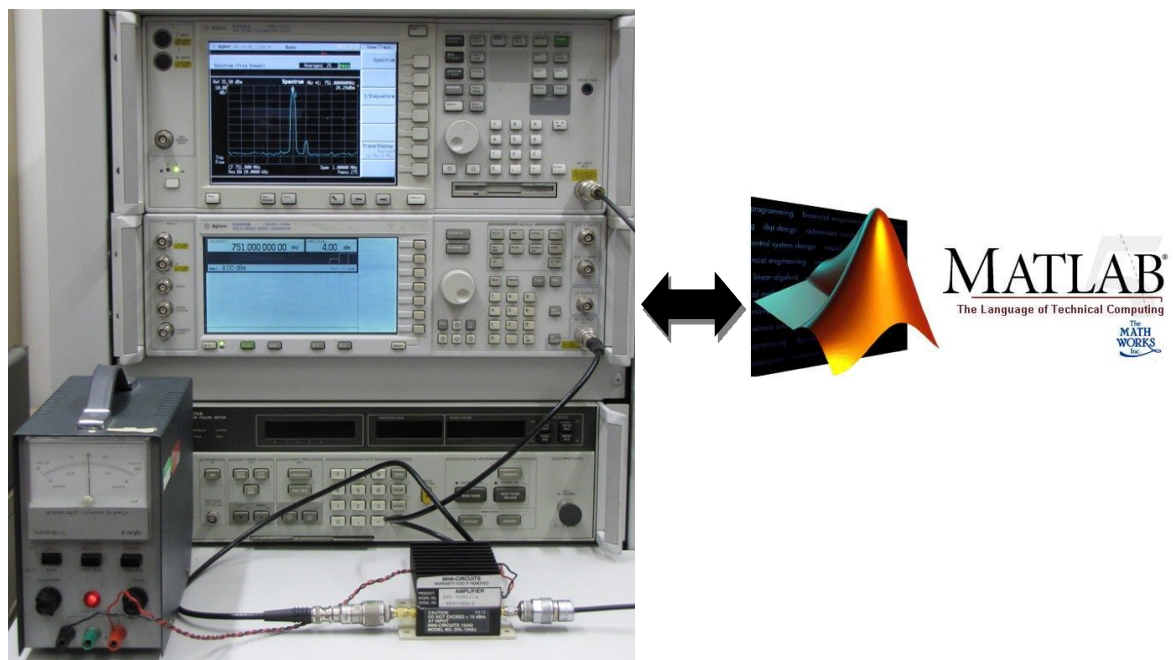


Figure 4-3: The experimental setup for PA characterisation

First, the input-output dataset from the experiment was transferred to PC with MATLAB software used for implementation of the described algorithm and offline processing of the data (Figure 4-3). The signal with strategically-chosen non-Gaussian distribution was added to the output data and after that the LS algorithm is run, for comparison with the proposed method. Later on, the explained estimation procedure is run, with initial values for θ acquired from the first algorithm and parameters $\gamma = 0.0001$ and $k = 0.75$ tuned to make a more accurate model. The input-output data, measured during the experiments, is given in the Table 4.1.

Table 4.1: Power levels from the experiment

Pin [dBm]	Pout [dBm]
-30	-2.01
-25	2.99
-20	7.98
-15	12.99
-10	18
-5	22.85
-4.5	23.3
-4	23.73
-3.5	24.13
-3	24.51
-2.5	24.89
-2	25.26
-1.5	25.58
-1	25.89
-0.5	26.08
0	26.2
1	26.3
2	26.33
3	26.34
4	26.26
5	26.16
6	26.03
7	25.93
8	25.83
9	25.75
10	25.73

From measured values a different number of samples n , $n > m$ (m is the order of nonlinearity equal to 5) was used for calculations with both algorithms. The Figures 4-4 and 4-5 present the results for 11 and 19 data, respectively.

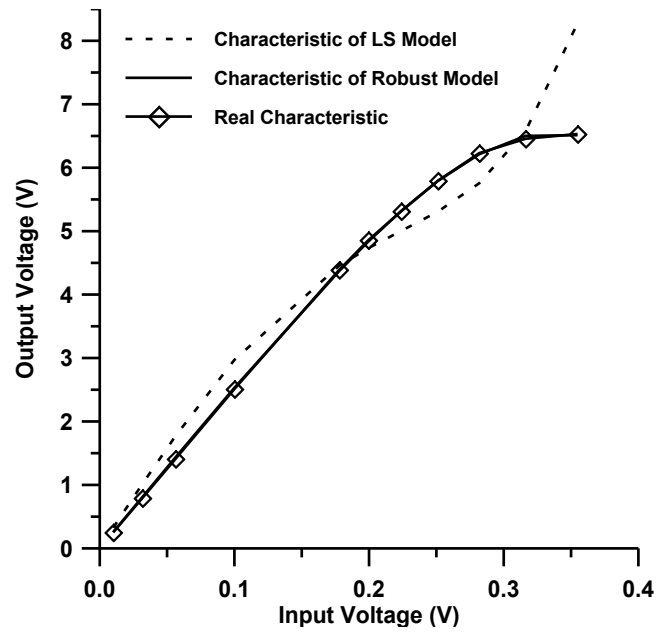


Figure 4-4: AM/AM characteristics of the measured and modelled PA ZHL-1042J at a 751 MHz carrier (11 data samples)

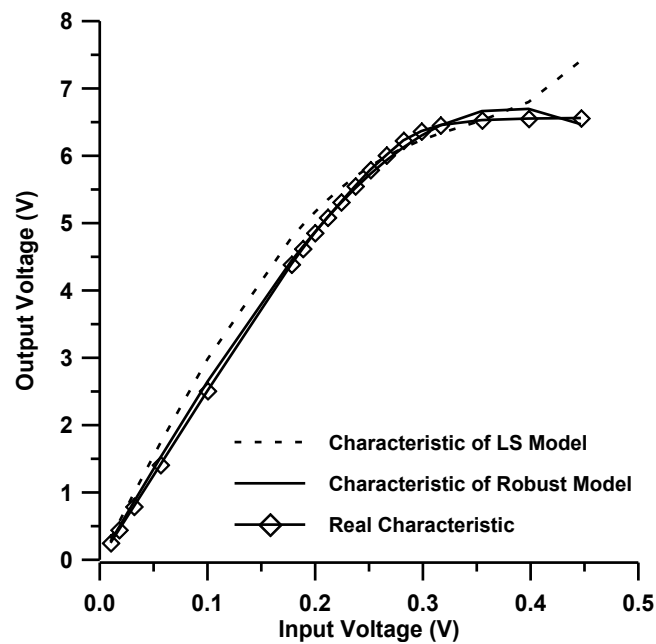


Figure 4-5: AM/AM characteristics of the measured and modelled PA ZHL-1042J at a 751 MHz carrier (19 data samples)

The Figures 4-4 and 4-5 show that in an impulsive noise environment the LS algorithm will not give acceptable results. If the DUT is in such environment it is

difficult to make an accurate model using the simple least squares (LS) method, as the correct LS result requires a lot of measured data, which is time-consuming, taking into account that the experiments require some time for one measure, and the goal was to make fast identification. That is why the robust method is better and therefore used for behavioural modelling of the PA. Secondly, it is proven that the proposed algorithm for parameters estimation gives a good outcome for further developing of the linearization technique, as a good model is required for the efficient linearization.

4.6. Conclusion

The proposed approach deploys a black-box modelling technique that utilises the data obtained from the experimentations with the modelled system. In particular we have addressed the issue of the data being corrupted by an impulsive noise and demonstrated that the method we propose is much more robust than the competing approach based on the least squares estimation. A very good agreement between modelled and experimental result has been obtained. In the next chapters the artificial intelligence system methods will be proposed, as these have very good ability to track nonlinear dynamics of a power amplifier. But they are nonlinear-based techniques. The method presented in this chapter uses a linear-based method, where output is presented as the linear function of the power functions of the input signal. Thus in the next chapter, a partial least squares method, as one of the linear-based methods, will be used for comparison with nonlinear-based ones.

4.7. References

- [4.1] J. C. Pedro, and S. A. Maas, "A comparative overview of microwave and wireless power-amplifier behavioral modeling approaches", *IEEE Transactions on Microwave Theory and Techniques*, vol. 53, no. 4, pp. 1150-1163, April 2005.
- [4.2] D. Bondar, and D. Budimir, "WiMax power amplifier linearization through injection of base-band component", in *Proc. 11th Int. Symp. Microw. Opt. Technol.*, Rome, pp. 293-297, December 2007.

- [4.3] N. Mizusawa, and S. Kusunoki, "Third- and fifth-order baseband component injection for linearization of the power amplifier in a cellular phone", *IEEE Trans. Microw. Theory Tech.*, vol. 53, no. 4, pp. 3327-3334, April 2005.
- [4.4] D. Bondar, D. Budimir, and B. Shelkovnikov, "A new approach for nonlinear analysis of power amplifiers", in *Proc. 18th Int. Crimean Conf. Microw. and Telecommun. Technology*, Sebastopol, Ukraine, vol. 1, pp. 125-128, September 2008.
- [4.5] D. Bondar, and D. Budimir, "A digital predistorter for wireless transmitters", *International Journal of RF and Microwave Computer-Aided Engineering*, 2009.
- [4.6] D. Bondar, and D. Budimir, "Digital baseband predistortion of wideband power amplifiers with improved memory effects", *IEEE Radio and Wireless Symposium*, pp. 284-287, January 2009.
- [4.7] M. Vaskovic, D. Bondar, Z. Djurovic, D. Budimir, "Analytical calculation of predistorter coefficients for any order of nonlinear distortion", *ETTRAN conference*, Donji Milanovac, Serbia, June 2010.
- [4.8] F. Perez, E. Ballesteros, J. Perez, "Linearisation of microwave power amplifiers using active feedback networks", *IEE Electronics Letters*, vol. 21, no. 1, pp. 9-10, January 1985.
- [4.9] M. Faulkner, "Amplifier linearization using RF feedback and feedforward techniques", *IEEE Transactions on Vehicular Technology*, vol. 47, pp. 209-215, February 1998.
- [4.10] J. C. Pedro and N. B. Carvalho, *Intermodulation Distortion in Microwave and Wireless Circuits*, Artech House, Norwood, 2003.
- [4.11] N. Mizusawa, and S. Kusunoki, "Third- and fifth-order baseband component injection for linearization of the power amplifier in a cellular phone", *IEEE Trans. Microw. Theory Tech.*, vol. 53, no. 4, pp. 3327-3334, April 2005.
- [4.12] G. Palumbo, and S. Pennisi "High-frequency harmonic distortion in feedback amplifiers: analysis and applications", *IEEE Transactions on Circuits and Systems-I: Fundamental Theory and Applications*, vol. 50, no. 3, pp. 328-340, March 2003.
- [4.13] N. B. De Carvalho, and J. C. Pedro, "Compact formulas to relate ACPR and NPR to two-tone IMR and IP3", *Microwave Journal*, vol. 42, no. 2, pp. 70-84, December 1999.

- [4.14] F. Perez, E. Ballesteros, J. Perez, "Linearisation of microwave power amplifiers using active feedback networks", *IEE Electronics Letters*, vol. 21, no. 1, pp. 9-10, January 1985.
- [4.15] W. N. Venables, and B. D. Ripely, *Modern Applied Statistics with S*, Springer, Berlin, 2002.
- [4.16] P. J. Huber, *Robust Statistics*, John Wiley, New York, 1981.
- [4.17] V. D. Barnett, and T. Lewis, *Outliers in Stochastic Data*, John Wiley, New York, 1978.
- [4.18] L. Ljung, and T. Soderstrom, *Theory and Practice of Recursive Identification*, MIT Press, Cambridge Mass, 1983.
- [4.19] Y. Z. Tsypkin, *Foundations of informational identification theory*, Nauka, Moscow, 1984.
- [4.20] V. Z. Filipovic, and B. D. Kovacevic, "On robust AML Identification Algorithms", *Automatica*, pp. 1775-1778, 1994.

5. MODELING AND PREDISTORTION OF POWER AMPLIFIERS USING NEURAL NETWORKS

5.1. Introduction

Linearization of power amplifiers is especially important when complex modulation procedures are used, such as orthogonal frequency-division multiplexing (OFDM). PAs are used close to saturation, in order to achieve a maximum output power. In that working range, OFDM signals are very sensitive to the PA nonlinear distortion. Digital predistortion techniques are widely used as the most cost-effective solutions for compensation of distortion effects [5.1]. Analogue techniques require vast hardware components to be employed in base stations. Using the DPD techniques, an inverse model of power amplifier behaviour can be derived, and in cascade with the PA makes the system with more or less improved linearization, depending on a method. The behavioural modelling methods mentioned in the Chapter 2.4 are also used for gaining the inverse models and predistortion procedures. Mostly used during the last decade are neural networks, as it has ability to adjust to different conditions [5.2]. As the LTE systems are going to be a state-of-the-art mobile communication solution in the future [5.3], modelling of the power amplifier behaviour and its linearization are important goals.

This chapter presents modelling and predistortion of the power amplifier MIMIX CFH2162-P3 using neural networks, and gives conclusions about advantages and disadvantages of this adaptive procedure.

5.2. Neural Network Models – Literature Overview

During last twenty years, few implementations of neural networks for modelling power amplifiers were explored. Depending on the network structure and its complexity the results can be more or less acceptable for implementation in real systems.

Some authors use the systems based on two separated networks [5.4]-[5.6]. One network is used for the dynamic AM/AM characterization, while the other one represents the AM/PM characteristic of DUT (Figure 5-1). A training dataset for supervised learning consists of an input dataset and desired output dataset, used for parameters update during the training procedure. If the training dataset have only real-valued samples, the parameters of the network will be also real. Such NNs are called real-valued neural networks (RVNNs). The structure from the Figure 5-1 consists of two RVNNs.

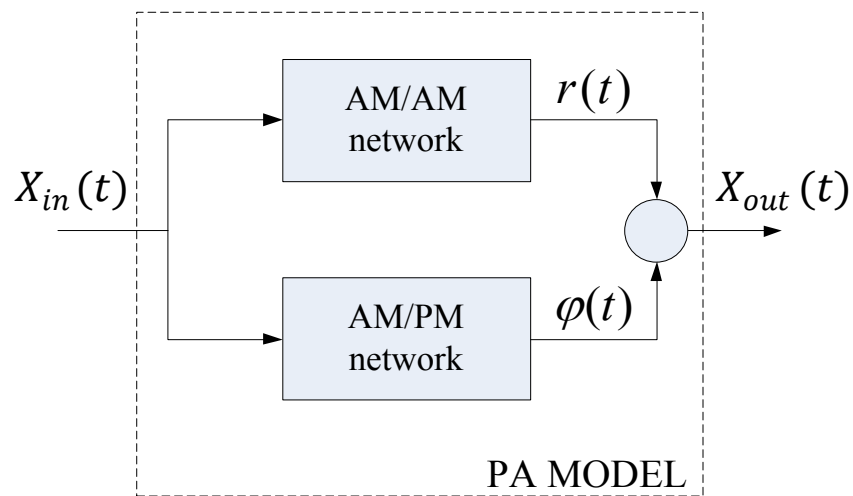


Figure 5-1: Power amplifier model structure with two separate networks

Training the dataset for AM/AM NN contains the amplitude of the PA input signal as the network training input, and the amplitude of the PA output signal as the desired output. The other network, AM/PM, has the training dataset composed of the amplitude of the PA input signal as the network training input, and the phase difference between the output and input signals of the PA as the desired output. Once the networks are trained, they are put in a parallel, creating a model of DUT. The AM/AM network will give the amplitude of the output signal $r(t)$, while the AM/PM network will give the phase of the output signal $\varphi(t)$. Their summation makes the overall NN power amplifier model output. The main drawback of this type of modelling is the convergence time of these two NNs. Thus the solution can be found in only one network mimicking the PA behaviour.

Other authors use one network for the behavioural modelling of a PA, but with complex input and output values (Figure 5-2), which makes the training procedure and network structure more complex [5.7]-[5.10].

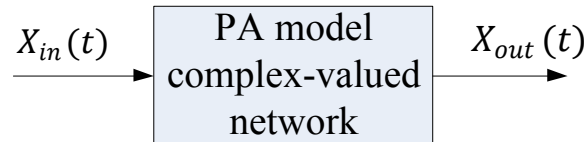


Figure 5-2: Power amplifier model structure with one complex-valued network

This model structure has complex parameters, e.g. network weights and biases, as the training dataset have complex samples. The training input in this case is the PA input signal $X_{in}(t)$, and the desired output is the complex output signal of the PA. In this case the training procedure is more time-consuming than the training of RVNNs.

Mostly used networks in last decade are the real-valued neural networks with multiple inputs and two outputs, using the different structures [5.1], [5.11]-[5.12]. The advantage of availability of the baseband in-phase $I(t)$ and quadrature $Q(t)$ components of the complex signal, which are real-valued data, is in avoiding necessity for the complex-valued NNs, or more separated NNs. Thus the network weights and biases are real values and the activation functions are also real.

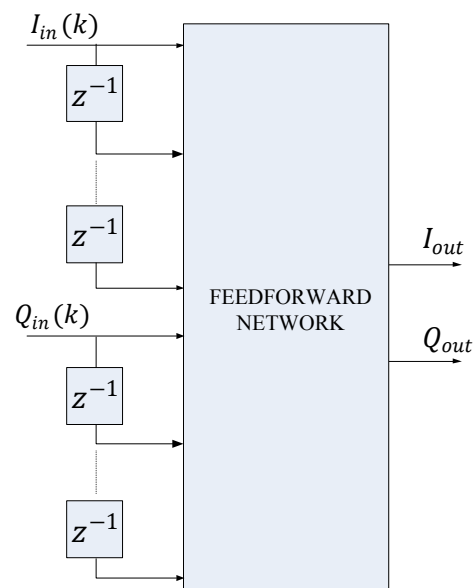


Figure 5-3: Feedforward real-valued neural network with multiple inputs and two outputs

In the dynamic systems with memory, RVNN with two inputs and two outputs cannot give good results, as the nonlinear output is not only dependent on the current time samples, but also on the previous time samples of the input signal. In order to

incorporate the memory effects existing in the PA behaviour RVNNs have to be recurrent. But, as it was mentioned in the Chapter 3, a recurrent network requires more time for training, and sometimes suffers from instability. Therefore, a feedforward network structure is used, with the time delayed inputs I and Q (Figure 5-3). These networks are called real-valued time-delay neural networks (RVTDNNs). Authors who confronted the PA modelling and predistortion problem so far [5.4]-[5.14], used RVTDNNs that have all linear activation functions in the output layer neurons. Unlike other authors, here we propose a NN structure with nonlinear activation functions in every output layer neuron.

5.3. Proposed Neural Network Structure

The Figure 5-4 shows the proposed structure for modelling a PA behaviour, and also for modelling of an inverse PA characteristic. It consists of $n + m + 2$ inputs, which are: one current in-phase component $I_{in}(k)$, its n delayed samples, one current quadrature component $Q_{in}(k)$ and its m delayed samples. The network is fully connected, as we cannot distinguish some of the modulation components. The number of hidden layers is two, and that was found as the most appropriate for this type of a nonlinear system during simulation tests of different structures, and also it is the type of network used in the literature, with regards to the number of layers. k_1 is the number of neurons in the first hidden layer, while k_2 is number of neurons in the second hidden layer.

The complex input signal in the time sample k has the Cartesian form:

$$X_{in}(k) = I_{in}(k) + j \cdot Q_{in}(k), \quad (5.1)$$

where $I_{in}(k)$ and $Q_{in}(k)$ are real values. The network outputs depend on network inputs:

$$\begin{bmatrix} I_{out}(k) \\ Q_{out}(k) \end{bmatrix} = \begin{bmatrix} f_I(I_{in}(k), I_{in}(k-1), \dots, I_{in}(k-n), Q_{in}(k), Q_{in}(k-1), \dots, Q_{in}(k-m)) \\ f_Q(I_{in}(k), I_{in}(k-1), \dots, I_{in}(k-n), Q_{in}(k), Q_{in}(k-1), \dots, Q_{in}(k-m)) \end{bmatrix} \quad (5.2)$$

$f_I(\cdot)$ and $f_Q(\cdot)$ are overall transfer functions.

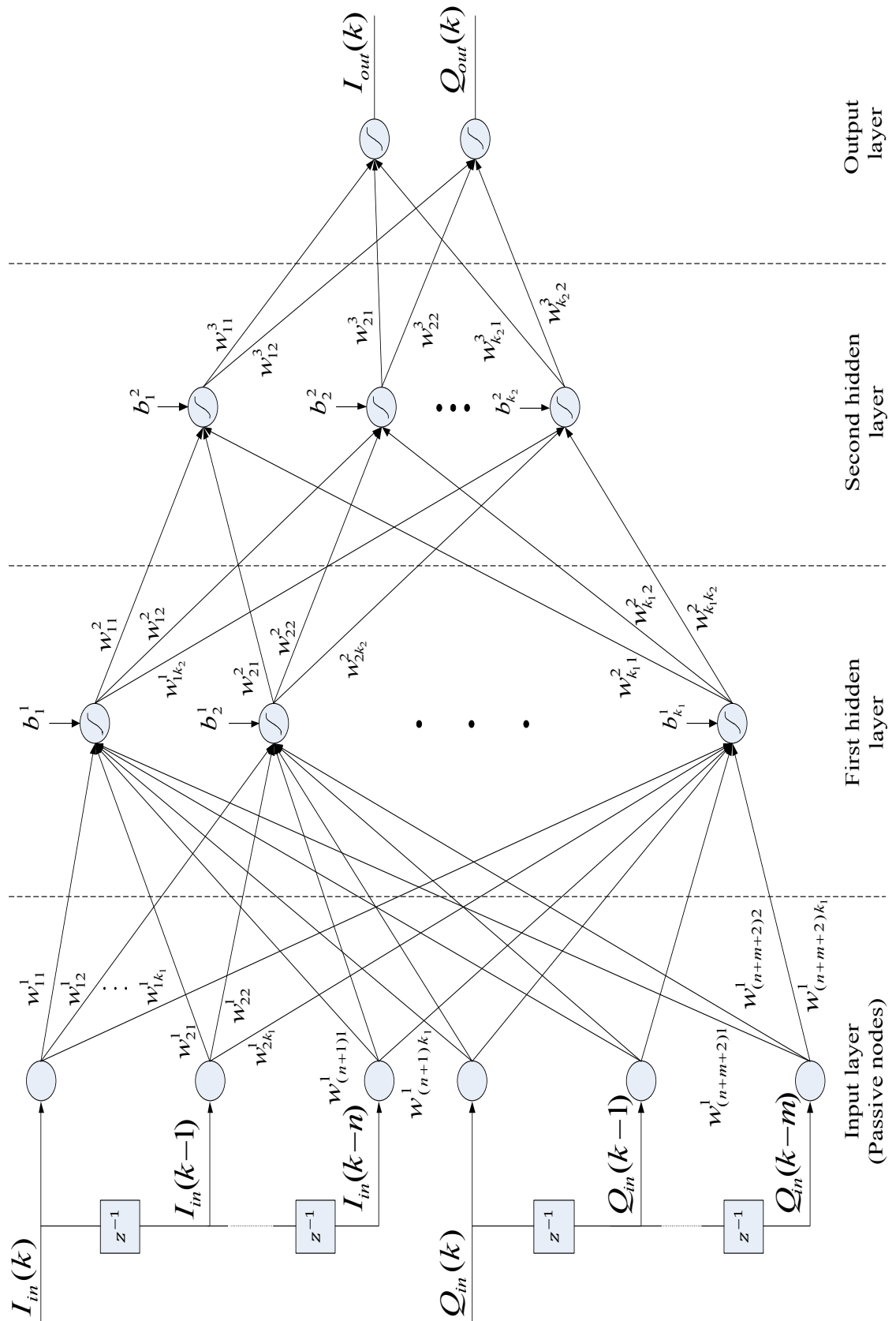


Figure 5-4: Proposed neural network structure for modelling

Through the next equations transfer functions will be derived. w_{ij}^l is the weight connecting i -th input with j -th neuron in l -th layer. b_j^l is the bias for j -th neuron in l -th layer. The output of the j -th neuron in the first layer will be:

$$out_j^1(k) = \text{Logsig} \left(b_j^1 + \sum_{r=0}^n w_{(r+1)j}^1 I_{in}(k-r) + \sum_{p=0}^m w_{(n+p+2)j}^1 Q_{in}(k-p) \right), \quad (5.3)$$

where $\text{Logsig}(\cdot)$ is log-sigmoid function defined in (3.4), and $j = 1, 2, \dots, k_1$. Similarly, the output of j -th neuron in the second hidden layer is described by:

$$out_j^2(k) = \text{Logsig} \left(b_j^2 + \sum_{r=1}^{k_1} w_{rj}^2 out_r^1(k) \right) \quad (5.4)$$

And finally, the outputs of the network are:

$$I_{out}(k) = \text{Logsig} \left(b_1^3 + \sum_{r=1}^{k_2} w_{r1}^3 out_r^2(k) \right) \quad (5.5)$$

$$Q_{out}(k) = \text{Logsig} \left(b_2^3 + \sum_{r=1}^{k_2} w_{r2}^3 out_r^2(k) \right) \quad (5.6)$$

The final functions are nonlinear functions, which include the delayed input samples for the memory tracking, and nonlinear activation functions which enable nonlinear modelling.

5.4. Neural Network Forward Model of Power Amplifier

5.4.1 Experimental Data Collection

The first step in modelling procedure is collection of the datasets for training. The proper data will provide good training and a good model. The test-bed for measurements is shown in the Figure 5-5. The setup consists of the signal generator Agilent MXG N5182A, the device under test (DUT) power amplifier MIMIX CFH2162-P3, with 1dB compression point at 27 dBm output power level, the vector signal analyser (VSA) Agilent E4406A and PC with adequate software. An attenuator of 30 dB attenuation was added after the amplifier, in order to make the signals appropriate for the VSA. The software used for these measurements contains MATLAB, for creating baseband signals for the signal generator; Agilent Signal Studio Toolkit, for assistance in the downloading process; and Agilent Distortion Suite 89604A for capturing the signals from the VSA to PC.

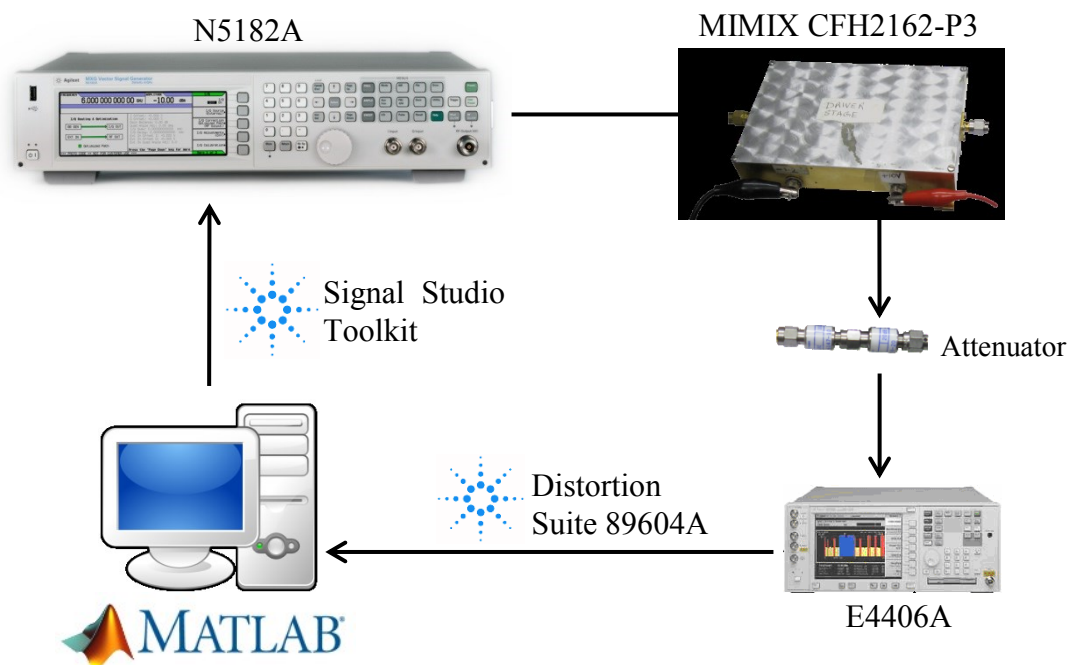


Figure 5-5: The experimental setup for data collection

The overall hardware system is implemented in the Wireless Communications Research Group laboratory at the University of Westminster and is presented in the Figure 5-6.

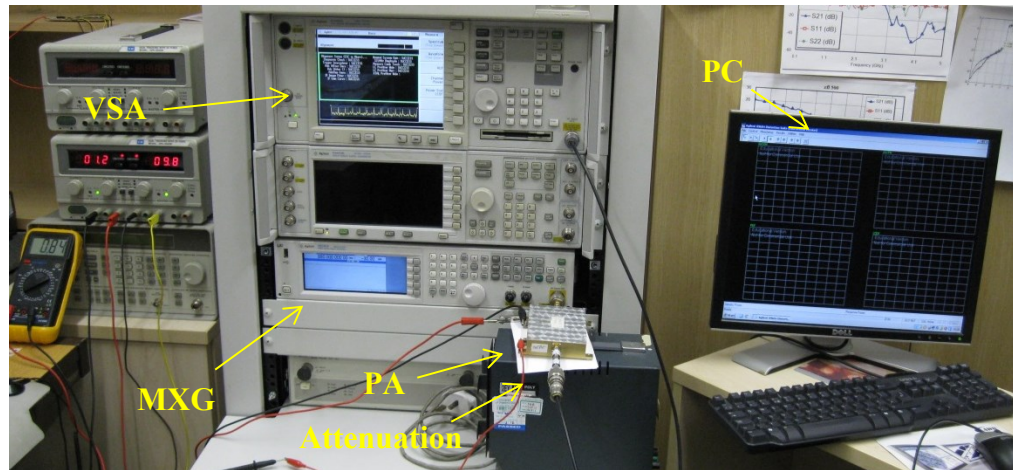


Figure 5-6: The hardware test-bench

Signals used as excitation of the DUT are the LTE 1.4 MHz 64 QAM and LTE 3 MHz 64 QAM signals created in MATLAB environment. After that the signal was downloaded to the MXG via General Purpose Interface Bus (GPIB) where it has been up-converted to the RF frequency of 880 MHz. Measurements were carried out at power level of 1dB compression point. Downloading process was performed by Agilent Signal Studio Toolkit assistance. The signal at the output of MXG was passed through the device under test. In order to capture the signal at the output of the DUT, an attenuator of 30dB was added. The signal was down-converted by VSA and captured on PC with Distortion Suite 89604A. The measurements were made for a system without a power amplifier and a system with an amplifier. The measured signals were transferred from the distortion suite to MATLAB for further processing and analysis.

5.4.2 Training the Neural Network with collected data

After the measurement procedure is completed, next step is the preparation of the collected data for the training process. In MATLAB environment the input and output signals are scaled in to the range [0.1, 0.9]. Normally a scaling range would be from 0 to 1. But, since the signal used for the training and the signal for testing can be in different

ranges, in case that the network has to extrapolate in order to track these differences, free sub ranges are left. Delayed inputs, e.g. training dataset with current and delayed I and Q are also created in MATLAB.

Once we prepare the signals for training, finding an optimal network structure in terms of the number of neurons in the layers and finding network training parameters starts. This procedure is based on trial and error, where the performance of the network is observed through the normalised mean square error (NMSE) which combines errors of both complex signal components, I and Q :

$$NMSE_{dB} = 10 \cdot \log_{10} \left(\frac{\sum_{n=1}^K (I_{meas}(n) - I_{est}(n))^2 + (Q_{meas}(n) - Q_{est}(n))^2}{\sum_{n=1}^K (I_{meas}(n)^2 + Q_{meas}(n)^2)} \right), \quad (5.7)$$

where I_{meas} and Q_{meas} are measurements of the baseband output signal, while I_{est} and Q_{est} are a model output signals. The NMSE is the mostly used parameter in the optimisation process [5.1], [5.11]-[5.14], which tells the user if the model is acceptable or not.

Conventional statistical measures for estimators are the mean square error (MSE) and root mean square error (RMSE), defined in (5.8) and (5.9). These performance parameters can be used for one component, I or Q . Thus the NMSE is much more convenient as a performance of the complete system.

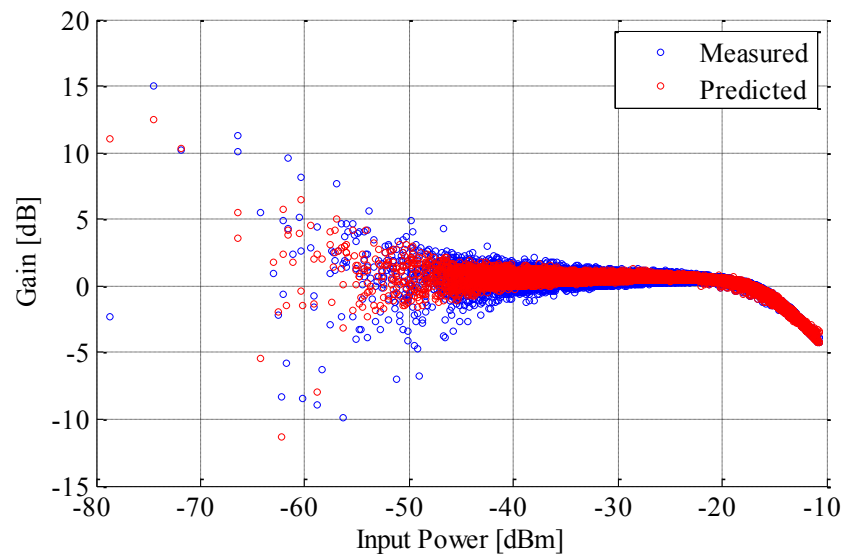
$$MSE = \frac{\sum_{n=1}^K (X_{meas}(n) - X_{est}(n))^2}{K} \quad (5.8)$$

$$RMSE = \sqrt{\frac{\sum_{n=1}^K (X_{meas}(n) - X_{est}(n))^2}{K}} \quad (5.9)$$

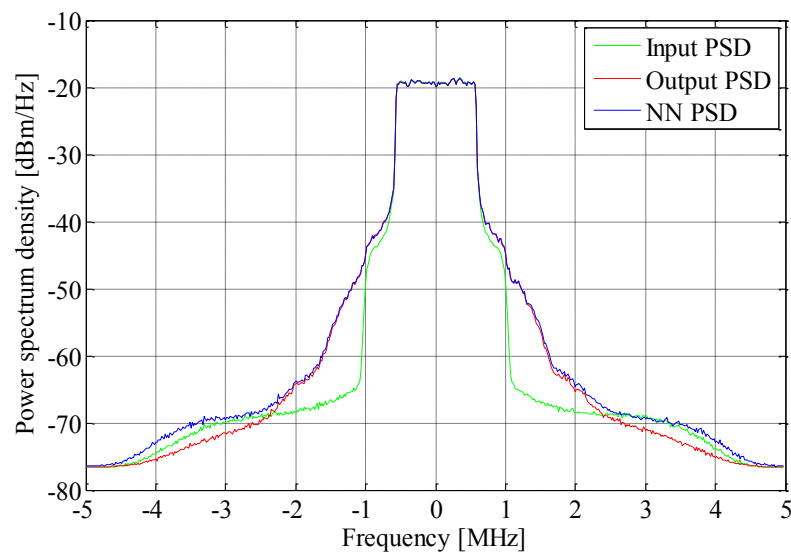
X_{meas} is the measured value of the in-phase or quadrature complex signal component, X_{est} is the estimated value, and K is the number of the data used for the model testing.

The network structure found as the most appropriate for this problem has an equal number of delay taps ($n = m$) for the I and Q components and has 20 nodes in the first, and 12 nodes in the second hidden layer. The memory depth is 3, so the network has

eight inputs. The learning rate for the training is $\alpha = 0.1$ while the momentum has the value $\eta = 0.2$. 30000 (30K) data were used for training the network. And once the training was complete, 100K data were used for testing the NN model. NMSEs for testing were -38.28dB for the LTE 1.4 MHz 64 QAM signal and -38.29dB for the LTE 3 MHz 64 QAM signal. Due to the complex modulation of signals, PAPR is 9.92dB for the LTE 1.4 MHz 64 QAM signal and 9.3dB for the LTE 3 MHz 64 QAM signal. The Figures 5-7 and 5-8 show the modelling results for the LTE 1.4 MHz 64 QAM and LTE 3 MHz 64 QAM signals, respectively.



a)



b)

Figure 5-7: Forward model results at 880 MHz: a) PA gain for the LTE 1.4 MHz 64 QAM signal; b) Power spectrum density of the RVTDNN model output vs. the real PA output for the LTE 1.4 MHz 64 QAM signal

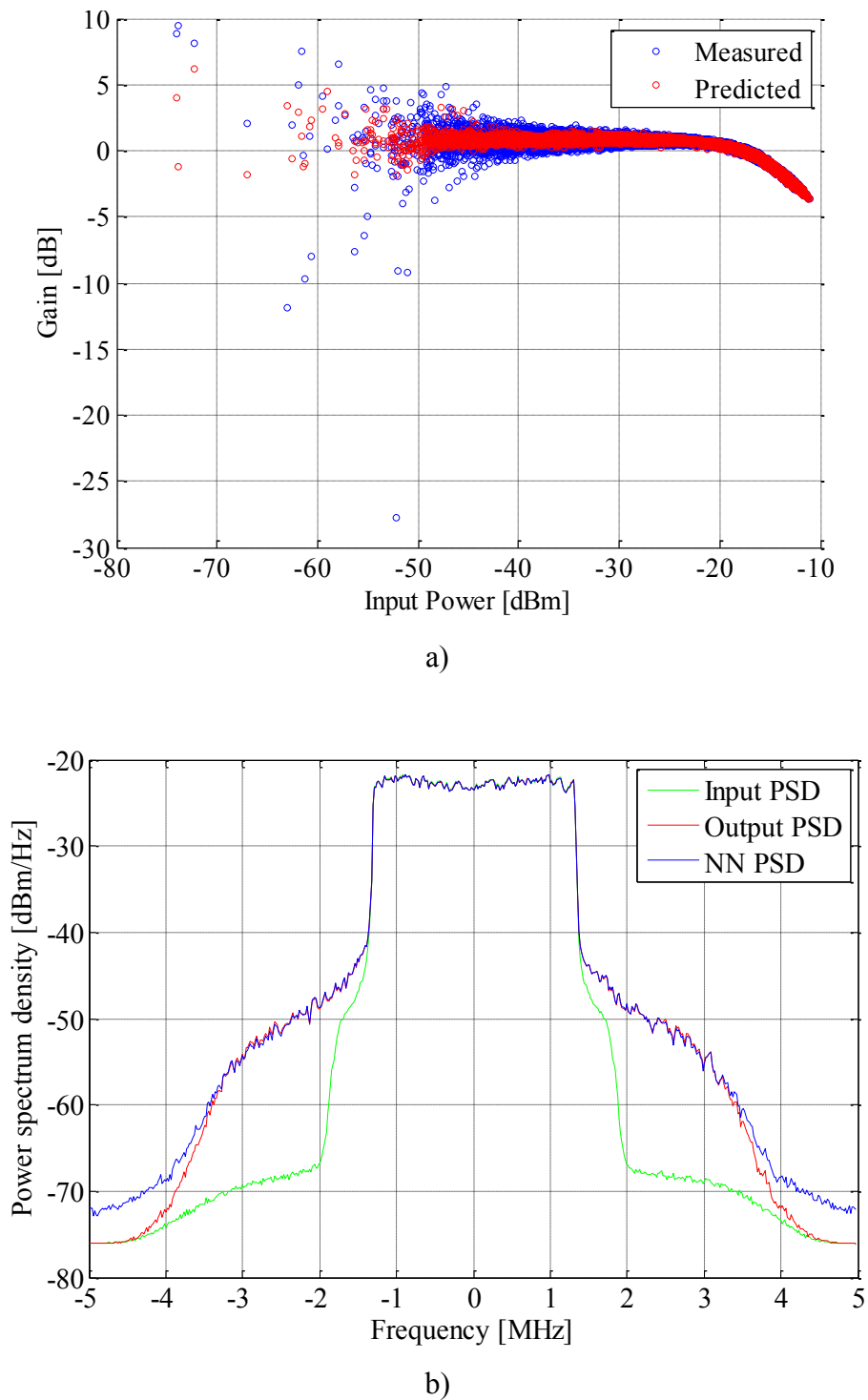


Figure 5-8: Forward model results at 880 MHz: a) PA gain for the LTE 3 MHz 64 QAM signal; b) Power spectrum density of the RVTDNN model output vs. the real PA output for the LTE 3 MHz 64 QAM signal

The Tables 5.1 and 5.3, given below, show parameters of the achieved models for the LTE 1.4 MHz 64 QAM signal and LTE 3 MHz 64 QAM signal, respectively. As can be seen from these results, the models for both signal bandwidths are very good. EVMs for the real output signals, and the output signals from the NN forward models are almost equal. ACPRs also show that the models are accurate enough. The difference between EVMs for the 1.4MHz signal and 3MHz signal is due to a different behaviour of the power amplifier for these two signal types. A signal is more distorted if it is wider, but PAPR is worse for a signal with smaller bandwidth. The Tables 5.2 and 5.4 show the statistical performances of the developed forward models for the LTE 1.4 MHz 64 QAM signal and LTE 3 MHz 64 QAM signal.

Table 5.1: Forward model performances compared with performances of real input and output for the LTE 1.4 MHz 64 QAM signal at 880 MHz centre frequency

	ACPR [dBc] ±1.4 MHz offset		EVM [%]
	LOW	HIGH	
PA input	-36.22	-34.30	/
Real PA	-30.90	-30.02	8.66
NN model	-30.85	-30.00	8.58

Table 5.2: Forward model statistical performances for the LTE 1.4 MHz 64 QAM signal at 880 MHz centre frequency

NMSE [dB]	-38.28	
MSE	<i>I</i>	6.34e-07
	<i>Q</i>	6.35e-07
RMSE	<i>I</i>	7.96e-04
	<i>Q</i>	7.97e-04

Table 5.3: Forward model performances compared with performances of real input and output for the LTE 3 MHz 64 QAM signal at 880 MHz centre frequency

	ACPR [dBc] ±3 MHz offset		EVM [%]
	LOW	HIGH	
PA input	-40.96	-39.50	/
Real PA	-29.66	-29.39	9.79
NN model	-29.64	-29.36	9.71

Table 5.4: Forward model statistical performances for the LTE 3 MHz 64 QAM signal at 880 MHz centre frequency

NMSE [dB]	-38.29	
MSE	<i>I</i>	6.73e-07
	<i>Q</i>	6.62e-07
RMSE	<i>I</i>	8.21e-04
	<i>Q</i>	8.13e-04

5.5. Neural Network Inverse Model of Power Amplifier

The same data collected for the neural network forward model of the DUT is used for inverse characterisation of a power amplifier. Idea is to create a neural network which will act in opposite of a PA. In cascade, an overall transfer function should be linear in the used frequency range and for that type of the signal. The inverse model of the power amplifier is trained with the same learning procedure, with the reverse input-output training set. The input signal is the desired output in this case, and the output baseband signal is the training dataset for the neural network. The network structure for the inverse problem has the memory depth 4 and has 15 nodes in the first and 6 nodes in the second hidden layer. The learning rate for the training is $\alpha = 0.1$ and the momentum is $\eta = 0.2$, same as for the forward model. 30000 (30K) data were used for training the networks and 100K data for testing the NN inverse models. NMSEs for testing were -36.67dB for the LTE 1.4 MHz 64 QAM signal and -37.4dB for the LTE 3 MHz 64 QAM signal. The Figures 5-9 and 5-10 show the inverse modelling results for the LTE 1.4 MHz 64 QAM and LTE 3 MHz 64 QAM signals, respectively.

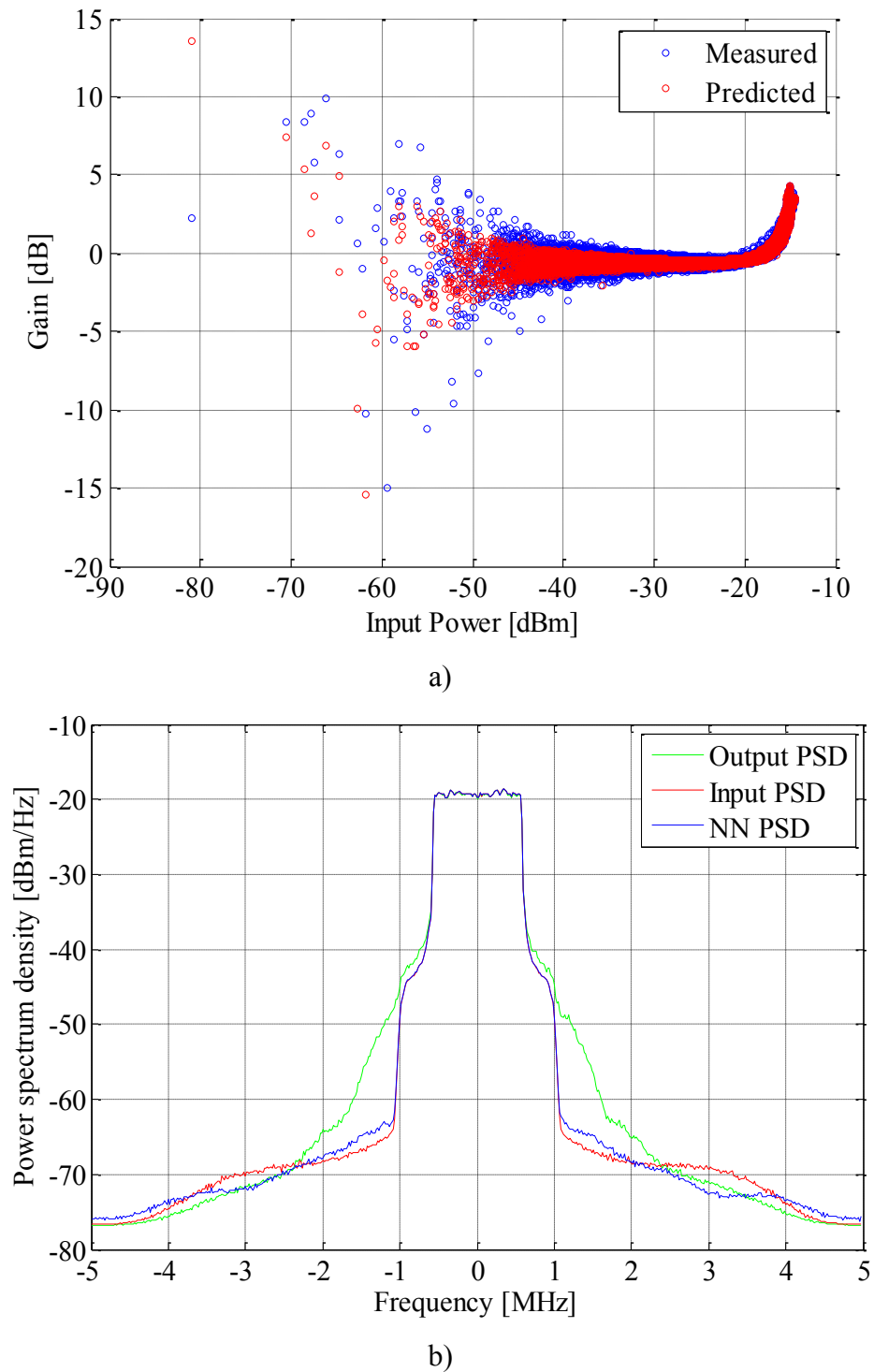


Figure 5-9: Inverse model results at 880 MHz: a) Inverse PA gain for the LTE 1.4 MHz 64 QAM signal; b) Power spectrum density of the RVTDNN model output vs. the real PA input for the LTE 1.4 MHz 64 QAM signal

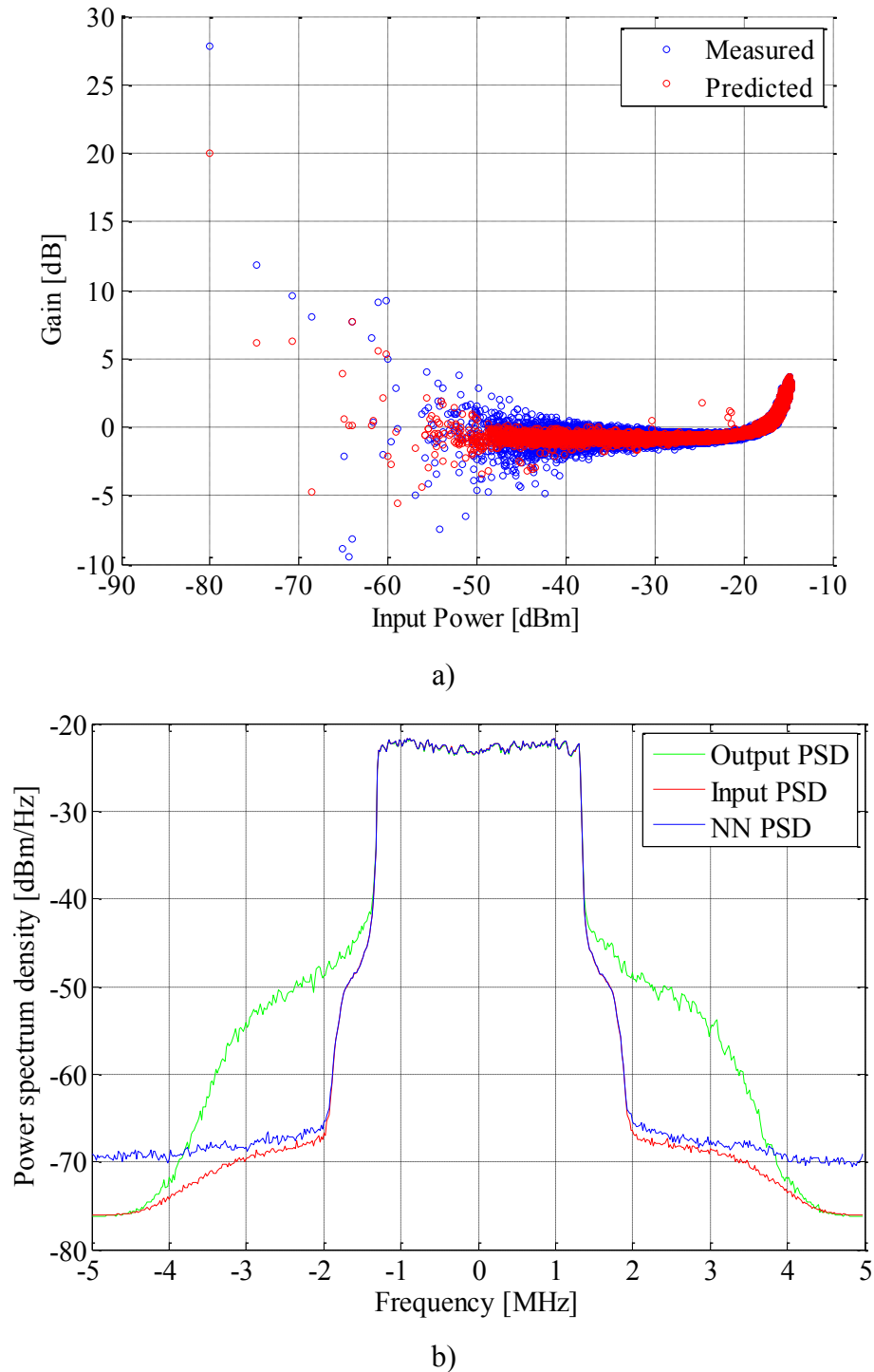


Figure 5-10: Inverse model results at 880 MHz: a) Inverse PA gain for the LTE 3 MHz 64 QAM signal; b) Power spectrum density of the RVTDNN model output vs. the real PA input for the LTE 3 MHz 64 QAM signal

Table 5.5: Inverse model performances compared with performances of real input and output for the LTE 1.4 MHz 64 QAM signal at 880 MHz centre frequency

	ACPR [dBc] ±1.4 MHz offset		EVM [%]
	LOW	HIGH	
PA input	-36.22	-34.30	/
Real PA	-30.90	-30.01	8.66
NN inverse model	-36.01	-34.15	1.47

Table 5.6: Inverse model statistical performances for the LTE 1.4 MHz 64 QAM signal at 880 MHz centre frequency

NMSE [dB]	-36.67	
MSE	<i>I</i>	9.28e-07
	<i>Q</i>	9.27e-07
RMSE	<i>I</i>	9.63e-04
	<i>Q</i>	9.63e-04

Table 5.7: Inverse model performances compared with performances of real input and output for the LTE 3 MHz 64 QAM signal at 880 MHz centre frequency

	ACPR [dBc] ±3 MHz offset		EVM [%]
	LOW	HIGH	
PA input	-40.96	-39.50	/
Real PA	-29.66	-29.39	9.79
NN inverse model	-40.44	-39.15	1.35

Table 5.8: Inverse model statistical performances for the LTE 3 MHz 64 QAM signal at 880 MHz centre frequency

NMSE [dB]	-37.40	
MSE	<i>I</i>	8.56e-07
	<i>Q</i>	8.01e-07
RMSE	<i>I</i>	9.25e-04
	<i>Q</i>	8.95e-04

As these inverse models have to mimic the inverse PA behaviour, ACPRs for the models' outputs have to be close to ACPR of the real PA input signal. EVMs should be as low as possible, which relates to the deviation from the ideal input signal constellation.

The Figures 5-7(a), 5-8(a), 5-9(a) and 5-10(a) present a comparison between the real characteristics and modelled transfer characteristics. As can be observed, the NN

models are very accurate. The scattered samples on lower power levels are consequence of the out-of-band model behaviour, which does not track the DUT perfectly. That also can be seen in the Figures 5-7(b), 5-8(b), 5-9(b) and 5-10(b) observing the spectra. The spectra of the models' output signals have mismatches in the beginning and ending frequency regions. This is especially seen in the models for 3MHz signals. The explanation for that can be found in the frequency range of the measurement. It is preferable that the measurement of the signals be in range five times bigger than the signal occupied bandwidth. Another explanation is down converting of the signals through the VSA and distortion suite. Filtering the signals for bringing them down to PC cuts the wider signals, and parts of the nonlinear samples are lost in that way. Still, the models are good enough while the main channel and adjacent channels are modelled correctly, which is seen through EVM and ACPR performances.

5.6. Power Amplifier Predistortion using Inverse Model

As we said earlier, in an ideal case, the inverse model of some nonlinear system in cascade with its nonlinearity make the linear characteristic. In this subsection the NN inverse models presented in the previous subsections will be tested as predistorters for the PA MIMIX CFH2162-P3. The Figure 5-11 shows a layout of a predistortion system. Both inverse models will be examined as predistorters in cascade with the forward NN models of the DUT. After that predistorter for the LTE 1.4 MHz 64 QAM signal will be tested in a real system.

In this stage there is no need for trainings and modelling. At this point checking of developed predistorters is done.

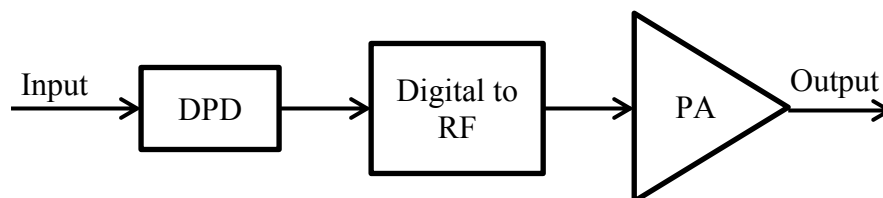


Figure 5-11: A layout of predistortion system

The idea is to bring an input signal to the predistorter first, e.g. to the inverse PA model, and after that to pass it through the PA, in order to get the linearly gained signal at the output. The input signals LTE 1.4 MHz 64 QAM and LTE 3 MHz 64 QAM are input signals from experiments, used for testing the networks. They are passed through the inverse model neural networks and after that through the forward model neural networks. The additional scaling of signals, between these two NNs, inverse and forward, is not needed, as both networks are modelled for the same range of input-output data. The spectra of real input signal, real output signal and signal at the output of the cascade DPD-PA are presented in the Figures 5-12 and 5-13. The spectral regrowth improvement for the 1.4MHz signal is 11.76dB for the upper band, and 11.44dB for the lower band. For the 3MHz signal spectral regrowth is 11.34dB for the upper band and 11.96dB for the lower band, as pointed in the Figure 5-13. The spectra show that it is possible to decrease the distortion coming from the PA. That is also observable through the performance parameters, ACPR and EVM. As can be seen from the Tables 5.9 and 5.10, ACPRs are very close to ACPR of the input signal and EVMs are very small. That means that the output of system with a predistorter is almost completely linear transformation from the original input.

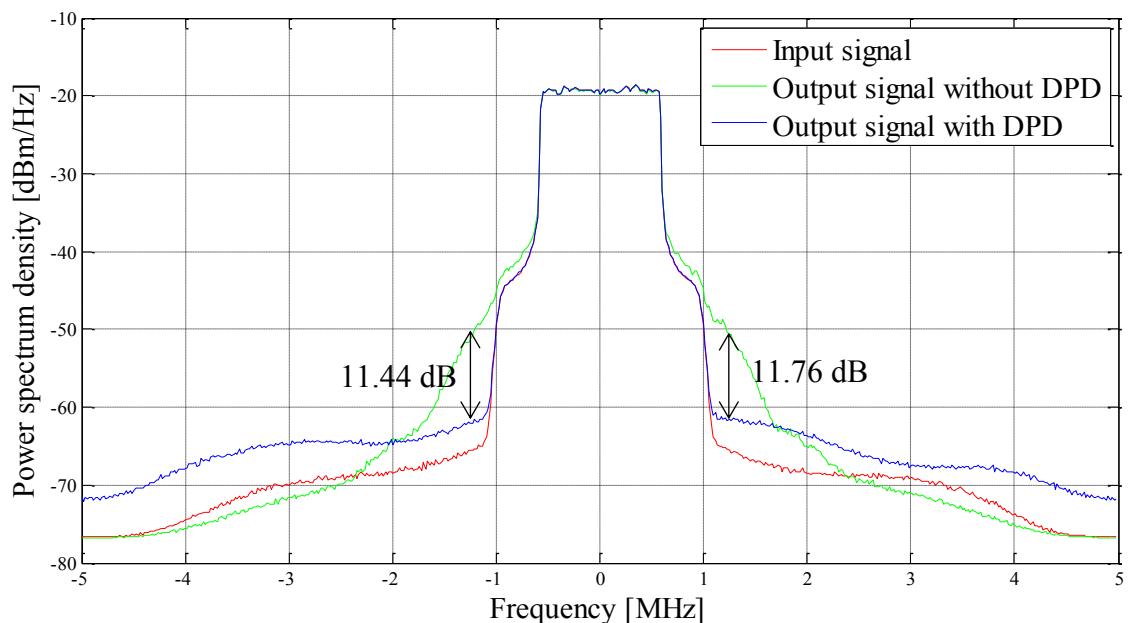


Figure 5-12: Power spectrum densities at 880 MHz for an input signal before predistortion, output signal with predistortion, and output signal without predistortion for the LTE 1.4 MHz 64 QAM signal

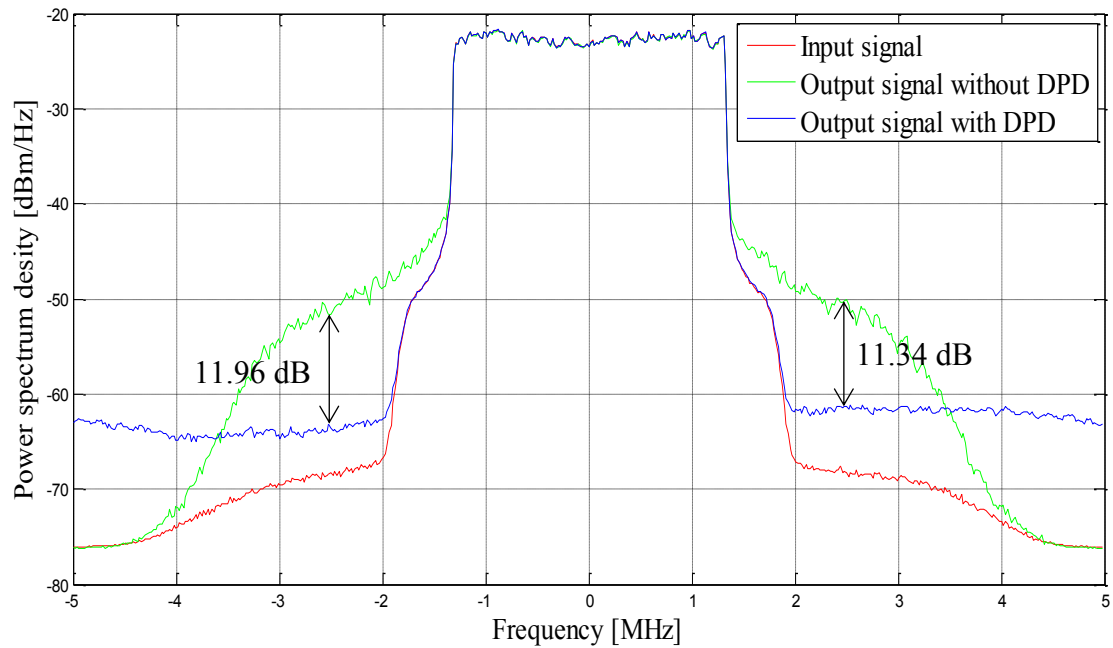


Figure 5-13: Power spectrum densities at 880 MHz for an input signal before predistortion, output signal with predistortion, and output signal without predistortion for the LTE 3 MHz 64 QAM signal

Table 5.9: Performances of output signal from a system with DPD compared with performances of real input and output signals from a system without DPD for the LTE 1.4 MHz 64 QAM signal at 880 MHz centre frequency

	ACPR [dBc] ±1.4 MHz offset		EVM [%]
	LOW	HIGH	
PA input	-36.22	-34.30	/
PA output without DPD	-30.90	-30.01	8.66
PA output with DPD	-35.73	-33.85	1.37

Table 5.10: Performances of output signal from a system with DPD compared with performances of real input and output signals from a system without DPD for the LTE 3 MHz 64 QAM signal at 880 MHz centre frequency

	ACPR [dBc] ±1.4 MHz offset		EVM [%]
	LOW	HIGH	
PA input	-40.96	-39.50	/
PA output without DPD	-29.66	-29.39	9.79
PA output with DPD	-38.70	-36.66	1.74

When the predistortion capability is proved using the NN models for forward and inverse characteristics of the DUT, the predistorted signal LTE 1.4 MHz 64 QAM signal was sent from MATLAB to the real test-bed (Figure 5-5). The results for this real testing of the designed predistorter are presented in the Figure 5-14 and Table 5.11.

Table 5.11: ACPR of output signal from a real system with DPD compared with ACPR of real input and output signals from a system without DPD for the LTE 1.4 MHz 64 QAM signal at 880 MHz centre frequency

	ACPR [dBc] ±1.4 MHz offset	
	LOW	HIGH
PA input	-36.69	-34.76
PA output without DPD	-26.98	-26.61
PA output with DPD	-33.73	-32.50

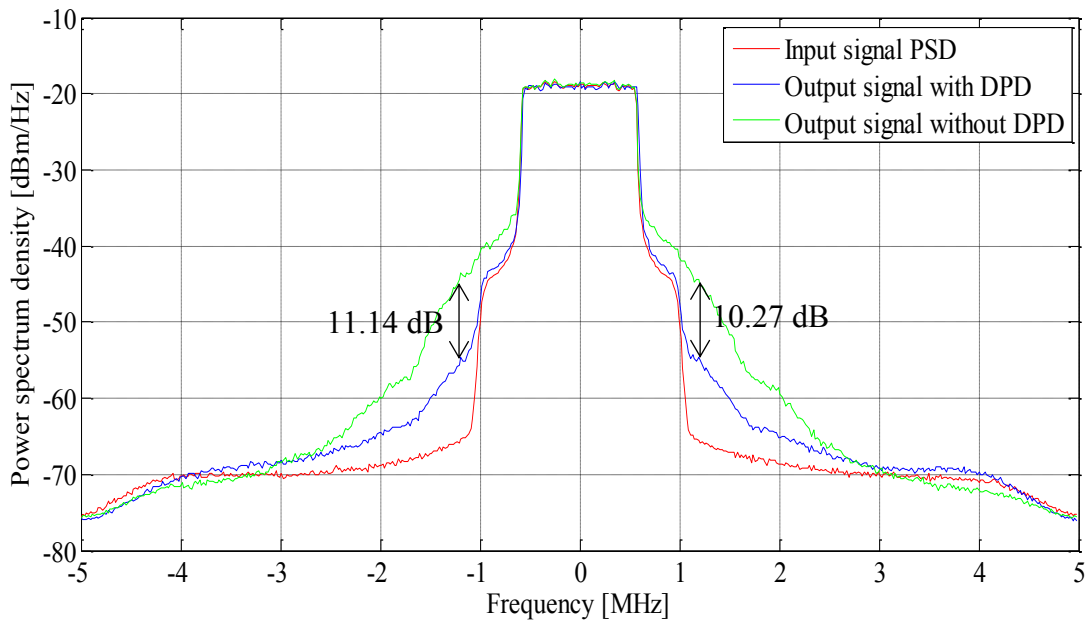


Figure 5-14: Power spectrum densities at 880 MHz for an input signal before predistortion, output signal with predistortion, and output signal without predistortion for the LTE 1.4 MHz 64 QAM signal (using the hardware test-bench)

The results acquired from testing the predistorter in real environment, not using the NN model for the device under test, show improvement of the spectral regrowth for 10.27dB in the upper band and 11.14dB in the lower band. Decrease in ACPR parameters comparing the output signals from the system without predistorter and the one with DPD also presents capability for the PA predistortion using inverse NN model.

5.7. Comparison with partial least squares method

In the Chapter 4 a linear-based technique was presented. In order to show the superiority of artificial neural networks over this type of modelling techniques, the partial least squares method (PLS) is used [5.15]. Forward and inverse models of a power amplifier were created. For forward PLS model 32 inputs is used, which means the current I component sample and the 15 times delayed I signal, plus the same for the Q component. This is a four times bigger input vector, and the performance is much worse (Table 5.12). A model is made for the LTE 1.4 MHz 64 QAM signal at 880 MHz centre frequency. For the same signal an inverse model is created. This one has the memory depth 21, e.g. 42 inputs. Statistical performance parameters are compared with NN model in the Table 5.13.

Table 5.12: Forward model statistical performances for RVTDNN and PLS for the LTE 1.4 MHz 64 QAM signal at 880 MHz centre frequency

	RVTDNN		PLS	
NMSE [dB]	-38.28		-21.26	
MSE	I	6.34e-07	I	3.05e-05
	Q	6.35e-07	Q	3.34e-05
RMSE	I	7.96e-04	I	5.50e-03
	Q	7.97e-04	Q	5.80e-03

Table 5.13: Inverse model statistical performances for RVTDNN and PLS for the LTE 1.4 MHz 64 QAM signal at 880 MHz centre frequency

	RVTDNN		PLS	
NMSE [dB]	-36.67		-21.68	
MSE	I	9.28e-07	I	2.81e-05
	Q	9.27e-07	Q	3.04e-05
RMSE	I	9.63e-04	I	5.30e-03
	Q	9.63e-04	Q	5.50e-03

As can be seen from the statistical performance parameters for the forward and inverse PLS models, these are much inferior to the artificial neural networks. Performances are given for two PLS models randomly chosen from a large pool of different PLS structures used for modelling. NMSEs for few PLS forward model structures are:

- with 10 inputs: -21.2623 dB
- with 46 inputs: -21.2672 dB
- with 100 inputs: -21.2719 dB,

and NMSEs for few inverse model structures are:

- with 10 inputs: -21.6483 dB
- with 46 inputs: -21.6851 dB
- with 100 inputs: -21.7161 dB.

Conclusion that can be made upon these normalised mean square errors for different PLS structures, is that the number of inputs does not change a model performance significantly. Thus this technique could not be used successfully for modelling, or predistortion of power amplifiers.

5.8. Conclusion

Literature overview of existing methods based on the artificial neural networks was given. The neural network structure that differs from the structures used in the literature was proposed. Verification of the forward and inverse models of the DUT was depicted through spectra of the input and output signals and signal performance parameters. The proposed method for predistortion was finally certified through the real experiment. Small difference between the spectral regrowth improvement gained through testing the DPD+PA system in MATLAB environment, and the spectral regrowth improvement gained through hardware testing of the developed predistorter, shows that the PA forward model has high accuracy. Superiority of the neural networks over the partial least squares method is presented at the end of this section. In the next chapter, the developed models will be used for creation of a predistorter based on different layout than the DPD+PA, and a comparison with another proposed method will be given.

5.9. References

- [5.1] F. Mkadem, M. B. Ayed, S. Boumaiza, J. Wood, and P. Aaen, "Behavioral modeling and digital predistortion of Power Amplifiers with memory using Two Hidden Layers Artificial Neural Networks", *IEEE MTT-S International Microwave Symposium Digest*, pp. 656-659, May 2010.
- [5.2] Q. J. Zhang, and K. C. Gupta, *Neural Networks for RF and Microwave Design*, Norwood, MA: Artech House, 2000.
- [5.3] H. Holma, and A. Toskala, *LTE for UMTS: Evolution to LTE-Advanced, 2nd Edition*, Wiley, 2011.
- [5.4] M. Ibnkahla, N. J. Bershad, J. Sombrin, and F. Castanie, "Neural network modeling and identification of nonlinear channels with memory: algorithms, applications, and analytic models", *IEEE Transactions on Signal Processing*, vol. 46, no. 5, pp. 1208-1220, May 1998.
- [5.5] B. E. Watkins, and R. North, "Predistortion of nonlinear amplifiers using neural networks", *Military Communications Conference, MILCOM '96, Conference Proceedings, IEEE*, vol. 1, pp. 316-320, October 1996.
- [5.6] A. Ahmed, E. R. Srinidhi, and G. Kompa, "Efficient PA modeling using neural network and measurement setup for memory effect characterization in the power device", *Microwave Symposium Digest, 2005 IEEE MTT-S International*, June 2005.
- [5.7] M. S. Kim, and C. C. Guest, "Modification of backpropagation networks for complex-valued signal processing in frequency domain", *International Joint Conference on Neural Networks, 1990 IJCNN*, vol. 3, pp. 27-31, June 1990.
- [5.8] H. Leung, and S. Haykin, "The complex backpropagation algorithm", *IEEE Transactions on Signal Processing*, vol. 39, no. 9, pp. 2101-2104, September 1991.
- [5.9] N. Benvenuto, F. Piazza, and A. Uncini, "A neural network approach to data predistortion with memory in digital radio systems", *IEEE International Conference on Communications, ICC '93 Geneva, Technical Program, Conference Record*, vol. 1, pp. 232-236, May 1993.

-
- [5.10] D. Liongyinh, and Y. Kwon, “Behavioral modelling of power amplifiers using fully recurrent neural networks”, *IEEE MTT-S International Microwave Symposium Digest*, pp. 1979-1982, June 2005.
- [5.11] L. Taijun, S. Boumaiza, and F. M. Ghannouchi, “Dynamic behavioral modeling of 3G power amplifiers using real-valued time-delay neural networks”, *IEEE Transactions on Microwave Theory and Techniques*, vol. 52, no. 3, pp. 1025-1033, March 2004.
- [5.12] H. Zihong, C. Wenhua, F. Zhenghe, and F. M. Ghannouchi, “Forward behavioral modeling of concurrent dual-band power amplifiers using extended real valued time delay neural networks”, *International Conference on Microwave and Millimeter Wave Technology*, vol. 5, pp. 1-4, 5-8. May 2012.
- [5.13] M. Rawat, K. Rawat, and F. M. Ghannouchi, “Adaptive Digital Predistortion of Wireless Power Amplifiers/Transmitters Using Dynamic Real-Valued Focused Time-Delay Line Neural Networks”, *IEEE Transactions on Microwave Theory and Techniques*, vol. 58, no. 1, pp. 95-104, January 2010.
- [5.14] K. Fu, C. L. Law, and T. T. Thein, “Novel Neural Network Model of Power Amplifier plus IQ Imbalances”, *Progress In Electromagnetics Research B*, vol. 46, pp. 177-192, 2013.
- [5.15] P. Geladi, and B. R. Kowalski, “Partial least-squares regression: a tutorial”, *Analytica Chimica Acta*, vol. 185, pp. 1-17, 1986.

6. MODELING AND PREDISTORTION OF POWER AMPLIFIERS USING NEURO-FUZZY SYSTEMS

6.1. Introduction

Identification of nonlinear systems and linearization of these systems for special applications have been extensively studied during the last decades. Power amplifiers fall into that category, and many techniques for its modelling and predistortion have been developed [6.1]-[6.11]. The artificial intelligence systems (neural networks, fuzzy systems and neuro-fuzzy systems) are mostly used for dynamic system identification [6.12]-[6.15]. NNs and fuzzy systems are both stand-alone systems, but both have disadvantages. Fuzzy rules and membership functions are difficult to develop when the complexity of a process being modelled increase, e.g. it is not possible to train a fuzzy system. On the other hand, neural networks are trainable, but it is very difficult to incorporate some prior knowledge into the system, and almost impossible to explain the behaviour of NN in a particular situation [6.16]. For this reason, the neuro-fuzzy methods are developed. In that way, advantages of both NNs and FSs are kept and their disadvantages are compensated.

Until now, for modelling and predistortion of power amplifiers authors have been using only ANFISs as a neuro-fuzzy technique for modelling and predistortion of PAs [6.16]-[6.21]. The main drawback of these systems is that they have only one output, and that creates request for more ANFIS structures, or more complex CANFIS structures.

This chapter proposes the adaptive fuzzy logic system (AFLS) introduced by Wang [6.22] with slightly different defuzzification for modelling and predistortion of a PA. Experimental results of modelling and predistortion of the power amplifier MIMIX CFH2162-P3 using the proposed technique will be presented and compared with the results from the previous chapter.

6.2. Proposed Adaptive Fuzzy Logic System

The Chapter 3.4.2 introduced the AFLS (Figure 6-1) proposed by Wang [6.22]. There are different defuzzification methods, but most popular among them is the centroid of area (3.24) which is computationally more complex with the increase of quantization levels of the output.

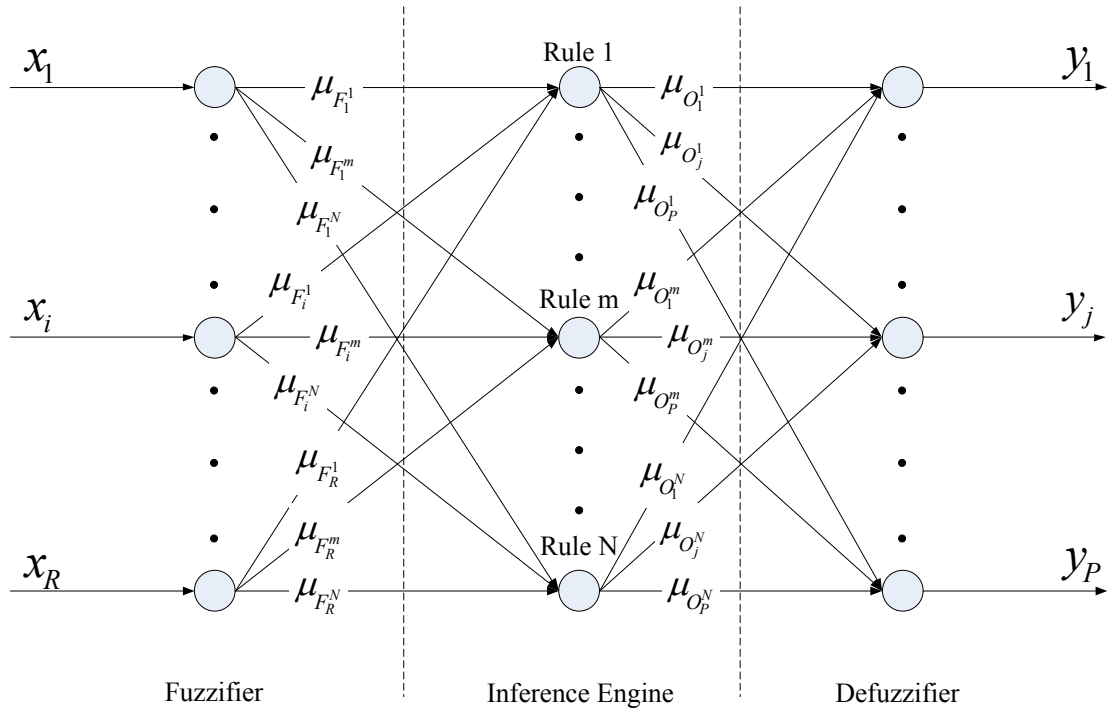


Figure 6-1: A multi-input multi-output AFLS architecture

Thus the defuzzification method used here is the “area of balance” (AOB) method, proposed by Kodogiannis [6.23]-[6-24] used in different applications of AFLS regardless of power amplifiers. This defuzzification method will be described further on, and the first two layers of the AFLS remain as in the Chapter 3.4.2.

First we have to presume that the output fuzzy set O_j^m (output fuzzy region of m -th rule for j -th overall output) has a symmetrical shape. The Gaussian and bell shape of the membership functions are always symmetrical, but a symmetrical triangular or trapezoidal can be used as well. The centre of gravity will pass through the halfway point of the base of O_j^m . In this thesis the triangular membership function is used in the consequent part, and the AOB will be explained through that example. The Figure 6-2

shows the shape of the consequent part of the m -th rule. The result of a max-product inference will be the membership function described by (3.23). As the membership function values $\mu_{O_j^m}$ will be the same for every j , we will note it as μ_m for simplicity.

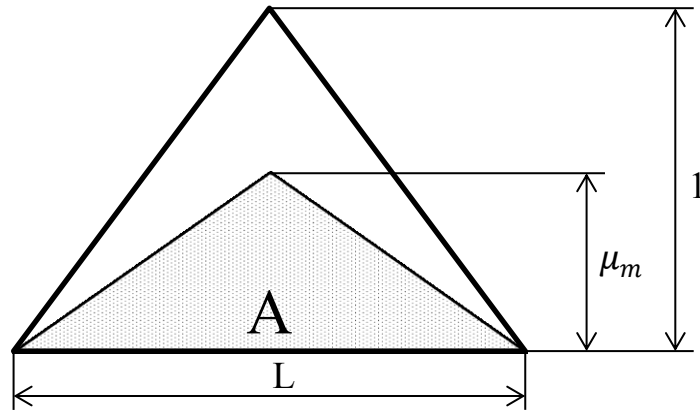


Figure 6-2: A triangular shape membership function

The area A is derived as:

$$A = \frac{1}{2} \mu_m L \quad (6.1)$$

Now let assume that the shape (Figure 6-3) have the density D and thickness T . Then the mass of this shape will be:

$$M = ATD \quad (6.2)$$

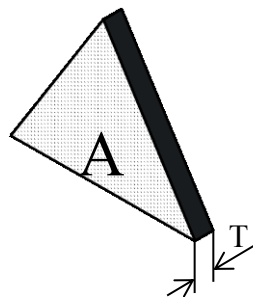


Figure 6-3: A consequent part shape

If we put the consequent parts of each rule on the massless beam with the pivot point at origin O (Figure 6-4), we can write down the balance of forces:

$$F = M_1g + M_2g + \dots + M_n g = \sum_{m=1}^n M_m g, \quad (6.3)$$

where n is the number of the rules. The momentum balance will be:

$$F y_j = M_1 g y_j^1 + M_2 g y_j^2 + \dots + M_n g y_j^n = \sum_{m=1}^n M_m g y_j^m, \quad (6.4)$$

where y_j^m is the centre of the membership function in the consequent part of the j -th output of the m -th rule. Substituting (6.3) into (6.4) we derive y_j as the j -th output of the system:

$$y_j = \frac{\sum_{m=1}^n M_m y_j^m}{\sum_{m=1}^n M_m} \quad (6.5)$$

Under assumption that D and T are the same for every consequent part, and after substituting (6.1) in (6.2) and after that in (6.5), the final form of the output of this AFLS will be:

$$y_j = \frac{\sum_{m=1}^n A_m T D y_j^m}{\sum_{m=1}^n A_m T D} = \frac{\sum_{m=1}^n \mu_m L_j^m y_j^m}{\sum_{m=1}^n \mu_m L_j^m} \quad (6.6)$$

y_j is the j -th output of the AFLS, μ_m is the membership value of the m -th rule, L_j^m is the spread parameter of the membership function in the consequent part of the j -th output of the m -th rule and y_j^m is the centre of the membership function in the consequent part of the j -th output of the m -th rule.

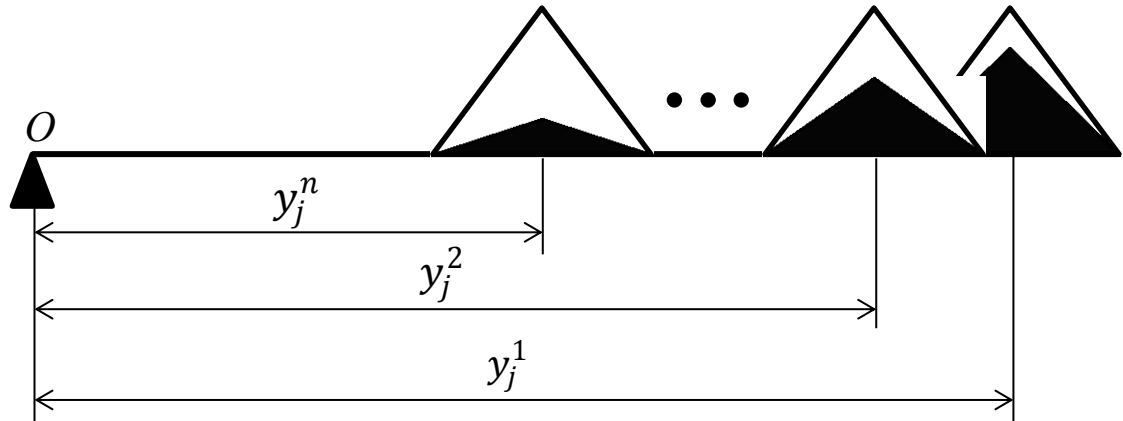


Figure 6-4: Consequent fuzzy sets of the j -th output placed on a massless beam

6.2.1 Training of Adaptive Fuzzy Logic System

During the training of AFLS the back-propagation algorithm is used. In order to derive update equations for training algorithm, first we have to define the objective function.

$$J = \sum_{p=1}^P J_p \quad (6.7)$$

where P is the number of the training patterns, and J_p is:

$$J_p = \frac{1}{2} \sum_{j=1}^N e_j(p)^2 = \frac{1}{2} \sum_{j=1}^N (y_j(p) - d_j(p))^2 \quad (6.8)$$

That is the sum of squared errors for the p -th pattern. N is the number of outputs, $y_j(p)$ is the AFLS output defined by (6.6) and $d_j(p)$ is the desired j -th output. The update equation of the centre of the membership function in the consequent part of the j -th output of the m -th rule y_j^m is:

$$y_j^m(k+1) = y_j^m(k) + m_y [y_j^m(k) - y_j^m(k-1)] - \eta_y \left. \frac{\partial J}{\partial y_j^m} \right|_k, \quad (6.9)$$

where m_y is the learning rate and η_y is the momentum for this parameter training. k is the iteration index. Partial derivative $\frac{\partial J}{\partial y_j^m}$ has form:

$$\frac{\partial J}{\partial y_j^m} = \frac{\partial J}{\partial J_p} \cdot \frac{\partial J_p}{\partial e_j} \cdot \frac{\partial e_j}{\partial y_j} \cdot \frac{\partial y_j}{\partial y_j^m} = \sum_{p=1}^P (y_j(p) - d_j(p)) \frac{\mu_m^p L_j^m}{\sum_{m=1}^n \mu_m^p L_j^m} \quad (6.10)$$

where μ_m^p presents the membership value of the m -th rule corresponding to p -th pattern in the training data. The update equation of the spread parameter of the membership function in the consequent part of the j -th output of the m -th rule, L_j^m , is in form:

$$L_j^m(k+1) = L_j^m(k) + m_L [L_j^m(k) - L_j^m(k-1)] - \eta_L \left. \frac{\partial J}{\partial L_j^m} \right|_k, \quad (6.11)$$

where m_L is the learning rate and η_L is the momentum for the spread parameter training.

$$\frac{\partial J}{\partial L_j^m} = \frac{\partial J}{\partial J_p} \cdot \frac{\partial J_p}{\partial e_j} \cdot \frac{\partial e_j}{\partial y_j} \cdot \frac{\partial y_j}{\partial L_j^m} = \sum_{p=1}^P \left[(y_j(p) - d_j(p)) \frac{\mu_m^p}{\sum_{m=1}^n \mu_m^p L_j^m} (y_j^m - y_j(p)) \right] \quad (6.12)$$

The update equation of the centre parameter of the Gaussian membership function of fuzzifier, c_i^m , defined in (3.22) will be in the form:

$$c_i^m(k+1) = c_i^m(k) + m_c [c_i^m(k) - c_i^m(k-1)] - \eta_c \left. \frac{\partial J}{\partial c_i^m} \right|_k, \quad (6.13)$$

where m_c is the learning rate and η_c is the momentum for training of the centre parameter.

$$\frac{\partial J}{\partial c_i^m} = \frac{\partial J}{\partial J_p} \cdot \frac{\partial J_p}{\partial e_j} \cdot \frac{\partial e_j}{\partial y_j} \cdot \frac{\partial y_j}{\partial \mu_m} \cdot \frac{\partial \mu_m}{\partial \mu_{F_i}^m} \cdot \frac{\partial \mu_{F_i}^m}{\partial c_i^m} \quad (6.14)$$

$$\frac{\partial \mu_m}{\partial \mu_{F_i}^m} = \prod_{\substack{j=1 \\ j \neq i}}^n \mu_{F_j}^m \quad (6.15)$$

$$\frac{\partial \mu_{F_i^m}}{\partial c_i^m} = \mu_{F_i^m} \frac{x_i(p) - c_i^m}{(\sigma_i^m)^2} \quad (6.16)$$

$$\frac{\partial J}{\partial c_i^m} = \sum_{p=1}^P \left\{ \left[\sum_{j=1}^N (y_j(p) - d_j(p)) \frac{L_j^m (y_j^m - y_j(p))}{\sum_{m=1}^n \mu_m^p L_j^m} \right] \mu_m^p \frac{x_i(p) - c_i^m}{(\sigma_i^m)^2} \right\} \quad (6.17)$$

The update equation of the spread parameter of the Gaussian membership function of fuzzifier, σ_i^m , defined in (3.22) is in the form:

$$\sigma_i^m(k+1) = \sigma_i^m(k) + m_\sigma [\sigma_i^m(k) - \sigma_i^m(k-1)] - \eta_\sigma \left. \frac{\partial J}{\partial \sigma_i^m} \right|_k, \quad (6.18)$$

where m_σ is the learning rate and η_σ is the momentum for the training of spread parameter.

$$\frac{\partial J}{\partial \sigma_i^m} = \frac{\partial J}{\partial J_p} \cdot \frac{\partial J_p}{\partial e_j} \cdot \frac{\partial e_j}{\partial y_j} \cdot \frac{\partial y_j}{\partial \mu_m} \cdot \frac{\partial \mu_m}{\partial \mu_{F_i^m}} \cdot \frac{\partial \mu_{F_i^m}}{\partial \sigma_i^m} \quad (6.19)$$

$$\frac{\partial \mu_{F_i^m}}{\partial \sigma_i^m} = \mu_{F_i^m} \frac{(x_i(p) - c_i^m)^2}{(\sigma_i^m)^3} \quad (6.20)$$

$$\frac{\partial J}{\partial \sigma_i^m} = \sum_{p=1}^P \left\{ \left[\sum_{j=1}^N (y_j(p) - d_j(p)) \frac{L_j^m (y_j^m - y_j(p))}{\sum_{m=1}^n \mu_m^p L_j^m} \right] \mu_m^p \frac{(x_i(p) - c_i^m)^2}{(\sigma_i^m)^3} \right\} \quad (6.21)$$

Derived equations (6.9)-(6.21) are used for update of the AFLS parameters during the training phase of this neuro-fuzzy system.

6.3. Experimental Results for Modelling and Predistortion of DUT

6.3.1 Modelling of Power Amplifier

Experimental setup for measurement and collection of the data for the training is described in the Chapter 5.4.1. For modelling and testing of this structure the LTE 1.4 MHz 64 QAM signal at 880MHz centre frequency is used. After the measurement procedure, the next step is preparation of the collected data for the training process. In MATLAB environment the input and output signals are scaled to the range [0, 1]. Delayed inputs, e.g. training dataset with current and delayed I and Q signals are also created in MATLAB.

The AFLS structure found as the most appropriate for this problem has four inputs ($I(p), Q(p), I(p - 1), Q(p - 1)$) and 30 rules. This structure was established during the optimisation procedure. The learning rates for the training of every parameter are 0.008, and the momentums for every parameter are 0.55. The initial centre parameters of the Gaussian membership functions of the fuzzifier layer are equally distributed in the range [0, 1]. The initial spread parameters of the Gaussian membership functions of the fuzzifier are all set to 0.2. The initial values for centres of the membership functions in the consequent part are equally distributed in the range [0, 1]. The initial values for the spread parameters of the membership functions in the consequent part are all set to 0.65. The training of proposed AFLS was carried out with 30000 (30K) patterns in the training dataset. And once the training was complete, 100K data were used for testing the AFLS model.

6.3.1.1 Forward AFLS Model

NMSE for testing with training 30K data was -43.54dB, and NMSE for testing with 100K data was -42.08dB for the LTE 1.4 MHz 64 QAM signal. PAPR of the input signal is 10.21dB for the LTE 1.4 MHz 64 QAM signal. The Figure 6-5 shows the modelling results for LTE 1.4 MHz 64 QAM. As can be seen from the spectrum plots, the forward model using the AFLS method is very accurate. The Table 6.1 gives the

performance parameters for the real input signal, real output signal, and modelled output signals when the testing is carried out with the training set, and when the new set of 100K data was used. Statistical performances for forward model are given in the Table 6-2.

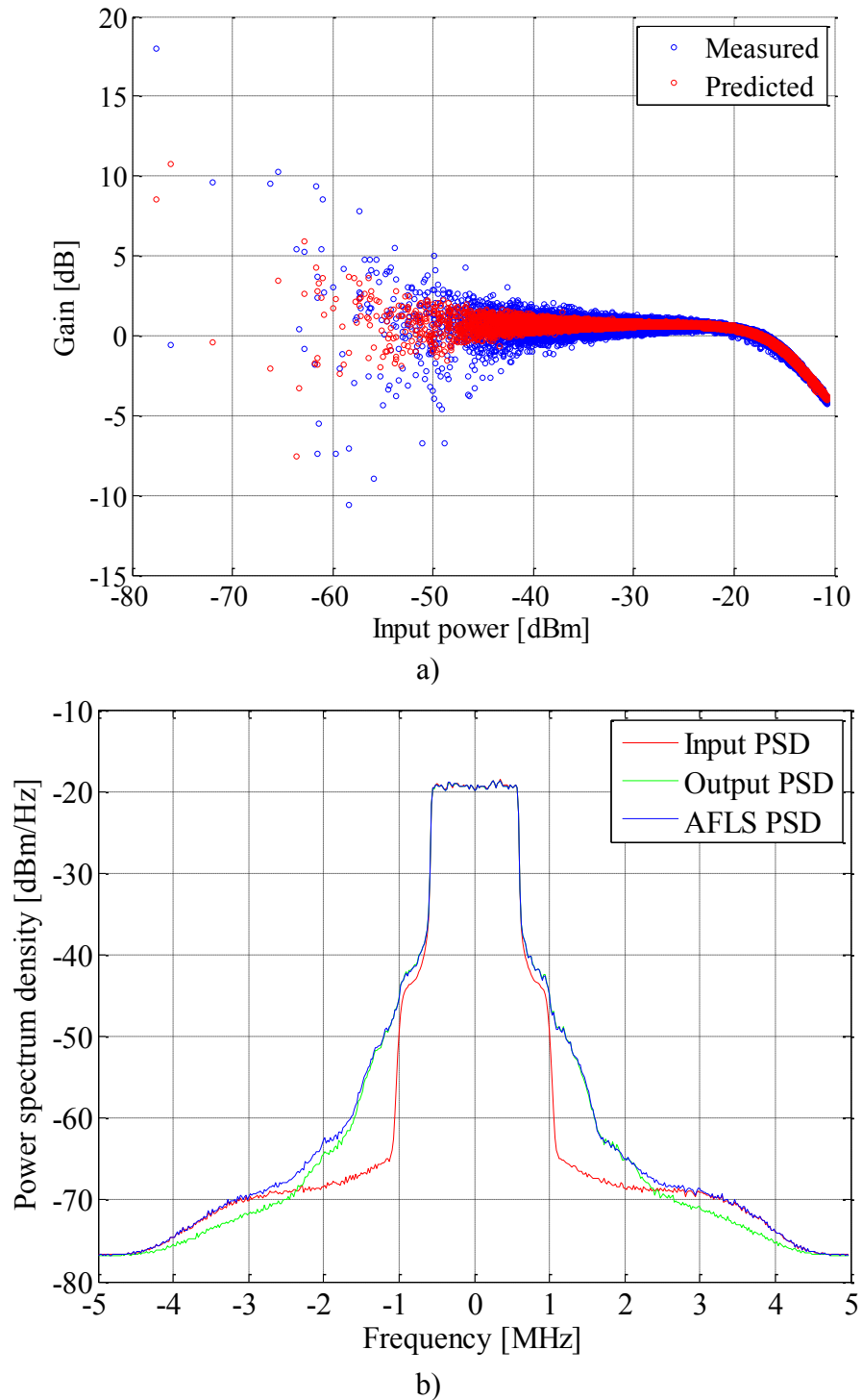


Figure 6-5: Forward model results at 880 MHz: a) PA gain for the LTE 1.4 MHz 64 QAM signal; b) Power spectrum density of the AFLS model output vs. the real PA output for the LTE 1.4 MHz 64 QAM signal

Table 6.1: Forward model performances compared with performances of real input and output for the LTE 1.4 MHz 64 QAM signal at 880 MHz centre frequency

	ACPR [dBc] ±1.4 MHz offset		EVM [%]
	LOW	HIGH	
PA input	-36.19	-34.28	/
Real PA	-30.89	-30.00	8.66
AFLS model tested with training dataset	-30.84	-29.98	8.54
AFLS model tested with different dataset	-30.82	-30.11	8.53

Table 6.2: Forward model statistical performances for the LTE 1.4 MHz 64 QAM signal at 880 MHz centre frequency

	AFLS model tested with training dataset		AFLS model tested with different dataset	
NMSE	-43.54		-42.08	
MSE	<i>I</i>	9.67e-07	<i>I</i>	9.47e-07
	<i>Q</i>	9.37e-07	<i>Q</i>	9.56e-07
RMSE	<i>I</i>	9.83e-04	<i>I</i>	9.73e-04
	<i>Q</i>	9.68e-04	<i>Q</i>	9.78e-04

The Figure 6-5 (a) shows very good matching results for the PA nonlinear gain. Almost identical spectra of the real PA output and AFLS output confirm the model accuracy which can be seen also from the EVM and ACPR performance parameters. Excellent NMSE parameter gives a proof of good modelling structure. The training of this model required around 90 minutes running on the laptop DELL Inspiron 5110. The computer contains the Intel Core i7-2630QM processor and 8GB of RAM memory. This is short time for the training, in comparison with a NN training duration. Later on a comparative review of these two techniques for modelling and predistortion will be presented.

6.3.1.2 Inverse AFLS Model

The inverse model structure is slightly different than the forward model one. The number of rules is increased to 40, and the memory depth is enlarged for one, e.g. the number of inputs for this structure is six. Learning rates and momentums are the same as for the forward model. The training procedure has been run, with the reverse input-output dataset. The input signal is the desired output in this case, and the output

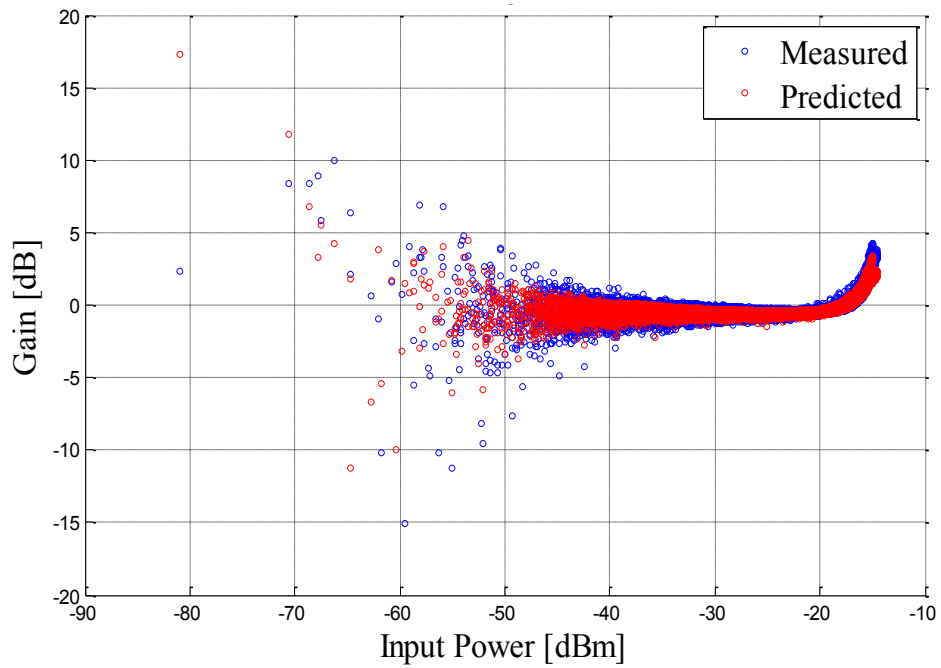
baseband signal is the training dataset for adaptive fuzzy logic system. 30K data were used for training the AFLS and 100K data from different period of time were used for testing the AFLS inverse model. The training procedure required two hours at the same PC stated in the above subsection. NMSE for testing with the training dataset was -44.27dB for the LTE 1.4 MHz 64 QAM signal. NMSE parameter for testing with new 100K data was -44.15dB. The Figure 6-6 shows inverse modelling results for the LTE 1.4 MHz 64 QAM signal at 880MHz centre frequency. The Table 6.3 presents the signal performances for the developed model, and the Table 6-4 presents statistical performances. EVM is low, which means that we managed to develop the system which will decrease spreading of the symbols in constellation diagram far from the ideal values. From this table one can observe very good modelling results with closer look at the ACPRs and EVMs of testing model with training dataset, and testing with the new dataset.

Table 6.3: Inverse model performances compared with performances of real input and output for the LTE 1.4 MHz 64 QAM signal at 880 MHz centre frequency

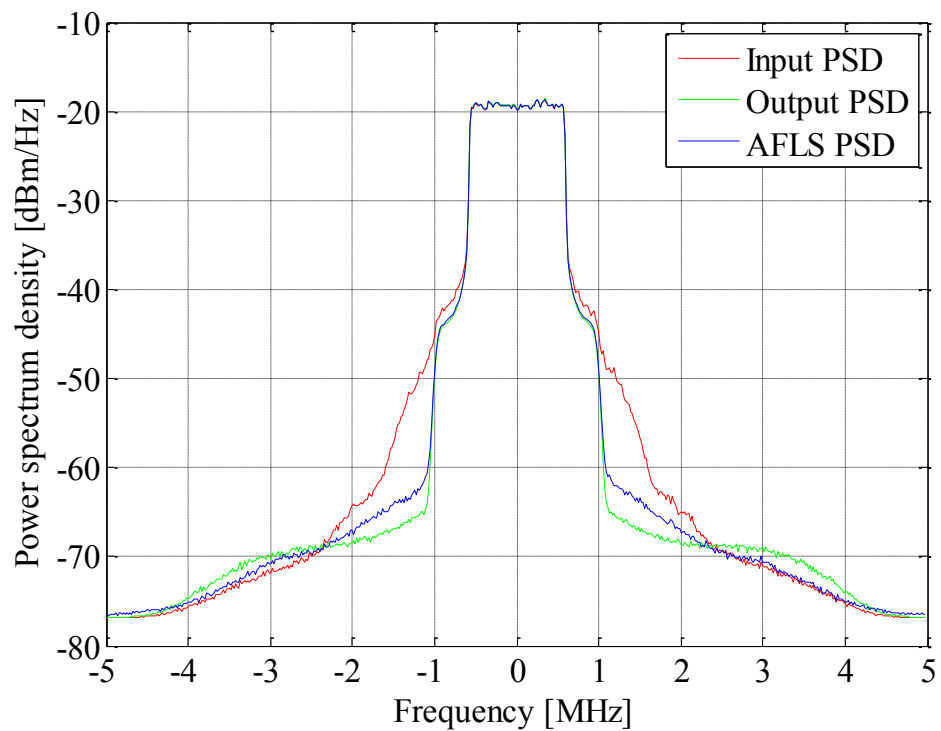
	ACPR [dBc] ±1.4 MHz offset		EVM [%]
	LOW	HIGH	
PA input	-36.19	-34.28	/
Real PA	-30.89	-30.00	8.66
AFLS model tested with training dataset	-35.56	-33.51	2.38
AFLS model tested with different dataset	-35.63	-33.76	2.42

Table 6.4: Inverse model statistical performances for the LTE 1.4 MHz 64 QAM signal at 880 MHz centre frequency

	AFLS model tested with training dataset		AFLS model tested with different dataset	
NMSE	-44.27		-44.15	
MSE	<i>I</i>	9.49e-07	<i>I</i>	2.80e-06
	<i>Q</i>	9.56e-07	<i>Q</i>	2.23e-06
RMSE	<i>I</i>	9.75e-04	<i>I</i>	1.70e-03
	<i>Q</i>	9.78e-04	<i>Q</i>	1.50e-03



a)



b)

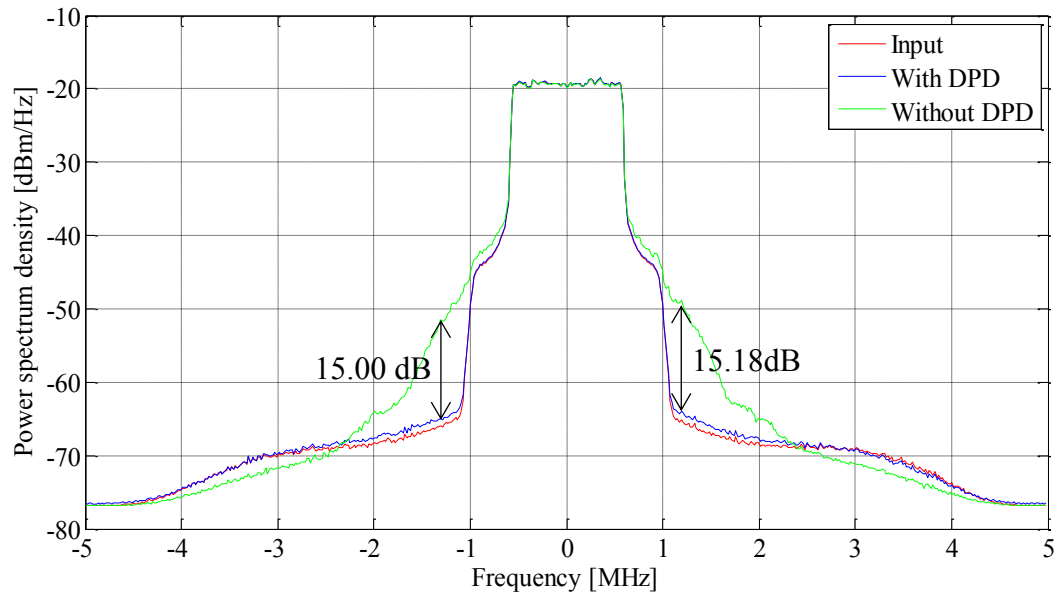
Figure 6-6: Inverse model results at 880 MHz: a) PA gain for the LTE 1.4 MHz 64 QAM signal; b) Power spectrum density of the AFLS model output vs. the real PA output for the LTE 1.4 MHz 64 QAM signal

The Figure 6-6 presents the inverse PA gain and a comparison of spectra. Based on this, we can expect that the model will have good results as a predistorter. It requires short time for training, which is an important advantage of this procedure. Next subsection will give the results for predistortion of the MIMIX CFH2162-P3 for LTE 1.4 MHz 64 QAM signal at 880MHz centre frequency.

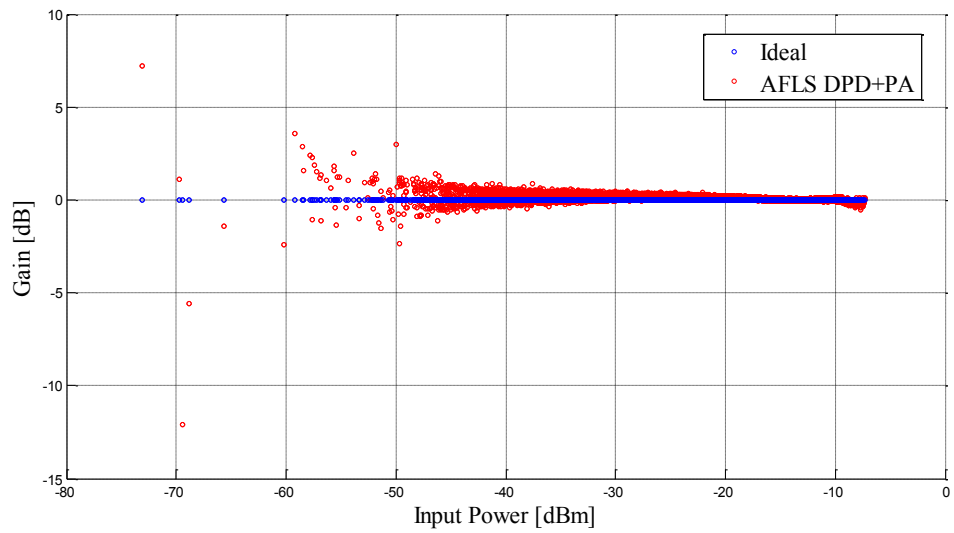
6.3.2 Predistortion of Power Amplifier using AFLS

6.3.2.1 DPD+PA system

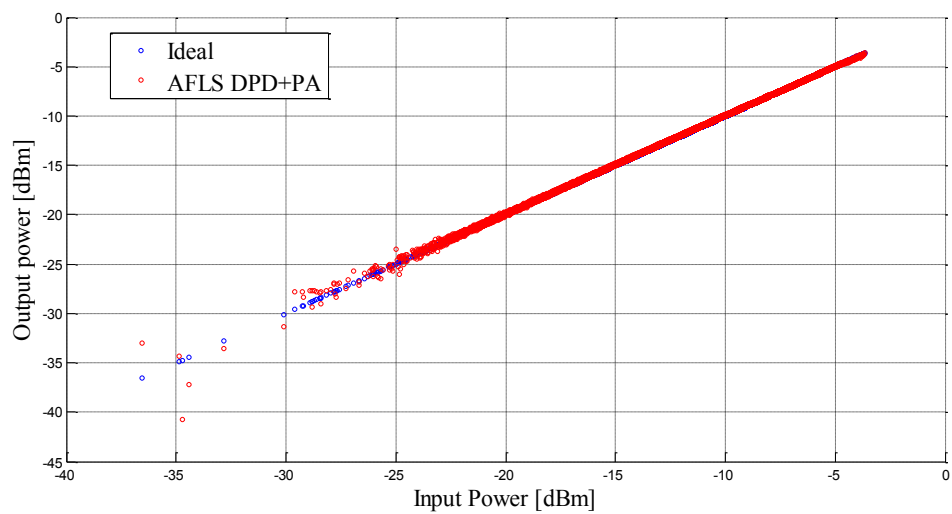
The Figure 5-11 presents the layout of a predistortion system and the procedure of testing the developed models for that application is the same as described in the Chapter 5.6. The input signal is used as the input of the predistorter, which is the first block in the DPD system. After the inverse PA model as DPD, the signal is further passed through the PA, in order to get a linearly gained signal at the output. The input signal LTE 1.4 MHz 64 QAM is used for testing developed AFLSs. The spectra of the real input signal, real output signal and signal at the output of the cascade DPD-PA are presented in the Figure 6-7. Spectral regrowth improvement for the LTE 1.4 MHz 64 QAM signal is 15.18dB for the upper band, and 15.00dB for the lower band. In order to present the predistortion ability of proposed method better, the nonlinear characteristics of the DPD-PA system are presented vs. characteristics of an ideally linear system. It can be seen from the PA gain graph (Figure 6-7 (b)) that this characteristic differs from its counterpart in modelling of the PA without using predistortion. The AM/AM characteristic (Figure 6-7 (c)), as well as the AM/PM dynamical characteristic (Figure 6-7 (d)), shows almost perfect matching with a linear system. The Table 6.5 presents the parameters of the signals at the output of the system without DPD and system formed of cascade of DPD and DUT.



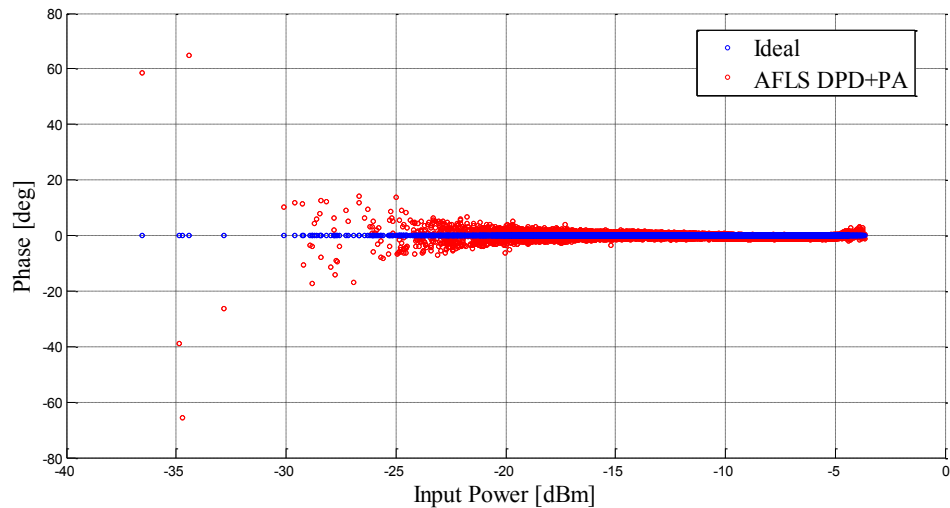
a)



b)



c)



d)

Figure 6-7: Predistortion results at 880 MHz: a) Power spectrum density of the DPD+PA model output vs. the real PA output for the LTE 1.4 MHz 64 QAM signal; b) PA gain; c) AM/AM characteristic; d) AM/PM characteristic

Table 6.5: Performances of output signal from DPD+PA system compared with performances of real input and output signals from a system without DPD for the LTE 1.4 MHz 64 QAM signal at 880 MHz centre frequency

	ACPR [dBc] ± 1.4 MHz offset		EVM [%]
	LOW	HIGH	
PA input	-36.19	-34.28	/
PA output without DPD	-30.89	-30.00	8.66
PA output with DPD	-36.06	-34.18	1.32

EVM of 1.32% and difference between the DPD-PA output signal ACPR and the real PA input signal ACPR of 0.13dB and 0.10dB for lower and upper adjacent channels, respectively, also confirms what can be seen from the spectra and nonlinear transfer characteristics.

6.3.2.1 PA+DPD system

As it was mentioned earlier, the inverse PA model and power amplifier in a cascade make a system expected to have an improved linearity. The Figure 5-11 shows one possible layout of a predistortion system, where the DPD part precedes the PA part of

the system. Another way of combining the PA and DPD parts is to put the PA first, and the DPD afterwards (Figure 6-8).

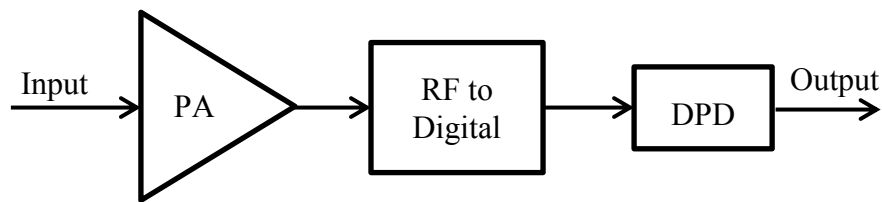
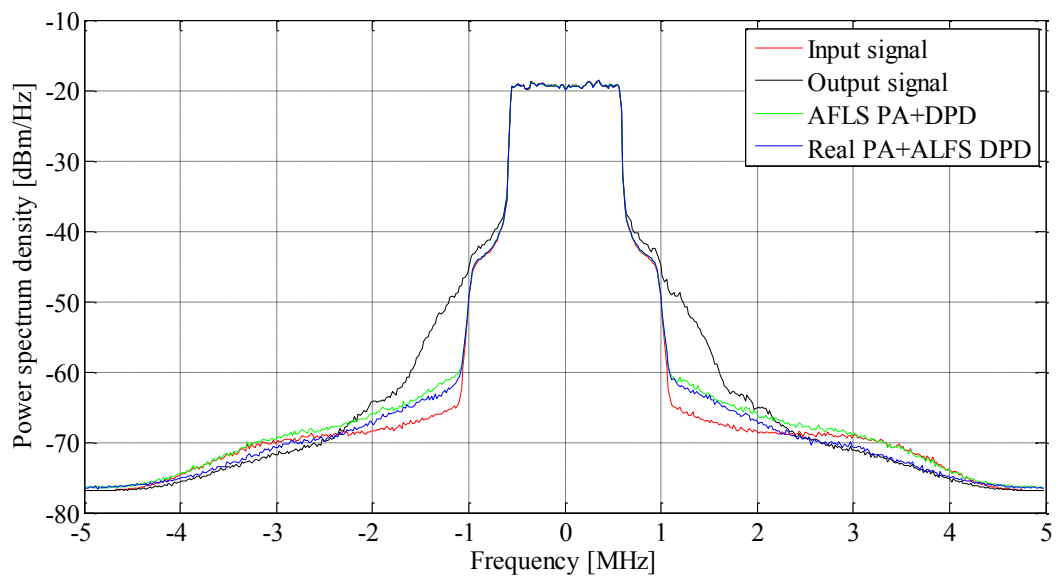


Figure 6-8: A layout of PA-DPD system

Creating presented layout using the forward and inverse models of a power amplifier, which were developed earlier, we expect to get a system with suppressed distortion. The input signal is used as the input of the power amplifier model, which is the first block in the DPD system shown in the Figure 6-8. After the PA model, the signal is further passed through the inverse model of the PA, in order to get a linearly gained signal at the output. The input signal LTE 1.4 MHz 64 QAM is used for testing this PA-DPD system. The spectra of the real input signal, real output signal, signal at the output of the cascade Real PA-DPD and signal at the output of the cascade PA Model-DPD are presented in the Figure 6-9 (a). Gain of the overall system, the AM/AM and AM/PM characteristics for the simulation and experimental tests are presented in the Figure 6-9 (b)-(d), respectively. It should be noted that the experiment in this case is basically the output of the inverse PA model, as the input comes from the output of the real power amplifier.



a)

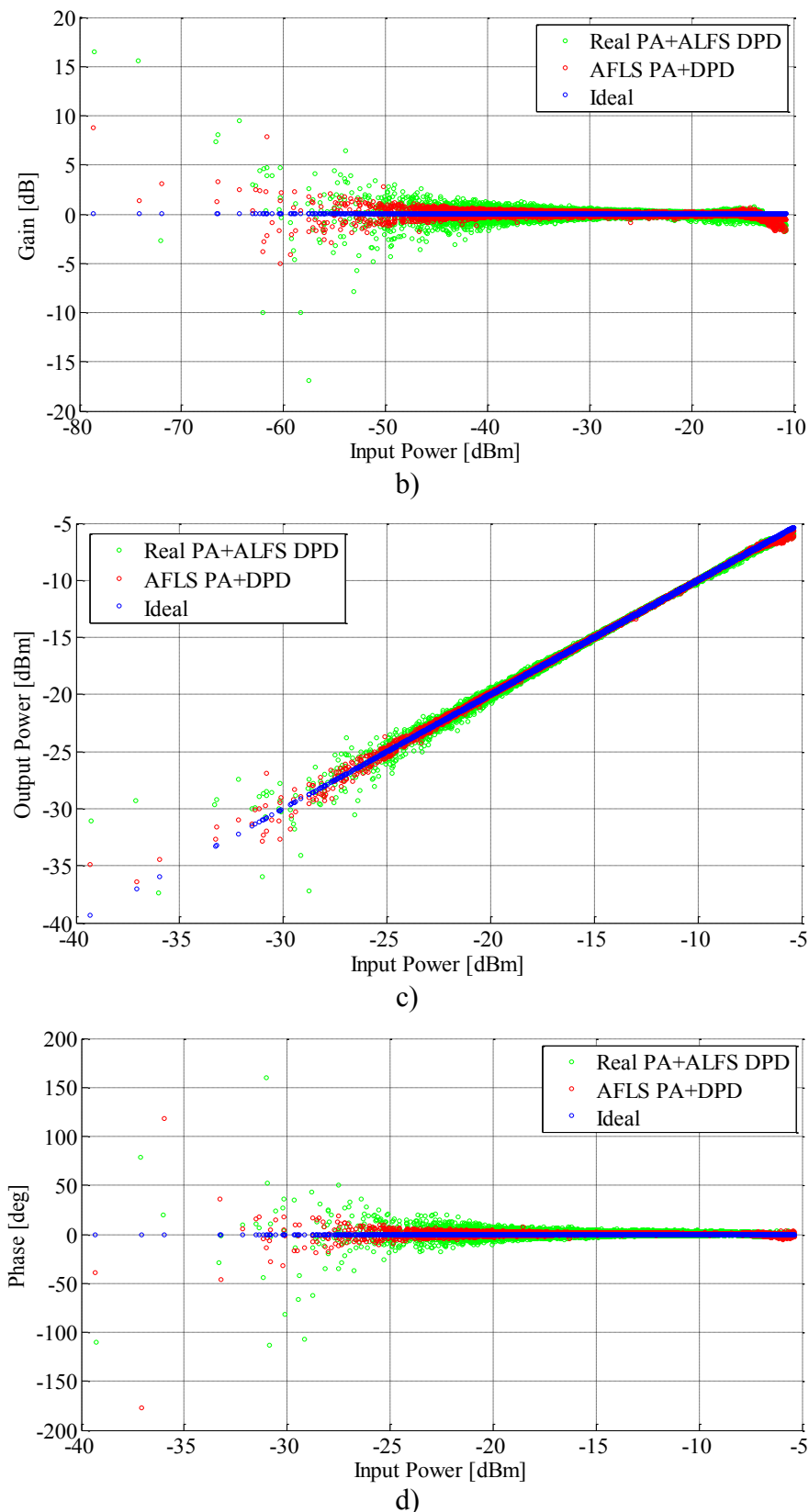


Figure 6-9: Comparison of simulation and experimental predistortion results at 880 MHz: a) Power spectrum density of a PA+DPD model output vs. output of the real PA for the LTE 1.4 MHz 64 QAM signal; b) PA gain; c) AM/AM characteristic; d) AM/PM characteristic

Table 6.6: Performances of output signal from PA+DPD system compared with performances of real input and output signals from a system without DPD for the LTE 1.4 MHz 64 QAM signal at 880 MHz centre frequency

	ACPR [dBc] ±1.4 MHz offset	
	LOW	HIGH
PA input	-36.19	-34.28
PA output without DPD	-30.89	-30.00
PA output with DPD (simulation)	-35.58	-33.78
PA output with DPD (experiment)	-35.63	-33.76

The Table 6.6 presents the signal performances for the experimental and simulation cases. ACPR of the output signal of the overall simulation system in comparison with ACPR of the input signal, is 0.61 dB and 0.5 dB higher in the lower and the upper channel, respectively. These indices for experimental case are 0.56 dB for the lower channel, and 0.52 dB for the upper channel. This shows a very good compensation of nonlinear distortion, as the output signal is very close to the linearly gained signal. The spectral comparison presented in the Figure 6-9 (a) also proves that this DPD system is effective. The matching between the simulation and experimental spectra means that the power amplifier AFLS model is very good. The spectral regrowth improvements at ±1.2 MHz offset are: for the simulation 11.79 dB in the lower band and 11.96 dB in the upper band; for the experiment 13.1 dB in the lower band and 13.31 dB in the upper band.

6.4. Comparison of used predistortion techniques

The main goal of this research was to compensate the distortion of the highly nonlinear power amplifier MIMIX CFH2162-P3. Two methods are proposed based on the artificial intelligence systems. The Chapter 5 gives the neural network approach with nonlinear activation function in the output layer, and this chapter presents the fuzzy logic system approach with the AOB defuzzification method. The Table 6.7 is overview of the simulation results for both DPD-PA and PA-DPD predistortion methods for the DUT and LTE 1.4 MHz 64 QAM signal, for which the comparison will be given later on.

Table 6.7: Comparative overview of used DPD techniques for the LTE 1.4 MHz 64 QAM signal at 88MHz centre frequency

		AFLS		RVTDNN	
DPD+PA system	ACPR difference between linearly gained signal and output of DPD+PA system [dB] ±1.4 MHz offset	LOW	-0.13	LOW	-0.49
		HIGH	-0.10	HIGH	-0.45
	EVM [%]	1.32		1.37	
	Spectral regrowth improvement [dB] ±1.2 MHz offset	LOW	15.00	LOW	11.44
HIGH		15.18	HIGH	11.76	
PA+DPD system	ACPR difference between linearly gained signal and output of PA+DPD system [dB] ±1.4 MHz offset	LOW	-0.61	LOW	-0.36
		HIGH	-0.50	HIGH	-0.26
	EVM [%]	1.79		1.13	
	Spectral regrowth improvement [dB] ±1.2 MHz offset	LOW	11.79	LOW	12.65
HIGH		11.96	HIGH	13.88	
Structure of predistorter		<ul style="list-style-type: none"> • 6 inputs • 40 rules 	<ul style="list-style-type: none"> • 10 inputs • 15 nodes in first hidden layer • 6 neurons in second hidden layer 		
Training time		~2h		>24h	
Number of parameters for training		640 (480 for fuzzifier, 160 for defuzzifier)		275 (165 in first hidden layer, 96 in second hidden layer, 14 in output layer)	

Table 6.8: Distortion suppression for presented methods for the LTE 1.4 MHz 64 QAM signal at 88MHz centre frequency

		AFLS		RVTDNN	
Distortion suppression [%]	DPD-PA	LOW	93.69	LOW	72.27
		HIGH	93.30	HIGH	72.28
	PA-DPD	LOW	73.64	LOW	79.91
		HIGH	73.51	HIGH	85.31

The comparison of the presented techniques was for the DUT at frequency of 880 MHz for the same LTE signal with 1.4 MHz bandwidth. Adjacent channels for measurement of the ACPR performance are at 1.4 MHz offset with bandwidth of 1.08 MHz. The trainings of the predistorters were carried out on the same PC, in order to have the same base for comparison. This 1.08 MHz channel bandwidth is the real occupied bandwidth of the used LTE 1.4 MHz 64 QAM signal. From the above comparison tables following conclusions can be derived. The ACPR difference and spectral regrowth show better performances of the AFLS method in the DPD-PA system and better performances of RVTDNN in the PA-DPD system. Furthermore, the time required for the AFLS training at the same computer is much smaller than for the neural network. The number of parameters of these structures, on the other hand, is smaller for the neural networks than for the neuro-fuzzy system. This makes the NNs requiring less memory for storage of these parameters, but the training algorithm is computationally more complex and more time-consuming. Both techniques were successfully used for the predistortion of the power amplifier. Depending on the user request, both of these can be incorporated in a real system. Even if the signals fed into the PA are beyond the range of the training signals, both structures would still have acceptably good results as they have an ability of interpolation and in some small range extrapolation. The advantage of the AFLS method is use of the Gaussian membership functions which provide a good local learning. On the other hand, the sigmoid activation functions in the neural networks provide a global learning. Thus the training of the AFLS network is quicker and more accurate than the training of the neural networks.

6.5. Conclusion

The proposed adaptive digital predistortion technique for linearizing the wireless highly nonlinear power amplifiers has been presented and verified by simulations and experiments. Theoretical concept and practical operation of the adaptive fuzzy logic systems were presented in the Chapter. The proposed digital predistortion technique is adjustable for achieving the best ratio of the linearization degree to the computational complexity for any particular application.

Unlike the published predistortion techniques which use the ANFIS networks for the power amplifier linearization, this presented method is less time-consuming and uses simpler structure than the multi-input multi-output ANFIS. Additionally, the distortion suppression of 93.3% is better in comparison with 72.28% achieved using the neural networks, when the DPD-PA structure is used.

6.6. References

- [6.1] M. Schetzen, *The Volterra and Wiener Theories of Nonlinear Systems*, New York: Wiley, 1980.
- [6.2] J. Mathews and G. Sicuranza, *Polynomial Signal Processing*, New York: Wiley, 2000.
- [6.3] H. W. Kang, Y. S. Cho, and D. H. Youn, "Adaptive precompensation of Wiener systems", *IEEE Transactions on Signal Processing*, vol. 46, no. 10, pp. 2825–2829, October 1998.
- [6.4] P. Celka, N. J. Bershad, and J.-M. Vesin, "Stochastic gradient identification of polynomial Wiener systems: analysis and application", *IEEE Transactions on Signal Processing*, vol. 49, no. 2, pp. 301–313, February 2001.
- [6.5] A. E. Nordsjo and L. H. Zetterberg, "Identification of certain time-varying nonlinear Wiener and Hammerstein systems", *IEEE Transactions on Signal Processing*, vol. 49, no. 3, pp. 577–592, March 2001.
- [6.6] T. J. Liu, S. Boumaiza, F. M. Ghannouchi, "Augmented Hammerstein predistorter for linearization of broad-band wireless transmitters", *IEEE Transactions on Microwave Theory and Techniques*, vol. 54, no. 4, pp. 1340–1349, April 2006.

- [6.7] D. R. Morgan, Z. Ma, J. Kim, M. G. Zierdt, and J. Pastalan, "A generalized memory polynomial model for digital predistortion of RF power amplifiers", *IEEE Transactions on Signal Processing*, vol. 54, no. 10, pp. 3852–3860, October 2006.
- [6.8] N. J. Bershad, P. Celka, and S. McLaughlin, "Analysis of stochastic gradient identification of Wiener–Hammerstein systems for nonlinearities with Hermite polynomial expansions", *IEEE Transactions on Signal Processing*, vol. 49, no. 5, pp. 1060–1072, May 2001.
- [6.9] S. Benedetto, and E. Biglieri, "Nonlinear equalization of digital satellite channels", *IEEE J. Select. Areas Commun.*, vol. SAC-1, pp. 57–62, January 1983.
- [6.10] A. Ahmed, E. R. Srinidhi, and G. Kompas, "Efficient PA modelling using neural network and measurement setup for memory effect characterization in the power device", *IEEE MTT-S International Microwave Symposium Digest*, June 2005.
- [6.11] S. Boumaiza, and F. Mkadem, "Wideband RF Power Amplifier Predistortion using Real-Valued Time-Delay Neural Networks", *European Microwave Conference, EuMC2009*, pp. 1449-1452, October 2009.
- [6.12] D. Culibrk, O. Marques, D. Socek, H. Kalva, and B. Furht, "Neural network approach to background modeling for video object segmentation", *IEEE Trans. Neural Netw.*, vol. 2, no. 5/6, pp. 673–689, June 2005.
- [6.13] T. Takagi and M. Sugeno, "Fuzzy identification of systems and its Applications to modeling and control", *IEEE Trans. Syst., Man, Cybern.*, vol. 15, no. 1, pp. 116–132, 1985.
- [6.14] N. Bawane, A. G. Kothari, and D. P. Kothari, "ANFIS based HVDC control and fault identification of HVDC converter", *HAIT J. Sci. Eng. B*, vol. 18, no. 6, pp. 1614–1627, November 2007.
- [6.15] J. S. R. Jang, "ANFIS: Adaptive-network-based fuzzy inference system", *IEEE Trans. Syst., Man, Cybern.*, vol. 23, no. 3, pp. 665–685, June 1993.
- [6.16] V. P. G. Jimenez, Y. Jabrane, A. G. Armada, B. A. Es Said, and A. A. Ouahman, "High Power Amplifier Pre-Distorter Based on Neural-Fuzzy Systems for OFDM Signals", *IEEE Transactions on Broadcasting*, vol. 57, no. 1, March 2011.
- [6.17] H. M. Deng, S. B. He, and J. B. Yu, "An adaptive predistorter using modified neural networks combined with a fuzzy controller for nonlinear power amplifiers", *International Journal of RF and Microwave Computer-Aided Engineering*, vol. 14, no. 1, pp. 15-20, January 2004.

-
- [6.18] K. C. Lee and P. Gardner, “Neuro-fuzzy approach to adaptive digital predistortion”, *Electronics Letters*, vol. 40, no. 3, February 2004.
- [6.19] Y. Li, and P. Yang, “Data predistortion with adaptive fuzzy systems”, *In Proc. IEE Int. Conf. Syst., Man, Cybern.*, vol. 6, pp. 168–172, 1999.
- [6.20] K. C. Lee, and P. Gardner, “A novel digital predistorter technique using an adaptive neuro-fuzzy”, *IEEE Commun. Lett.*, vol. 7, no. 2, pp. 55–57, February 2003.
- [6.21] K. C. Lee, and P. Gardner, “Adaptive neuro-fuzzy inference system (ANFIS) digital predistorter for RF power amplifier linearization”, *IEEE Trans. Veh. Technol.*, vol. 55, no. 1, pp. 43–51, January 2006.
- [6.22] L. X. Wang, and J. M. Mendel, “Generating Fuzzy Rules by Learning from Examples”, *IEEE Transactions on Systems, Man, and Cybernetics*, vol. 22, no. 6, December 1992.
- [6.23] V. S. Kodogiannis, M. Boulougoura, J. N. Lygouras, and I. Petrounias, “A neuro-fuzzy-based system for detecting abnormal patterns in wireless-capsule endoscopic images”, *Neurocomputing*, vol. 70, no. 4-6, pp. 704-717, January 2007.
- [6.24] V. S. Kodogiannis, I. Petrounias, and J. N. Lygouras, “Intelligent classification using adaptive fuzzy logic systems”, *4th International IEEE Conference on Intelligent Systems, IS '08.*, vol.1, pp.9-8,9-13, September 2008.

7. CONCLUSION

This Chapter presents summary of the thesis and suggestions for the future work.

7.1. Thesis Summary

Linearization of power amplifiers is essential considering requirements of nowadays communication systems. Complex modulation schemes, like wideband code division multiple access (WCDMA) and orthogonal frequency division multiplexing (OFDM), have a high peak to average power ratios, and the need for linearization of power amplifiers becomes more important in order to back off the amplifier working range from the saturation point.

A research work on the topic of linearization of power amplifiers for mobile communication systems has been presented in this thesis. A robust method for memoryless modelling of power amplifiers is proposed. Two new methods for modelling and linearization based on artificial intelligence systems are presented. Digital predistortion techniques are represented by theoretical concepts, practical implementation and validation by simulation and experimental results.

This thesis started off by developing a brief understanding of the nonlinearity of power amplifiers. A nonlinear analysis was described through analytical expressions and graphics of characteristics of a power amplifier. Overview of modelling and predistortion techniques for memoryless amplifiers, as well as for the ones without memory effects, was performed. The nonlinear analysis of the commercially available power amplifier ZHL-1042J with the two-tone test was depicted through simulations done in ADS software. The RF feedback compensation of distortion components is explained and verified for the same amplifier.

In the Chapter 3 introduction to the artificial intelligence systems was given. Every part of an artificial neural system is briefly explained. After that the fuzzy logic theory was introduced. In order to overcome disadvantages of both neural networks and fuzzy logic systems, neuro-fuzzy systems are described as basics for future developing modelling and linearization techniques. The adaptive neuro-fuzzy inference systems structure was explained.

A robust method for estimation of nonlinear parameters of memoryless model of power amplifiers was presented in the Chapter 4. An analysis of an output signal distortion as a consequence of memoryless nonlinearity was first presented over general formulas. Furthermore, the theory of baseband linearization was depicted. The application and verification of proposed robust method was performed through MATLAB environment. The experimental setup for collecting the data for the robust algorithm was described. The results of proposed method for estimation of nonlinear parameters were presented for the power amplifier Mini-Circuits ZHL-1042J.

Modelling of power amplifiers with memory was topic in the Chapter 5. Literature overview of existing methods based on the artificial neural networks was given. A neural network structure that differs from the structures used in literature was proposed. Complete systems for forward model as well as for the inverse model of power amplifier were described. The experimental setup based in Wireless Communications Research Laboratory at the university used for collection of data for training of the proposed networks was presented. Additionally, the modelling algorithms implemented in MATLAB software were explained in this Chapter. A power amplifier used for modelling and predistortion was the MIMIX CFH2162-P3 power amplifier. The verification of forward and inverse models of the DUT was depicted through the spectra of the input and output signals and the signal performance parameters. The proposed method for predistortion was finally certified through a real experiment. Modelling and predistortion were carried out for the LTE 1.4 MHz 64 QAM signal and LTE 3 MHz 64 QAM signal at 880 MHz as centre frequency. A small difference between the spectral regrowth improvement gained through testing the DPD+PA system in MATLAB environment, and the spectral regrowth improvement gained through hardware testing of the developed predistorter, is a proof that the PA forward model has high accuracy.

In the Chapter 6 a novel technique for modelling and linearization based on the neuro-fuzzy approach was described. A detailed structure explanation was presented as well as the training procedure and the update of system parameters. This technique was explored for the LTE 1.4 MHz 64 QAM signal at 880 MHz as centre frequency driven to the MIMIX CFH2162-P3 power amplifier. Models for forward and inverse characteristics were validated through NMSE and matching spectra. Predistortion of the device under test was best shown through the spectral regrowth improvement. A comparative overview of the neural network based, and the neuro-fuzzy based systems

was given in this Chapter, where superiority of AFLS over the NN was shown. That was especially dominant for the training time and for improvement in spectral regrowth.

An overall conclusion can be set. Presented research work has achieved aims of developing digital predistortion systems for highly nonlinear power amplifiers. The feasibility and performances of the proposed DPD were validated by simulations using MATLAB, and by experiments which were described for every used amplifier.

7.2. Contributions to Knowledge

The research focuses on a novel solution for the adaptive distortion reduction of power amplifiers that can be used with OFDM digitally modulated signal for a number of different wireless applications such as next generation mobile and wireless communications systems. The main contributions of this work are:

- A new robust method of extracting the PA polynomial model based on the frequency response analysis. Using this method for memoryless nonlinearity characterisation, current and voltage changes, especially in older systems, can be overcome.
- Improvements in the neural network structure for modelling and predistortion of power amplifiers using the nonlinear activation functions in the output layer. Performance, advantages and limitations of the developed method for compensation of real-life imperfections of the power amplifier in wireless transceivers were presented.
- For the first time the adaptive fuzzy logic systems are used for modelling and predistortion of power amplifiers. It results in a reduction of almost 20dB in spectral regrowth.

7.3. Future Work

The first direction in future work would be testing the proposed DPD technique on the used device under test for the wider LTE signals, and on different frequencies, as the nonlinear behaviour of an amplifier changes over the frequency range.

Secondly, modelling and predistortion procedures should be carried out on a various amplifiers, to create a wider range of possible usage in real-life. Upon achieving successful results, the method would be investigated for improving the linearity and compensating the real-life imperfections of the complete transmitter.

Another area of the suggested future work is creation of recurrent neural network structures instead of RVTDDNs in order to avoid large vectors of input variables, and comparison of those results with real valued time delayed neural network structures, used in the presented research.

Developing of the pre-processing part of adaptive fuzzy logic system, possibly clustering stage would be an interesting part of the future research, as this would reduce complexity of AFLS network, thus shortening training time and making system more convenient for use in real-life systems.

Extension of the AFLS training algorithm with tracking the trend of the NMSE parameter through the training process and update the learning rates and momentums according to that trend, would speed up the training process and provide a better convergence of the network. For example, update of the learning rates and momentums could be performed when the NMSE parameter has three decreases in a row, and update factor would depend on the NMSE changing rate.

Furthermore, investigation of applicability of the proposed methods on different physical devices like Field Programmable Gate Array (FPGA) evaluation platform should be carried out.

After that, a real-life implementation of the designed adaptive DPD would become a part of the further studies. Experiments which include closed loop with an online processing of signals would evaluate the overall performance of the system before mass production. Also, in a real-life implementation tracking of changes in power amplifiers behaviour due to environmental conditions could be tested and ability of adaptation proved in that way.

LIST OF PUBLICATIONS

- [1] M. Vaskovic, and D. Budimir, "Compensation of Nonlinear Distortion in RF Power Amplifiers for LTE Applications", *Microwave and Optical Technology Letters*, vol. 56, pp. 1910-1913, August 2014.
- [2] M. Vaskovic, M. Cabarkapa, and D. Budimir, "PA Modelling using Robust Estimation Method", *In Proceedings of 56th ETRAN Conference*, Zlatibor, Serbia, June 2012.
- [3] M. Vaskovic, Z. Djurovic, A. Tarczynski, and D. Budimir, "Robust estimation of nonlinear model coefficients for RF power amplifiers", *10th International Conference on Telecommunications in Modern Satellite, Cable and Broadcasting Services – TELSIKS '11*, Nis, Serbia, October 2011.
- [4] M. Vaskovic, D. Bondar, and D. Budimir, "Analytical calculation of predistorter coefficients for any order of nonlinear distortion", *In Proceedings of 54th ETRAN Conference*, Donji Milanovac, Serbia, June 2010.
- [5] D. Bondar, N. Perisic, M. Vaskovic, and D. Budimir, "Signal processing technique for compensation of nonlinear distortion", *In Proceedings of 53th ETRAN Conference*, Vrnjacka Banja, Serbia, June 2009.

APPENDIX-A

Data Sheets for the Power Amplifiers

Coaxial
Amplifier

ZFL-500

50Ω Low Power 0.05 to 500 MHz

Features

- wideband, 0.05 to 500 MHz
- rugged, shielded case
- low noise, 5.3 dB typ.
- protected by US Patent, 6,943,629

Applications

- instrumentation
- lab use
- VHF/UHF



SMA version shown

CASE STYLE: Y460

Connectors	Model	Price	Qty.
SMA	ZFL-500	\$69.95	(1-9)
BNC	ZFL-500-BNC	\$74.95	(1-9)
BRACKET (OPTION "B")		\$2.50	(1+)

Amplifier Electrical Specifications

MODEL NO.	FREQUENCY (MHz)		GAIN (dB)		MAXIMUM POWER (dBm)			DYNAMIC RANGE		VSWR (:1) Typ.		DC POWER	
	f_L	f_U	Min.	Flatness Max.	Output (1 dB Compr.)	Input (no damage)	NF (dB) Typ.	IP3 (dBm) Typ.	In	Out	Volt (V) Nom.	Current (mA) Max.	
ZFL-500	0.05	500	20	±1.0	-	+9	+5	5.3	+18	1.9	1.9	15	80

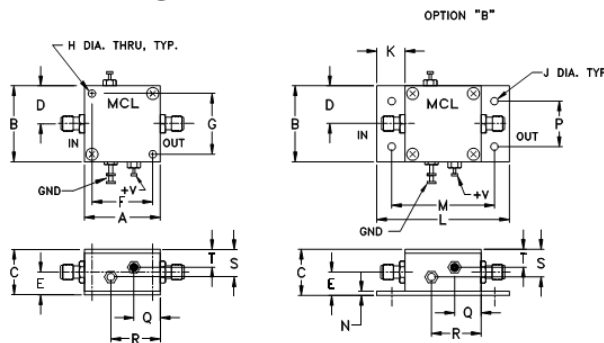
Open load is not recommended, potentially can cause damage.
With no load derate max input power by 20 dB

L= low range (f_L to $f_U/2$)U= upper range ($f_U/2$ to f_U)

Maximum Ratings

Operating Temperature	-20°C to 71°C
Storage Temperature	-55°C to 100°C
DC Voltage	+17V Max.

Outline Drawing



Outline Dimensions (inch/mm)

A	B	C	D	E	F	G	H	J	K
1.25	1.25	.75	.63	.36	1.000	1.000	.125	.125	.46
31.75	31.75	19.05	16.00	9.14	25.40	25.40	3.18	3.18	11.68
L	M	N	P	Q	R	S	S		wt.
2.18	1.688	.06	.750	.50	.80	.45	.29		grams
55.37	42.88	1.52	19.05	12.70	20.32	11.43	7.37		38

INTERNET <http://www.minicircuits.com>

P.O. Box 350166, Brooklyn, New York 11235-0003 (718) 934-4500 Fax (718) 332-4661

Distribution Centers NORTH AMERICA 800-654-7949 • 417-335-5935 • Fax 417-335-5945 • EUROPE 44-1252-832600 • Fax 44-1252-837010

Mini-Circuits ISO 9001 & ISO 14001 Certified

REV. OR
M98087
ZFL-500
051228
Page 1 of 2

Coaxial Amplifier

ZHL-1042J

50Ω Medium Power 10 to 4200 MHz



Features

- wideband, 10 to 4200 MHz
- high IP3, +30 dBm typ.
- low noise, 6 dB typ.

Applications

- laboratory
- communication systems

CASE STYLE: NN92			
Connectors	Model	Price	Qty.
SMA	ZHL-1042J	\$495.00	(1-9)

Amplifier Electrical Specifications

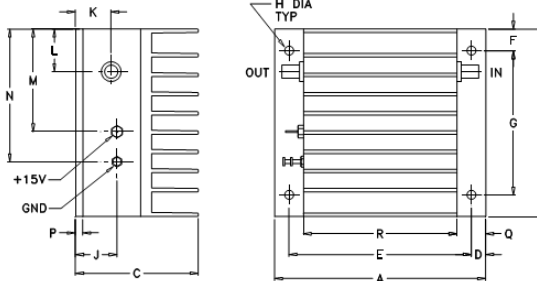
MODEL NO.	FREQUENCY (MHz)		GAIN (dB)			MAXIMUM POWER (dBm)		DYNAMIC RANGE		VSWR (∶1) Typ.		DC POWER	
	f_L	f_U	Typ.	Min.	Flatness Max.	Output (1 dB Compr.)	Input (no damage)	NF (dB) Typ.	IP3 (dBm) Typ.	In	Out	Volt (V) Nom.	Current (mA) Max.
ZHL-1042J	10	4200	—	25	±1.5	+20	+10	6	+30	2.5	2.5	15	330

Open load is not recommended, potentially can cause damage.
With no load derate max input power by 20 dB

Maximum Ratings

Operating Temperature	-20°C to 65°C
Storage Temperature	-55°C to 100°C
DC Voltage	+20V Max.

Outline Drawing



Outline Dimensions (inch/mm)

A	B	C	D	E	F	G	H	J
3.66	3.25	2.13	.25	3.16	.38	2.50	.156	.72
92.96	82.55	54.10	6.35	80.26	9.65	63.50	3.96	18.29
K	L	M	N	P	Q	R	wt	
.64	.74	1.78	2.30	.125	.50	2.66	grams	
16.26	18.80	45.21	58.42	3.18	12.70	67.56	440.0	



INTERNET <http://www.minicircuits.com>

P.O. Box 350166, Brooklyn, New York 11235-0003 (718) 934-4500 Fax (718) 332-4661

Distribution Centers NORTH AMERICA 800-654-7949 • 417-335-5935 • Fax 417-335-5945 • EUROPE 44-1252-832600 • Fax 44-1252-837010

Mini-Circuits ISO 9001 & ISO 14001 Certified

REV. OR
M98088
ZHL-1042J
051229
Page 1 of 2



CFH2162-P3

Advanced Product Information
May 1996

(1 of 2)

1.8 to 2.0 GHz +36 dBm Power GaAs FET

Features

- High Gain
- +36 dBm Power Output
- Proprietary Power FET Process
- >45% Linear Power Added Efficiency
- +33 dBm with 30 dBc Third Order Products

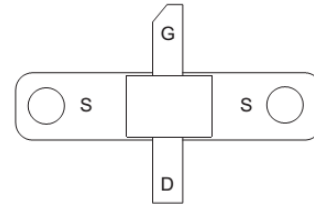
Applications

- PCS/PCN Base Stations
- Wireless Local Loop

Description

The CFH2162-P3 is a high-gain, linear FET intended for driver amplifier applications in high-power systems, and output stage usage in medium power applications at power levels up to +36 dBm. The device is easily matched and pro-

Package Diagram



vides excellent linearity at 4 Watts. Manufactured in Celeritek's proprietary power FET process, this device is assembled in a power flange package.

Specifications (TA = 25°C) The following specifications are guaranteed at room temperature in Celeritek test fixture at 1.95 GHz.

Parameters	Conditions	Min	Typ	Max	Units
$V_d = 10V, I_d = 1100 \text{ mA}$ (Quiescent)					
P-1dB		36.0	37.0	—	dBm
G-1 dB		13.0	14.0	—	dB
3rd Order Products (1)		30	35	—	dBc
Efficiency	@ P1dB	—	45	—	%
$V_d = 8V, I_d = 1300 \text{ mA}$ (Quiescent)					
P-1dB		—	36.0	—	dBm
G-1 dB		—	13.0	—	dB

Parameters	Conditions	Min	Typ	Max	Units
g_m	$V_{ds} = 2.0V, V_{gs} = 0V$	—	1700	—	mS
I_{dss}	$V_{ds} = 2.0V, V_{gs} = 0V$	—	2.8	—	A
V_p	$V_{ds} = 3.0V, I_{ds} = 65 \text{ mA}$	—	-1.8	—	Volts
BV_{GD}	$I_{gd} = 6.5 \text{ mA}$	20	24	—	Volts
Θ_{JL} (2)	@150°C TCH	—	8	—	°C/W

Absolute Maximum Ratings

Parameter	Symbol	Rating
Drain-Source Voltage	V_{DS}	15V ⁽³⁾
Gate-Source Voltage	V_{GS}	-5V
Drain Current	I_{DS}	I_{dss}
Continuous Dissipation	P_T	10W
Channel Temperature	T_{CH}	175°C
Storage Temperature	T_{STG}	-65°C to +175°C

Notes:

- Sum to two tones with 1 MHz spacing = 33 dBm.
- See thermal considerations information.
- Maximum potential difference across the device ($V_d + V_g$) cannot exceed 18V.

Power Flange Package Physical Dimensions

